

# **Fibre Models for Shear Failure and Plasticity**

Von der Fakultät Mathematik und Physik der Universität Stuttgart  
zur Erlangung der Würde eines Doktors der  
Naturwissenschaften (Dr. rer. nat.) genehmigte Abhandlung

Vorgelegt von

**Frank Raischel**

aus Würzburg

Hauptberichter: Prof. Dr. H. J. Herrmann  
Mitberichter: Prof. Dr. A. Muramatsu

Tag der mündlichen Prüfung: 5. Februar 2007

Institut für Computerphysik der Universität Stuttgart

2007



# Contents

<b>Zusammenfassung</b>	<b>5</b>
<b>1 Introduction</b>	<b>13</b>
1.1 Motivation . . . . .	13
1.2 State of Research . . . . .	19
1.3 Overview of the Research Conducted . . . . .	21
<b>2 The Classical Fibre Bundle Model</b>	<b>25</b>
<b>3 A Simple Beam Model for the Shear Failure of Interfaces</b>	<b>31</b>
3.1 Properties of the model . . . . .	31
3.2 Constitutive behaviour . . . . .	34
3.2.1 <i>OR</i> breaking rule . . . . .	34
3.2.2 Von Mises type breaking rule . . . . .	37
3.3 Computer simulations . . . . .	38
3.4 Progressive failure of the interface . . . . .	41
3.5 Avalanche statistics . . . . .	45
3.6 Local load sharing . . . . .	46
3.7 Concluding remarks . . . . .	49
<b>4 Failure Process of a Bundle of Plastic Fibres</b>	<b>51</b>
4.1 Model . . . . .	51
4.2 Transition to perfect plasticity . . . . .	52
4.3 Avalanches of fibre breakings . . . . .	58
4.4 Local load sharing . . . . .	60
4.4.1 Macroscopic response . . . . .	61
4.4.2 Bursts of fibre breakings . . . . .	63

---

4.4.3	Spatial structure of damage . . . . .	64
4.4.4	Random crack nucleation versus crack growth . . . . .	68
4.5	Summary . . . . .	74
<b>5</b>	<b>Local Load Sharing Fibre Bundles with a Lower Cutoff of Strength Disorder</b>	<b>75</b>
5.1	Critical Failure Threshold Distributions . . . . .	75
5.2	Discussion . . . . .	82
<b>6</b>	<b>Extensions of the continuous damage model</b>	<b>85</b>
6.1	Introduction . . . . .	85
6.2	CDFBM with a randomly distributed number of maximum failures . . . . .	86
6.3	CDFBM with sorted failure thresholds . . . . .	90
6.4	Conclusions . . . . .	102
<b>7</b>	<b>Discussion and Outlook</b>	<b>105</b>
7.1	Summary of the Results . . . . .	105
7.2	Open Questions . . . . .	108
7.3	A perspective . . . . .	110
	<b>Bibliography</b>	<b>113</b>
	<b>Acknowledgments</b>	<b>121</b>
	<b>Lebenslauf</b>	<b>124</b>

# Zusammenfassung

Diese Dissertation behandelt die Anwendung einer Klasse statistischer Modelle, der sogenannten Faserbündelmodelle, auf aktuelle Fragestellungen in Bezug auf das Bruchverhalten ungeordneter Materialien, insbesondere der faserverstärkten Verbundstoffe. Es handelt sich hierbei im Einzelnen um die Probleme des Schubversagens geklebter Verbindungen, die Darstellung von Plastizität, entgegengesetzt dazu das Auftreten von ausgeprägter Sprödigkeit, und zuletzt die schrittweise Schwächung von Materialien mit einer extremalen Defektverteilung. Die Notwendigkeit dieser Untersuchungen wird in Kapitel 1 begründet, eine Darstellung der grundlegenden Eigenschaften von Faserbündelmodellen erfolgt in Kapitel 2. Die vorgestellten Ergebnisse sind für sich alleine genommen gültig, weisen aber auch Beziehungen zueinander auf. So ist das Balkenmodell, welches in Kapitel 3 vorgestellt und behandelt wird, zur Beschreibung der Faser-Matrix-Grenzfläche in Verbundwerkstoffen prädestiniert, eine Anwendung in der auch Plastizität, für die in Kapitel 4 ein einfaches Faserbündelmodell dargestellt wird, zum Tragen kommt. In diesem plastischen Faserbündelmodell wiederum tritt unter bestimmten Annahmen eine Auffälligkeit zu Tage, die signifikante Änderung der Häufigkeitsverteilung von Bruchereignissen, welche der Gegenstand von Kapitel 5 ist, und zudem auch in ausgeprägter Weise in Kapitel 6 im Rahmen eines graduellen Schädigungsmodelles auftritt. Dies spiegelt die Tatsache wieder, dass alle Modelle auf gemeinsamen theoretischen und experimentellen Erkenntnissen aufbauen, und im gleichen Formalismus der Faserbündelmodelle (FBM, *engl.* fibre bundle models) behandelt werden.

Das Gebiet der Bruchmechanik, welches durch experimentelle Studien von Galilei und da Vinci begründet wurde, hat in den letzten Jahren gesteigerte Aufmerksamkeit in Zusammenhang mit dem mechanischen Versagen ungeordneter Systeme und Materialien erhalten, für dessen Beschreibung die Methoden der statistischen Physik in besonderem Maße geeignet sind [1]. Unter den ungeordneten Materialien bildet die Klasse der faserverstärkten Werkstoffe einen Schwerpunkt dieser Arbeit. Als Beispiele für diese Materialien sind hierbei Holz, Stahlbeton, d.h. eine mit Stahlfasern verstärkte Betonmatrix, und die Klasse der faserverstärkten Compositmaterialien zu nennen, die in den letzten Jahren zu eminenter Bedeutung insbesondere in der Luft- und Raumfahrtindustrie gelangt sind, da sie bei geeigneter Faserorientierung außergewöhnliche Festigkeit mit geringer spezifischer Masse vereinigen. Einhergehend mit diesem Bedeutungszuwachs war auch die Erkenntnis, dass die gängigen ingenieurwissenschaftlichen Methoden die spezifischen Eigenschaften dieser Werkstoffe nicht vollständig erfassen können, insbesondere wenn es um Effekte der Unordnung geht, wie der statistischen Verteilung von Defektstellen. In Abb. 1 sind der faserige Aufbau von Holz und Faserbeton und der hierarchische Aufbau

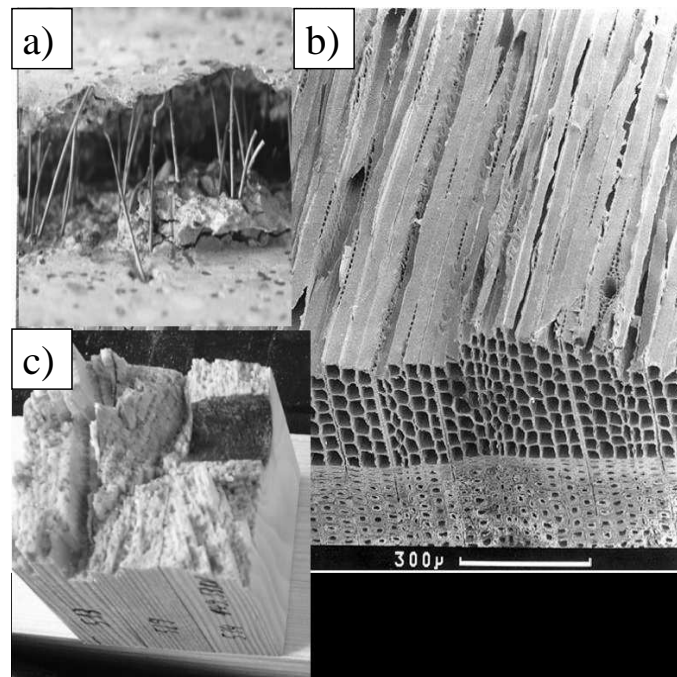


Abbildung 1: Beispiele für den faserigen Aufbau von Stahlbeton (a) und Holz (b,c). Der hierarchische Aufbau von Holz wird bei Betrachtung einer Weichholzprobe in mikroskopischem Maßstab (b) und bei einer anderen Holzprobe im mesoskopischen Bereich (c) ersichtlich. Quellen: (a) aus Ref. [2], (b) aus Ref. [3], (c) Foto eines Holzbalkens, welcher im Rahmen eines Zugversuches am Insitut für Werkstoffe im Bauwesen der Universität Stuttgart versagt hat.

von Holz zu erkennen.

Das klassische Faserbündelmodell, welches auf wegweisende Arbeiten von Peires [4] und Daniels [5] zurückgeht, wird in Kapitel 2 umrissen. Kurz gefasst besteht das Modell aus einer Menge an parallelen Fasern, welche auf einem kubischen zweidimensionalen Gitter angeordnet werden. Die Fasern werden unter Zug belastet und verhalten sich hierbei linear elastisch, bis sie einen spezifischen Lastwert erreichen an dem sie vollständig versagen, wobei die Last einer Faser nach Versagen auf Null fällt. Die jeweiligen Lastwerte für das Versagen unterliegen einer Wahrscheinlichkeitsverteilung, welche die Unordnung in dem zu betrachtenden Material abbildet; üblicherweise findet hier eine Weibull-Verteilung mit Maßstabsparameter  $m$  und Formparameter  $\lambda$  Verwendung; letzterer dient zur direkten Modellierung der Unordnung. Beim Versagen muss die Last, welche von der versagenden Faser getragen wird, auf die umliegenden intakten Fasern übertragen werden, was entweder lokal (LLS, *engl.* local load sharing) auf die benachbarten, oder global (GLS, *engl.* global load sharing) auf alle intakten Fasern im Bündel erfolgen kann. Bei beständigem Fortschreiten der von außen angelegten Zugspannung kann schon bei Versagen einer einzelnen Faser eine Kaskade von weiteren Versagensprozessen eintreten, da durch die Lastumlagerung von der versagenden auf die intakten Fasern eventuell weitere Schwellwerte überschritten werden. Die Größenverteilung  $D(\Delta)$  dieser lawinenartigen Prozesse ist neben dem makroskopischen Spannungs-Dehnungs-Diagramm  $\sigma(\varepsilon)$  das Hauptcharakter-

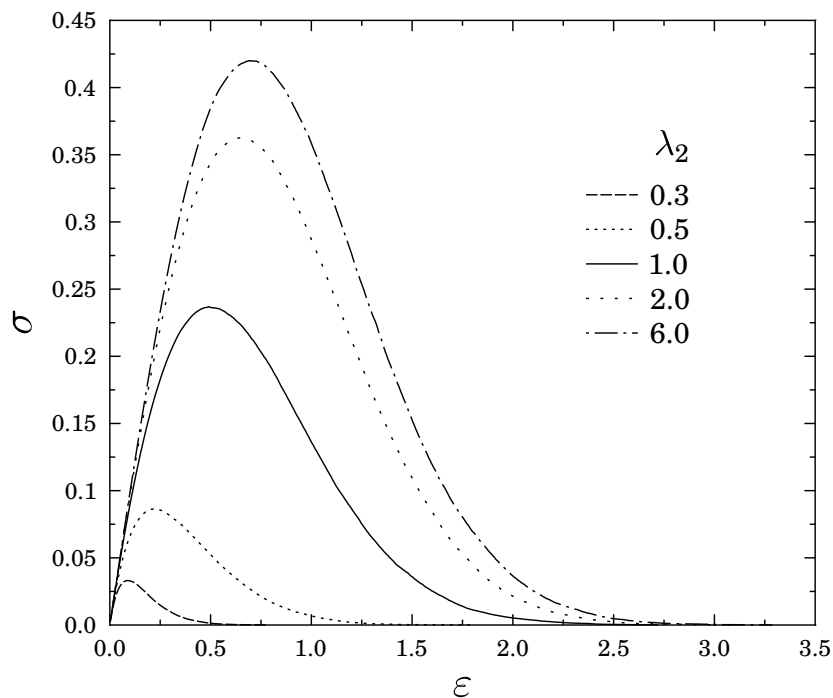


Abbildung 2: Spannungs-Dehnungs-Diagramm im Balkenmodell von Kapitel 3, wobei der relative Einfluss der unabhängigen Bruchmodi durch Variation des Weibull-Parameters  $\lambda_2$  für die Verteilung der Schwellwerte für Versagen durch Biegung variiert wird. Mit zunehmendem Wert von  $\lambda_2$  gewinnt der Zugmodus an Bedeutung und dominiert schließlich das Verhalten des Systems (nicht gezeigt), so dass das Balkenmodell einem reinen Faserbündelmodell entspricht.

teristikum der Faserbündelmodelle, und bei Betrachtung unter globaler Wechselwirkung findet man hierbei für das klassische Faserbündelmodell wie auch für die meisten seiner Derivate ein Potenzgesetz mit einem universalen Exponenten  $5/2$ , der sich auch mit analytischen Methoden herleiten lässt [6].

Mit der genannten Konstruktionsvorschrift bildet schon das klassische Modell die wesentlichen Eigenschaften von faserverstärkten Werkstoffen unmittelbar ab: die Anwesenheit einer statistischen Verteilung für die Festigkeit der einzelnen Elemente, die ausgeprägte Anisotropie sowie die Lastumlagerung bei Versagen eines Elementes sind integrale Bestandteile dieser Beschreibung.

Das Studium der Faserbündelmodelle und verwandter Methoden wie etwa dem *random fuse model* ist nicht nur aus Sicht der Materialwissenschaften von Bedeutung, sondern hat in den vergangenen Jahren auch wichtige Einblicke in die physikalischen Grundlagen des Versagens ungeordneter Stoffe geliefert [7]. Auch Anwendungen außerhalb des bisherigen Definitionsbereiches, etwa auf biologische Systeme oder Erdbeben, sind in letzter Zeit populär geworden.

Im Folgenden wird ein kurzer Abriss der vorgestellten Forschungsergebnisse gegeben.

Das klassische Faserbündelmodell beschreibt eine Belastung in Faserrichtung. Um aber den Fall einer Schubbelastung senkrecht zur Faserrichtung zu modellieren, muss eine Modifikation vorgenommen werden. Dies geschieht in der Absicht, das Schubversagen von faserverstärkten Compositen, welches wesentlich durch die Eigenschaften der Faser-Matrix-Grenzfläche bestimmt wird, abzubilden. Als einfaches Modellbild wird in Kapitel 3 das Schubversagen geklebter Verbindungen zwischen zwei festen Körpern unter Betrachtung eines neuartigen Modells untersucht. In dem Modell wird die Verbindung als Menge elastischer Balken diskretisiert, welche unter Schubbelastung gedehnt und gebogen werden. Das Versagen eines Balkens kann demzufolge durch zwei Bruchmodi verursacht werden, nämlich Spannung und Biegung, welche durch zufallsverteilte Schwellwerte beschrieben werden. Diese zwei Bruchmodi können entweder unabhängig voneinander wirken, oder in der Form eines von Mises-artigen Kriteriums kombiniert werden. Im Falle langreichweitiger Wechselwirkungen zwischen den Balkenelementen kann die vollständige Lösung für das makroskopische Verhalten sowie für den mikroskopischen Schädigungsprozess der Verbindung angegeben werden. Es zeigt sich, dass die Anwesenheit zweier unabhängiger Bruchmodi sowohl die kritische Spannung als auch die kritische Dehnung im Vergleich zum Vorliegen nur eines Bruchmodus herabsetzt, wovon die statistischen Häufigkeitsverteilungen der mikroskopischen Bruchereignisse unberührt bleiben. Die Kopplung der Bruchmodi führt zu einer weiteren Herabsetzung der mechanischen Festigkeit der Verbindungsschicht. Das mechanische Ansprechverhalten der Verbindung ändert sich bei Einstellung unterschiedlicher relativer Stärke beider Bruchmodi in einem weiten Bereich, wie in Abb. 2 anhand des konstitutiven Verhaltens sichtbar wird. Auch im Grenzfall stark lokalisierter Wechselwirkungen, in dem Balkenelemente ausschließlich mit den nächsten und übernächsten Nachbarelementen auf dem Gitter wechselwirken, wird das konstitutive Verhalten und die Größenverteilung der Bruchereignisse betrachtet. Ferner wird eine effiziente Simulationsmethode vorgestellt, welche die Betrachtung hinreichend großer Systeme ermöglicht. Auf Grundlage der vorgestellten Untersuchungen kann das Balkenmodell auf das klassische Faserbündelmodell abgebildet werden.

Zur Beschreibung der in diesem Zusammenhang relevanten makroskopischen Plastizität wird in Kapitel 4 eine Erweiterung der klassischen Faserbündelmodelle und des Balkenmodells aus Kapitel 3 vorgestellt, in welcher Oberflächenelemente auch nach ihrem Versagen weiterhin eine gewisse Fähigkeit zur Lastaufnahme besitzen. Die materielle Unordnung der Verbindung wird durch eine parallele Anordnung von Faserelementen mit zufallsverteilten Versagensgrenzwerten repräsentiert, welche bis zum jeweiligen Versagenspunkt linear elastisch reagieren. Es wird angenommen, dass die Fasern nach ihrem Versagen eine konstante Last annehmen, welche ein Bruchteil  $0 \leq \alpha \leq 1$  ihrer Last unmittelbar vor dem Versagen ist. Der Parameter  $\alpha$  des Modells interpoliert hierbei zwischen den Grenzwerten des vollständig plastizitätsfreien und des vollständig plastischen konstitutiven Verhaltens des Faserbündels. Auf der Grundlage analytischer Berechnungen und von Computersimulationen erweist sich die Fähigkeit der versagten Fasern zur Lastaufnahme als wesentlicher Einfluss sowohl auf das makroskopische Ansprechen des Systems, als auch auf seinen mikroskopischen Schädigungsprozess. Im Falle kurzreichweitiger Wechselwirkungen lässt sich ein interessanter Phasenübergang bei einem klar definierten Wert von  $\alpha$  feststellen. In der Nähe dieses kritischen Wertes von  $\alpha$  treten un-



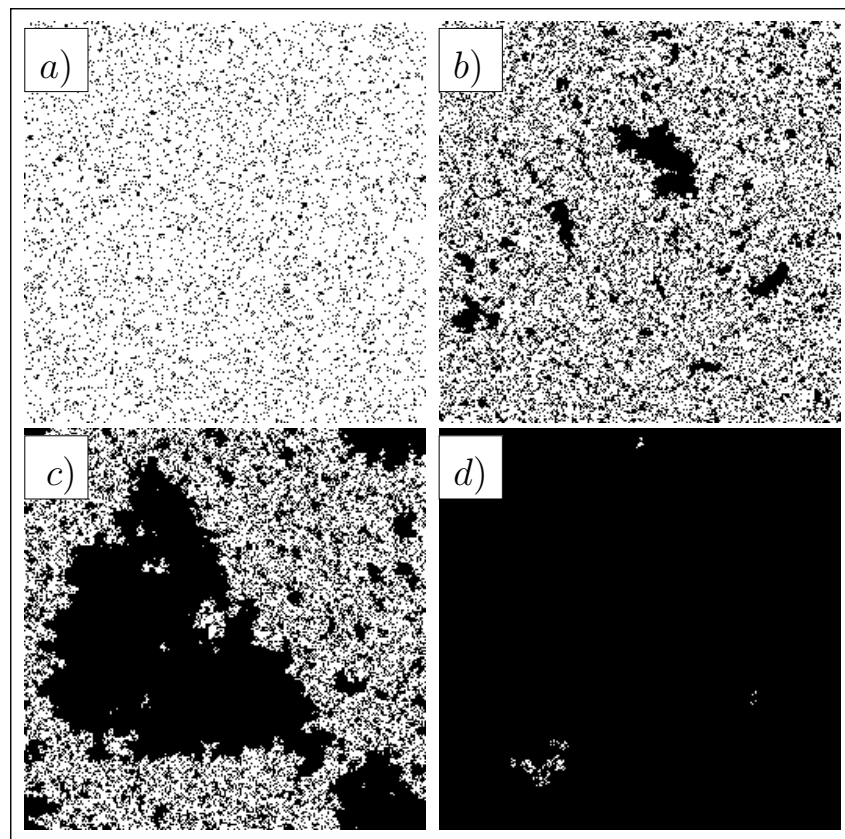


Abbildung 3: Das Erscheinen ausgedehnter zusammenhängender Bereiche im plastischen Faserbündelmodell von Kapitel 4 bei Variation des Plastizitätsparameters  $\alpha$  in der Nähe des kritischen Wertes  $\alpha_c \approx 0,4$ . a)  $\alpha = 0$ . b)  $\alpha = 0,35$ . c)  $\alpha = 0,4$ . d)  $\alpha = 0,6$ .

mittelbar vor dem globalen Systemversagen großflächige zusammenhängende Bereiche von versagten Fasern auf (s. Abb. 3), deren Beschreibung mit den Methoden der statistischen Physik weitere Einblicke in den mikroskopischen Schädigungsprozess liefert.

Wie vor kurzem erkannt wurde, hat die Existenz einer unteren Grenze  $\varepsilon_L$  für die Versagenswahrscheinlichkeiten in einem Faserbündel einen ausgeprägten Einfluss auf den Schädigungsfortschritt. In Kapitel 5 wird dieser Fall betrachtet, wobei die effektive Reichweite der Wechselwirkungen zwischen den Grenzfällen einer vollständig lokalisierten und einer globalen Lastumlagerung variiert wird. Simulationsergebnisse zeigen, dass für jede effektive Reichweite der Wechselwirkungen ein kritischer Wert dieser unteren Grenze existiert, an dem das makroskopische Verhalten eines Faserbündels vollständig spröde wird. Dies äußert sich in einem rein elastischen Verhalten bis der globale Versagenspunkt erreicht wird, an welchem plötzliches Versagen schon nach dem Bruch einer kleinen Anzahl von Fasern eintritt. Als Erweiterung bisheriger Arbeiten im Falle globaler Wechselwirkungen [8] zeigen wir, dass sich bei Annäherung an den kritischen Grenzwert ein Übergang der Größenverteilung der mikroskopischen Schadereignisse einstellt, hin zu einem universalen Potenzgesetz mit einem Exponenten  $3/2$ , welcher unabhängig von der Reichweite der Wechselwirkungen ist. Dieser Übergang ist in Abb. 4 dargestellt.

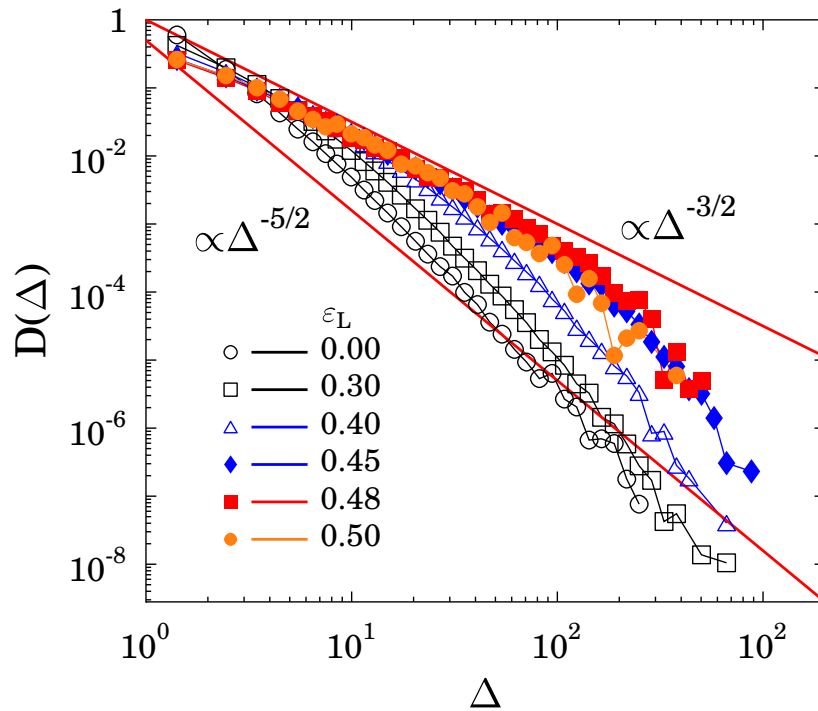


Abbildung 4: Verteilung  $D(\Delta)$  mikroskopischer Schadensereignisse der Größe  $\Delta$  in Abhängigkeit einer unteren Grenze  $\varepsilon_L$  für die Versagenswahrscheinlichkeiten, s. Kapitel 5. Für die Wahrscheinlichkeiten wird eine Gleichverteilung im Intervall  $[\varepsilon_L, 1]$  angenommen; die Lastumlagerung ist lokalisiert. Mit zunehmendem  $\varepsilon_L$  ist das Auftreten eines Potenzgesetzes der Form  $D(\Delta) \propto \Delta^{-3/2}$  sichtbar. Zu beachten ist, dass auch in Abwesenheit einer Begrenzung, d. h. für  $\varepsilon_L = 0$ , kein reines Potenzgesetz  $D(\Delta) \propto \Delta^{-5/2}$  wie im Falle globaler Lastumlagerung auftritt.

In ungeordneten Materialien mit hierarchischem Aufbau, wie z. B. Holz, können einige wenige makroskopische Defekte das Bruchverhalten entscheidend beeinflussen, insbesondere durch Arretierung und Umlenkung von Rissen. Die Anzahl dieser Fehlstellen kann hierbei von Probe zu Probe signifikanten Schwankungen unterliegen. Aus diesem Grund werden in Kapitel 6 zwei frei kombinierbare Erweiterungen der Modelle für die schrittweise Schädigung von Materialien, der sogenannten CDFBM (*engl.* continuous damage fibre bundle models) vorgestellt. In der ersten Modellvariante wird die maximale Anzahl von Schädigungsereignissen eines Elementes als Poisson-verteilte Zufallsvariable mit einem Mittelwert  $\kappa$  modelliert, um den Einfluss von Unordnung nicht nur auf den Schwellwert für das Versagen eines Elementes, sondern auch auf die Anzahl der makroskopisch wirksamen Defektstellen abzubilden. Als Folge dieser Änderung erscheint ein asymptotischer linearer Härtungsbereich im konstitutiven Verhalten des Faserbündels. Die Größenverteilung der mikroskopischen Schadensereignisse bleibt hiervon unberührt. Zusammenfassend ergibt die Einführung einer Zufallsvariablen für die maximale Anzahl der signifikanten Schadereignisse eine bessere Darstellung der Verteilung der makroskopischen Fehlstellen in Materialien mit ausgeprägt hierarchischem Aufbau, wie etwa geklebten Strukturelementen aus Holzlamellen, deren beobachtetes Bruchverhalten unter

Zugbelastung als Ausgangspunkt dieser Betrachtung dient.

In den genannten Materialien treten unter Belastung makroskopische Risse auf, welche sich unter zunehmender Last vergrößern. Diese Risse können aber auch an besonders festen Materialstellen arretiert werden, ehe unter weiter zunehmender Last globales Versagen eintritt. Um eine kohärente Beschreibung dieses Verhaltens zu erreichen, wird in einem zweiten Schritt eine Sortierung der zufällig verteilten Versagensschwellwerte, welche nach dem Versagen eines Elementes seinen nächsten Versagenspunkt bestimmen, vorgenommen. Im Rahmen des CDFBM werden den Fasern —welche Bestandteile eines Materials auf der untersten Hierarchieebene darstellen— wie im klassischen FBM Schwellwerte für das erstmalige Versagen bei einer bestimmten Dehnung  $\varepsilon$  (äquivalent einer Spannung  $\sigma$ ) zugeordnet. Anschließend wird für jeden Schädigungsschritt ein neuer Schwellwert gewählt, welcher entweder identisch mit dem ersten ist (eingefrorene Unordnung, *engl.* quenched disorder), oder anhand einer Zufallsverteilung bestimmt wird (thermische Unordnung, *engl.* annealed disorder). Das hier vorgestellte Modell stellt ein Gemenge der genannten Umordnungsformen dar, da die Zufallszahlen im voraus gezogen und in aufsteigende Reihenfolge gebracht werden. Mit dieser Vorschrift zeigt sich ein divergentes Verhalten der kritischen Spannung und der kritischen Dehnung mit ansteigender maximaler Anzahl der singulären Schadereignisse. Vor dem Erreichen der kritischen Spannung bzw. Dehnung ist ein langes nichtlineares Regime in der konstitutiven Kurve vorhanden. Für hohe numerische Werte der maximalen Anzahl der Schadereignisse treten Oszillationen der konstitutiven Kurve auf, die von ungewöhnlichen Kaskaden mikroskopischer Schadereignisse begleitet werden. Auch erscheint in diesem Falle wieder das Potenzgesetz für die Kaskaden mit einem Exponenten  $3/2$ , welches im Rahmen von Kapitel 5 behandelt wird. Eine konsistente Erklärung für dieses Phänomen wird angegeben, und das Auftreten der Oszillationen, welche exemplarisch in Abb. 5 dargestellt sind, wird im Parameterraum lokalisiert.

Zum Schluss, in Kapitel 7, erfolgt eine Zusammenstellung der in den vorangegangenen Kapiteln gewonnenen Ergebnisse und deren Einordnung in Hinblick auf den derzeitigen Stand der Forschung. Auch werden weitere mögliche theoretische und experimentelle Arbeiten im Zusammenhang mit diesen Ergebnissen vorgeschlagen, und eine Prognose über die zukünftige Entwicklung der Faserbündelmodelle abgegeben.

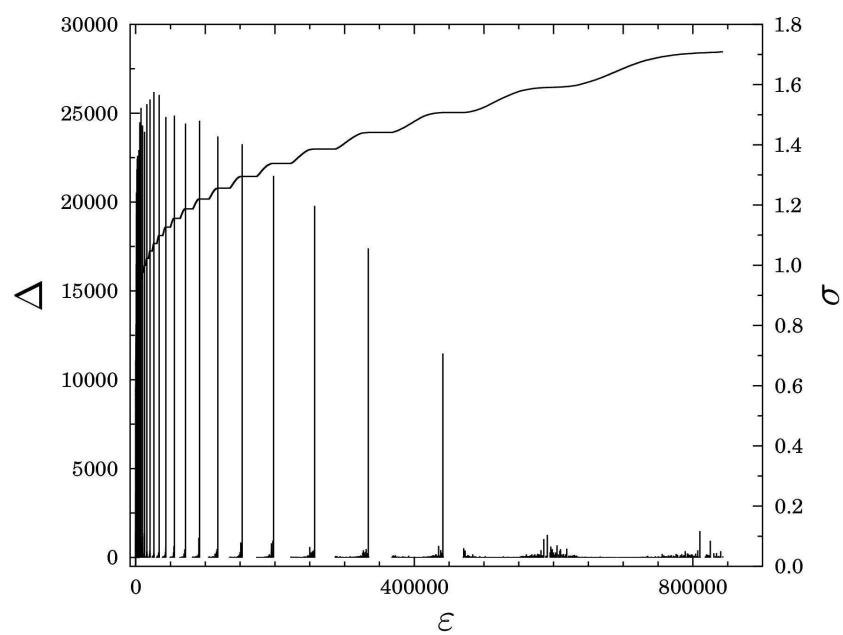


Abbildung 5: Im graduellen Schädigungsmodell mit sortierten Versagenswahrscheinlichkeiten erscheinende Oszillationen der konstitutiven Kurve  $\sigma(\varepsilon)$  (durchgezogene Linie) und synchron dazu auftretende mikroskopische Schadensereignisse der Größe  $\Delta$ , vgl. Kapitel 6.

# Chapter 1

## Introduction

### 1.1 Motivation

This thesis deals with the application of fibre bundle models, a class of statistical fracture models, on several current issues in the fracture of disordered materials, and fibrous composites in particular: the shear failure of glued interfaces, relevant to the failure of fibre-matrix interfaces in composite materials under external shear; the question of plasticity, which is related to this interfacial failure mode; the appearance of perfect brittleness when no weak fibres are present in the bundle; and finally the gradual degradation process of materials with an extremal distribution of defects. All these discussions are based on the classical fibre bundle model, which will be introduced in Chapter 2, or recent extensions thereof, and numerical simulations as well as analytical results will be presented.

Why do things break? Fracture of structures that surround us is a well known phenomenon in everyday life, and a fundamental manifestation of the second law of thermodynamics. The more important question therefore is how things break, and in which time. The systematic study of the mechanics of fracture, which was probably initiated by Leonardo da Vinci [9] and Galileo Galilei [10], has received renewed interest from the point of statistical physics in recent decades, especially for the case of disordered materials. Statistical models such as the fibre bundles are inherently suitable to capture the physical aspects of fracture in disordered materials, and applying the results obtained in this dissertation to models of material failure can aid a better understanding of the fracture mechanisms for a wide class of ubiquitous materials such as wood, concrete, fibre reinforced polymers or ceramics. Increased knowledge in this field can therefore enhance the lifetime, decrease the production and maintenance costs, and —most importantly— increase the safety of buildings, vehicles and structural components.

It may be advantageous to first highlight the importance of the materials considered, and to introduce some characteristic mechanical properties, i. e. their loading behaviour and fracture characteristics. Disordered materials are materials which display inhomogeneities, typically on the mesoscale of the sub-cm regime. An example for the microstructure of two fibrous materials, wood and fibre-reinforced concrete, is given in Fig. 1.1, where

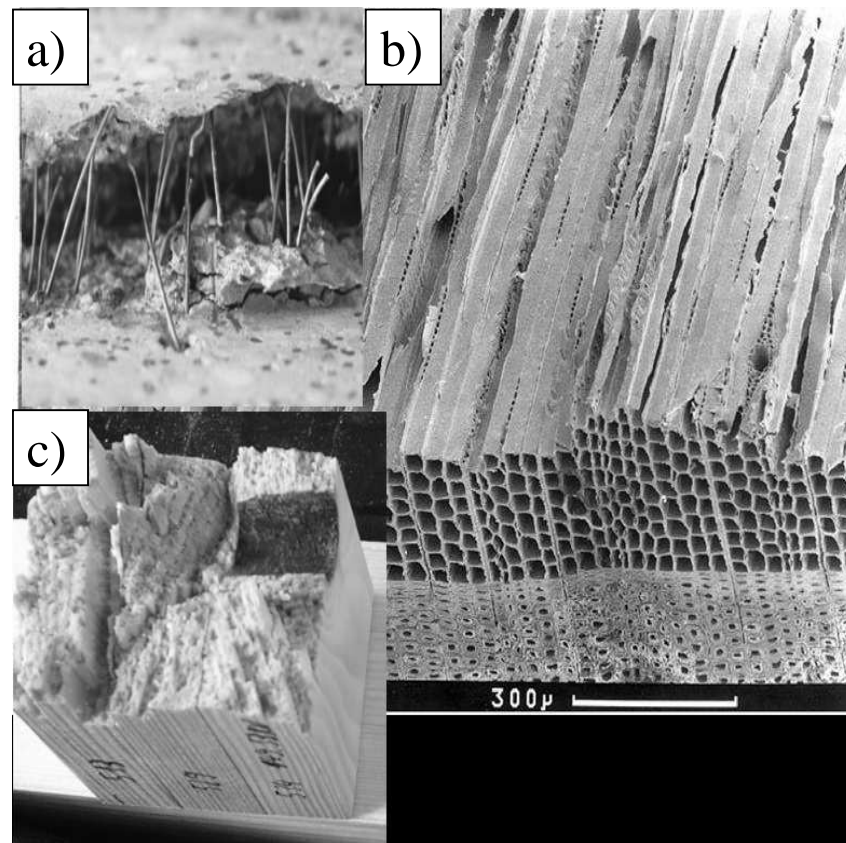


Figure 1.1: The structure of some fibrous composites. a) Steel reinforced concrete, from [2]. b) Microstructure of a softwood sample, from [3]. c) Fibrous mesostructure of another wood sample with a macroscopic knothole defect. Photograph taken in IWB, University of Stuttgart.

the fibrous structure and also the hierarchical properties of wood are clearly visible. Statistically seen, the presence of disorder can be modeled through random variables, which enter into the continuum mechanics and determine the rich microscopic behaviour [1; 7]. It turns out that the presence of disorder substantially reduces the fracture toughness and therefore effectively determines the mechanical stability of a material, as the order-of-magnitude difference between the ab-initio calculated strength of an ideal crystal and the experimentally measured strength of a real solid demonstrates [1; 11]. The effect of disorder is also visible in size effects, particularly when the strength of a material decreases with growing size, and strongly fluctuates between different samples. Fracture mechanics is a lasting problem in engineering and physics, and it is a generally accepted fact that the powerful computational and theoretical machinery employed in engineering tasks is not so well equipped when it comes to dealing with strong disorder, a shortcoming that statistical models such as the fibre bundle model and its derivatives may help to overcome. At the core of the problem is the question at which external load a given material fails, if there are precursors of failure (and how to measure them), and how the critical load scales with the size of materials.

An important subclass of disordered materials are the fibrous composites [12], or fibre reinforced composites (FRCs). In general, such a composite consists of a fibre reinforcement embedded in a matrix material, where the fibres are capable of sustaining a large amount of longitudinal stress. The material properties are determined not only by the respective constituent properties, but also by their mixing ratio, i. e. the volume fraction, the average fibre orientation and the deviation therefrom, and very prominently also by the fibre-matrix interface. Many of these factors can be adjusted in the manufacturing process, but a lack of control in the production gives rise to strong inter-sample fluctuations of the mechanical properties. Generally speaking, a hierarchy of length scales can be identified in composite materials, which is illustrated in Fig. 1.1. On the smallest scale the fibres and their bonds with the matrix can be identified. The fibres form sub-bundles and later on bundles, which are organized into a ply.

A technologically important example of fibrous composites are the fibre reinforced polymers, which have gained an unique standing in the aerospace, automotive and sporting goods industries due to their excellent strength at a low specific mass. The simplest layout of a fibre reinforced polymer is a unidirectional composite, where the fibres are all arranged in parallel. In practice, to account for various external loading conditions, the fibres may also be interwoven, and layers of uni- or multidirectional setups are frequently glued together into laminae. Under external loading, cracks first appear at the lowest level, i. e. in the matrix, at the fibre-matrix interface, and in the form of individual fibre fractures. The entire system and its elements experience a gradual reduction of stiffness as damage accumulates by nucleation of micro-cracks. The debonding of the fibre-matrix interface can propagate and lead to delamination, i. e. separation of entire layers. Finally, whole bundles of fibres will rupture, and the material fails catastrophically.

The usual starting point in the discussion of the failure characteristics of disordered materials is to consider the macroscopic, bulk averaged loading behaviour, which is represented by the stress-strain curve. This curve is the representative response obtained from loading a sample, typically by exerting tension on a long and —macroscopically speaking— homogeneous bar. Three fundamentally different types of behaviour are usually distinguished: a linear relation between stress and strain is called linear elastic behaviour, where a single parameter, the Young modulus, completely characterizes the loading behaviour, which is typically the case in the early stage of the loading of most materials, distant from the failure point. After a certain amount of loading, many materials then enter a nonlinear regime, a process that is called strain-hardening, and which is typically irreversible in the sense that after unloading, the sample will possess a reduced stiffness upon reloading. Other materials, however, display a behaviour that is labeled perfect plasticity after passing a material dependent yield point of loading, where the slope of the stress-strain curve vanishes, an effect that may be visualized as tearing apart a piece of chewing gum. All models presented in this work fit into one of these schemes, or compositions thereof. This classification is also useful in terms of fracture: a brittle material breaks before reaching the yield point, whereas a ductile material reaches the plastic regime first.

In contrast to other materials, e. g. glass, the assessment of damage in fibrous composites is not always a straightforward task, and visual inspection may not be able to discover

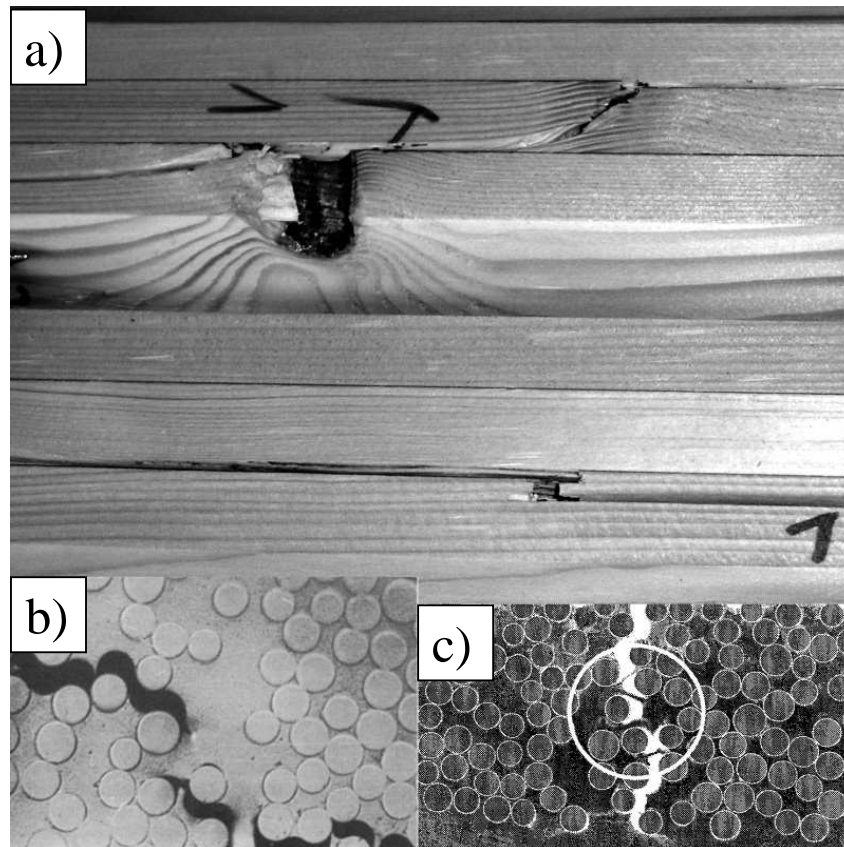


Figure 1.2: Examples for failure modes in fibrous composites. a) Cracks in timber lamellae, which follow the macroscopic structures. Photograph taken at a tension experiment at IWB, University of Stuttgart. b) Transversal cracks in a glass fibre reinforced polymer, from [13]. The cracks propagate along the fibre-matrix interfaces, and beginning plastic flow is visible. c) Microscopic plasticity in a glass fibre reinforced polymer that has failed displaying macroscopic brittleness under transversal loading, from [14].

even near catastrophically accumulated damage. For example, in layered composites delaminations may occur in deeper layers of a component and critically impair the structural stability, so elaborate visualization techniques such as ultrasound imaging are required in order to discover the damage [15].

It can therefore be assessed that in the experimental testing of fibrous composites not only a variety of material and production parameters appear, but that there are also a multitude of coexisting and mutually influencing failure modes, which explains the high volatility of results obtained even if different samples are taken from the same production batch. Consequently, these fluctuations together with the need for reliable monitoring and failure prediction capabilities have led to the development of an impressive array of technologically advanced non-destructive testing (NDT) methods [2]. However, safe and economic material design relies also on theoretical considerations, and finally on simulation. So far, the practical applicability of composite materials in weight sensitive environments is somehow limited by a certain lack of knowledge of the failure mechanisms. As a con-



sequence, to make sure that all safety requirements are met, composites employed under these conditions have to be more massive than might be necessary, which has a detrimental economic impact. Computer simulations, as a cost effective tool to clarify damage mechanisms, can contribute to overcome these shortcomings.

At this point, fibre bundle models (FBM) enter as a simple yet elegant method to capture the most significant characteristics shared by random materials in general and fibrous composites: they inherently feature disorder, anisotropy and dynamical load transfer [16], the dominant features in the breakdown of FRCs. Initially proposed as a model to capture the failure behaviour of a bundle of fibres in textile yarns, their behaviour can be summarized in a nutshell as follows: a thread of parallel single fibres is under an external uniaxial tension. They load in a linear elastic way until they reach their respective failure thresholds, which are randomly distributed. If a fibre fails, the load on it drops to zero, and has to be passed to the remaining fibres, which can result in cascades of further breaking events. Obviously, fibre bundle models are therefore well suited to describe uniaxial composites under tension, and have been applied successfully for this loading condition, since under tension the load on a composite is sustained almost exclusively by the fibres. Is it worth mentioning here that fibre bundle models possess no explicit time dependency—although such extensions have been developed; rather, there is an implicit dependence through the progress of external loading.

However, composite materials are not always loaded under pure tension, although this is attempted in order to utilize the fibres' high tensile strength; more importantly, in a real material there exist no pure loading states, but the different internal loading states are always present to some extent. One of the modes that has not been modeled extensively in the past is the shear state. Under shear loading, composite materials have been shown to develop a variety of coexisting failure phenomena. It has been found that under in-plane shear stress not only matrix shear failure, but also fibre-matrix debonding plays a crucial role [12; 17], some studies finding that the debonding of the fibre-matrix interface actually is the limiting factor in shear strength [12; 18; 13]. It is therefore of high importance to improve the available models for this case, and also for the more general case of sheared states of glued interfaces, i.e. elastic or elasto-plastic connections between two rigid semispaces, where one can assume that the glued connection possesses disordered properties.

In fibrous composites the macroscopic loading behaviour under tension typically displays a nonlinear regime prior to fracture, although this may be rather short; under shear loading of glued interfaces, one may expect however a high degree of plasticity, which can actually develop the outlook of perfect plasticity depending on the composition of the glue.

Monitoring stressed systems and predicting imminent failure is an important aspect in the study of composite materials; recent events have shown that even state-of-the-art building structures, which had been under constant supervision, can catastrophically collapse in the presence of merely a minor external stimulus. One particularly tragic event led to the disintegration of the wooden roof skeleton spanning an ice-skating rink in southern Bavaria in 2006 [19], which caused the death of 15 persons. A subsequent investigation suggested the main cause to be the chemical decomposition of the glue between the

wooden components, a decade long process preceding the sudden collapse, which was finally triggered by the unusually heavy snow load of this season.

Along with similar building collapses in the winter of 2005/2006, live monitoring techniques have received growing attention and recent innovations in terms of wireless techniques render the equipment of precarious structures such as buildings and bridges with sensors for strain, temperature or noise possible [20]. Of particular importance can be the detection of noise signatures indicating the imminent collapse of a material system, or some of its components. As a matter of fact, acoustic emission (AE) techniques have been employed in materials testing in the past, and most fibrous composite materials exhibit a signature power law for the distribution of avalanche sizes. Detecting deviations from this power law could be highly beneficial, and the existence of such deviations in the context of a specific FBM will be examined in Chapter 5 of this thesis.

Another important aspect that links composite materials to an advanced class of FBMs, the continuous damage fibre bundle models (CDFBM) [21], is the inclusion of hierarchical failure levels. Experiments have revealed that long fibre composites loaded parallel to the fibre orientation experience a gradual degradation process such that the macroscopic constitutive curve  $\sigma(\varepsilon)$  of the composite develops a plastic plateau and the global failure is preceded by a strain hardening regime.

This effect mirrors the presence of a hierarchical organization in the material, where the failure mechanisms relevant at the lower length scales (at the scale of fibres) gradually activate the breaking of higher order substructures (sub-bundles, bundles, and plies) of the system. With fibres embedded in a matrix material, the breaking of a fibre causes debonding of the fibre-matrix interface in the vicinity of the crack [22]. Due to the frictional contact at the interface, the load of failed fibres builds up again over a certain stress recovery length and consequently the broken fibre can still contribute to the overall load bearing capacity of the system. On a more abstract level, the CDFBMs —an extension of which will be presented in this thesis— are not restricted to the length scales of fibres, fibre bundles etc., but can be applied to any hierarchical system where a failure event triggers the activation of internal degrees of freedom.

As a widely used tool in computational material research, one can observe that fibre bundle models address two major challenges: on the one hand, they serve as a starting point to develop more realistic models of material failure, which then comprise a detailed representation of the microstructure of a material, the local stress fields, and their complex transmission. Since efficient techniques have been developed to study large scale fibre systems both through analytical calculations and simulations, FBMs and models based on them allow to investigate the influence of microscopic material parameters on the macroscopic response of disordered systems, and on fibre reinforced composites in particular. On the other hand, the study of damage and fracture in disordered systems has evolved into a fascinating branch of statistical physics, where researchers have accomplished to find a link between breakdown phenomena and phase transitions, as well as critical phenomena in general. Pursuing this analogy, there are now ongoing research efforts to embed fracture phenomena into the framework of statistical physics.

In summary, FBMs are an established method that have aided the understanding of material breakdown and failure, they are deeply rooted in the contemporary understanding of disordered systems, and they are certainly suitable to accomplish the tasks laid out in the beginning of this section: first, to describe the shear failure of bonded interfaces between solid structures, which requires a reformulation in terms of a sheared state as opposed to a tensional one. Secondly, to find a simple representation of the damage law that describes the limiting cases of elasticity and plasticity, and a parameterization for all cases in between. Furthermore, if a critical failure threshold distribution with finite-range interactions is considered, there is a need to quantify the distribution of failure event sizes, which can be measured by recording acoustic emissions from a material. And finally, for materials that fail under continuous restructuring and hardening, certain constraints on the failure threshold distribution and the maximum number of failures of a fibre (or another elementary constituent) in a modified continuous damage FBM capture some aspects observed in the fracture process.

## 1.2 State of Research

Historically, the first appearance of the fibre bundle model can be traced back to the year 1927, when Peires introduced this approach in order to understand the strength of cotton yarns [4]. The first consistent stochastic formulation of the model, together with a comprehensive study of bundles of threads —assuming equal load sharing after subsequent failure— was presented by Daniels [5]. Early attempts to capture fatigue and creep effects led Coleman to propose a time dependent formulation of the model [23], where the strength of loaded fibres was proposed to diminish with time.

These first developments have been ensued by intense research in both the engineering [22] and physics [1; 24] communities, so that nowadays fibre bundle models are considered one of the most important theoretical approaches to the damage and fracture of disordered materials. A recent comprehensive review of failure in disordered materials prominently features fibre bundle models [7].

As mentioned previously, FBMs are a sound choice in modeling fibrous composites under loading parallel to the fibre direction, where most of the load is carried by the fibres, and the matrix material and properties of the fibre-matrix interface mainly determine the interaction (load transfer) among fibres [25; 26; 27; 28]. Still, some adaptations are necessary to make the model more realistic. The first step in doing so is to find a means to interpolate between the limiting cases of global and local load sharing, which obviously constitute extremal abstractions of the finite range interaction present in a real material. In 2002, such a model was proposed by Hidalgo et al. [29], where the load shared by the unbroken fibres decays as a power law with the distance from a broken fibre. This model was subsequently applied to explain the size dependence of softwood samples under tension [3].

After fibre breakings, the material yields due to fibre-matrix debonding in the vicinity of the crack [22], a gradual degradation process which can be arrested due to frictional con-

tacts at the interface. Macroscopically, this leads to the appearance of a strain hardening regime prior to failure. The gradual degradation is a trademark sign of a hierarchical organization of the material, where failure mechanisms relevant at the lower length scales, i.e. the dimension of the fibres, gradually activate the breaking of higher order substructures (sub-bundles, bundles, and plies) of the system. A continuous damage model has been proposed which mirrors this effect [21], and it has been investigated in terms of macroscopic behaviour and avalanche characteristics [30]. Furthermore, it has been employed to explain the restructuring of force chains in granular materials under compression [31].

Another branch of FBM developments aims at modeling the viscous behaviour of fibrous reinforced composites (FRCs), which under high stresses deform gradually, a time dependent process which can finally result in creep rupture. A viscoelastic model has been suggested [32], and investigated in terms of the usual macro- and microscopic characteristics, and the universality of the failure process [33; 34]. The same model and some variants have been proven to give a good description of creep tests on FRC samples [35; 36].

In terms of materials, fibre bundle models have also been applied to model the failure behaviour of fibre reinforced concrete [37; 38]) and, very recently, asphalt [39; 40], where the reversal of microscopic crack opening must be considered.

Most of the theoretical studies on the failure of interfaces, where disordered properties assume a crucial role, rely on discrete models [1; 41] which are able to capture heterogeneities and can account for the complicated interaction of nucleated cracks. In studies of the progressive failure of glued interfaces under a uniform load perpendicular to the interface, several aspects of the failure process have been revealed such as the macroscopic constitutive behavior, the distribution of avalanches of simultaneously failing constituents and the structure of failed glue regions [42]. Considering a hierarchical scheme for the load redistribution following fibre failure, a cascading mechanism was proposed for the softening interface in Ref. [43; 44]. The roughness of the crack front propagating between two rigid plates due to an opening load was studied in the framework of the fuse model. The microcrack nucleation ahead the main crack and the structure of the damaged zone were analyzed in detail [45]. The shear failure of an interface between two rigid blocks has very recently been investigated by discretizing the interface in terms of springs. It was shown that shear failure of the interface occurs as a first order phase transition [46].

The original idea behind the invention of FBMs had been to describe material degradation and failure. However, it turned out that—due to their simplicity and their inherent features—they have also earned appreciation as a general model for the breakdown of a broad class of disordered systems, in which many interacting elements are loaded externally. Some examples that have been mentioned are magnets driven by an applied field [47; 48] and scale-free networks [49; 50]. Fibre bundle models also capture important aspects of geological phenomena [51], and it has been shown that a generalization of the fibre bundle model with long-range interactions is equivalent to a mean field formulation of the Burridge-Knopoff model frequently used in the investigation of earthquakes [52].

Thus, several novel aspects of breakdown phenomena have been revealed by the study of FBMs in recent years. The introduction of thermal noise leads to the reduction of

the strength of materials, and in the presence of thermally activated cracking sub-critical crack growth and a finite lifetime of materials are observed [53; 54]. The effect of healing of microscopic cracks has also been addressed by thermodynamical fibre bundle models [55].

A crossover in the avalanche size distribution  $D(\Delta)$  from the power law of exponent  $5/2$  to another power law regime with a lower exponent  $3/2$  has been observed, when the avalanches of fibre failures are solely recorded in the vicinity of the point of macroscopic failure, i.e. the strength distribution of the remaining intact fibres is close to critical [56; 57]. The connectivity properties of the bundle turned out to play an important role in breakdown processes, i.e. considering locally interacting fibres of a bundle on the nodes of a Barabasi-Albert network (instead of placing them on lattice sites) substantially alters the failure process [50]; these models are closely related to the statistical properties of social interactions [47]. Similarly, a random fuse model—a close relative of the FBM—on a network may be applicable to predict the failure of electric grids [58], and has been applied for biological materials [59; 60]

Finally, FBMs also played a crucial role in clarifying the fundamental relation between the breakdown of disordered materials, critical phenomena [48; 61; 62; 63; 64; 65], and self-organized criticality [66]. Under GLS, the microscopic quantities—such as the distribution of bursts of fibre breakings—when approaching the point of macroscopic failure under a quasi-statically increasing load were found to exhibit a scaling behaviour which is typical of continuous phase transitions [67; 6; 68; 65; 63; 69; 70; 71]. It has been suggested that the macroscopic failure of GLS bundles is analogous to first order phase transitions close to a spinodal [72; 48; 62; 21], since macroscopic quantities like the Young modulus of the bundle display a finite discontinuity at the same time. An interesting mapping of the fracture process of fibre bundles to Ising-like models, widely studied in statistical physics, has been suggested [73; 74; 69], which provides further hints on how to embed fracture phenomena into the general framework of statistical physics. An important aspect of this attempt is the possibility to obtain analytical solutions under GLS conditions; this also helped to explain the power law behaviour of avalanche statistics [68; 75; 6]. Although deviations from this power law should exist for small avalanches, their role is limited even if considering mixed threshold distributions [76].

### 1.3 Overview of the Research Conducted

Technical applications often require solid blocks that are connected by welding or gluing of the interfaces, and the structures need to sustain various types of external loads. If these solid interfaces are subject to shear, the interface elements experience not only longitudinal deformation (compression and elongation), but also bending deformation. This kind of loading of joined blocks is a model picture also for interfacial failure which occurs in fibre reinforced composites, where debonding of the fibre-matrix interface can even be the dominating damage mechanism when the composite is sheared. The complex deformation that appear in this context cannot be captured by discretizing the interface in terms of fibres, as they can only support longitudinal deformation in the classical FBM.

As a first step to model shear failure, we propose in Chapter 3 a novel beam model, that perpetuates the classical fibre bundle models and the extensions developed for them to a pure shear state, i.e. we change the loading direction by 90 degrees and model a novel situation: two rigid plates are coupled by elastic beams, which are subject to both stretching and bending under shear load. The beams fail if the two deformation modes exceed randomly distributed breaking thresholds. The two breaking modes can be independent or combined in the form of a von Mises-type breaking criterion. Under a global load sharing condition following the beam breaking, the macroscopic constitutive behaviour of the system can be obtained, and the microscopic process of the progressive interface failure has to be explored. An efficient simulation technique is mandatory in order to study large systems. Also, the limiting case of very localized interaction of surface elements has to be taken into account, which again requires computer simulations. Following this approach, the “beam model” of interface failure can then be mapped onto the classical fibre bundle model, preserving the theoretical apparatus that has been made available for the latter and allowing the use of modifications and extensions that have been developed for the FBM.

Secondly, to account for macroscopic plasticity, specifically in the context of glued interfaces, a modification to the damage law of fibre bundle models is presented in Chapter 4, assuming that failed fibres still carry a fraction  $0 \leq \alpha \leq 1$  of the load they sustained before failure. This introduces an additional parameter  $\alpha$ , whose value interpolates between the limiting cases of perfectly brittle failure ( $\alpha = 0$ ) and perfectly plastic behaviour ( $\alpha = 1$ ) of fibres. After having examined the macroscopic properties and obtaining an analytical formulation of the constitutive curve, the focus will be on investigating the usual microscopic characteristics of the system. Since under localized load sharing a nonzero value of  $\alpha$  softens the stress concentrations around broken fibres, the morphology, size distribution and evolution of clusters of broken fibres is of fundamental importance to understand the progressive damage of the model system. The competition between failure due to localization and the quenched disorder imposed by the failure threshold distribution can be tuned by varying  $\alpha$ , which has a substantial effect also on the avalanche size distribution and shows interesting links to the problem of random percolation. It should be noted that, since the mapping of the aforementioned beam model on the classical FBM will be derived, the application of this plastic model to the problem of glued interfaces under shear is straightforward.

A third aspect that will be investigated in Chapter 5 focuses on a recently discovered phenomenon, the change in the power law for the avalanche size distribution under certain choices of the failure threshold distribution. Specifically, it was shown in [56] for GLS loading conditions that the existence of a lower cutoff of this distribution results in a change of the exponent from  $5/2$  to  $3/2$ , which is tantamount to a delayed recording of the avalanches, starting only shortly prior to catastrophic failure. This discovery can have a strong impact in the field of acoustic monitoring as such a drastic change in the size distribution of microscopic fracture events can be measured by means of acoustic emission technologies — the possible benefits of which have been stressed previously. We will present a detailed numerical study of this situation under localized load sharing, employing the variable range model to interpolate between GLS and LLS and detect the change of exponent for all effective ranges of interaction; in addition, a discussion of this effect with respect to ductile vs. brittle fracture will be provided.

Finally, we will suggest two possible modifications to the continuous damage fibre bundle models in Chapter 6, which can account for gradual failure of a hierarchical, disordered system. The model that will be proposed overcomes the restriction of a fixed value for the maximum number of failures that a constituent element can sustain. This has been motivated by the existence of a multitude of coexisting damage mechanisms with different activation energies and failure mechanisms, especially in experiments on timber lamellae under tension. A second modification that we introduce to the CDFBM allows to model the arrest of cracks by introducing a sorting of the particular failure thresholds for each breaking event. These two extensions will be studied extensively and the differences in comparison to the CDFBM will be highlighted.

In Chapter 7 a discussion of the research efforts presented in this thesis will be given, and a comparison to the state of research will be drawn. This is followed by suggestions on further research and a brief outlook.





## Chapter 2

# The Classical Fibre Bundle Model

In this section we will outline the main properties of the classical fibre bundle model in order to facilitate the comprehension of the modified FBMs presented in the subsequent chapters.

To generate a computationally feasible fibre bundle model, a couple of simplifying assumptions have to be made [5; 22; 69; 77; 61; 6]:

The disordered model is discretized as a two-dimensional regular lattice, where the lattice sites represent parallel fibres, see Fig 2.1. Although triangular lattices or even networks of fibres have also been studied, we will restrict ourselves to the most commonly studied rectangular lattice type, with side length  $L$ , and a number of fibres  $N = L^2$ . The fibres are loaded under uniaxial tension parallel to the fibres' direction.

The constituent fibres behave perfectly brittle under an incremental external load, which means they load linearly elastic with a Young modulus  $E$  until they break at their respective failure load  $\sigma_{th}^i$ ,  $i = 1, \dots, N$ , which is illustrated in Fig. 2.1. The Young modulus  $E$  is identical for all fibres. The failure process of a single fibre is instantaneous and irreversible, so the load on a broken fibre vanishes (see Fig. 2.2). Broken fibres in the classical FBM cannot be restored, i.e. there is no healing without modifying the failure law.

Of crucial importance in the construction of the fibre bundle model is the range of load redistribution after fibre failure, which is prescribed in the form of a load sharing rule. Two extreme cases for the form and range of interaction have evolved as standards, and they constitute two sub-classes of fibre bundle models with substantially different micro- and macro-behaviour. The first form of global load sharing (GLS), sometimes termed equal load sharing (ELS), prescribes that the load of a failed fibre is distributed on all intact fibres in the array irrespective of their distance from the failed fibre, which as a mean field approach renders the topology of the model irrelevant. It reflects the experimental situation of loading a set of parallel fibres between two rigid plates, and usually it serves as a starting point for investigating more complex variations of this type, since GLS models usually can be treated analytically [6; 68; 56; 69; 77].

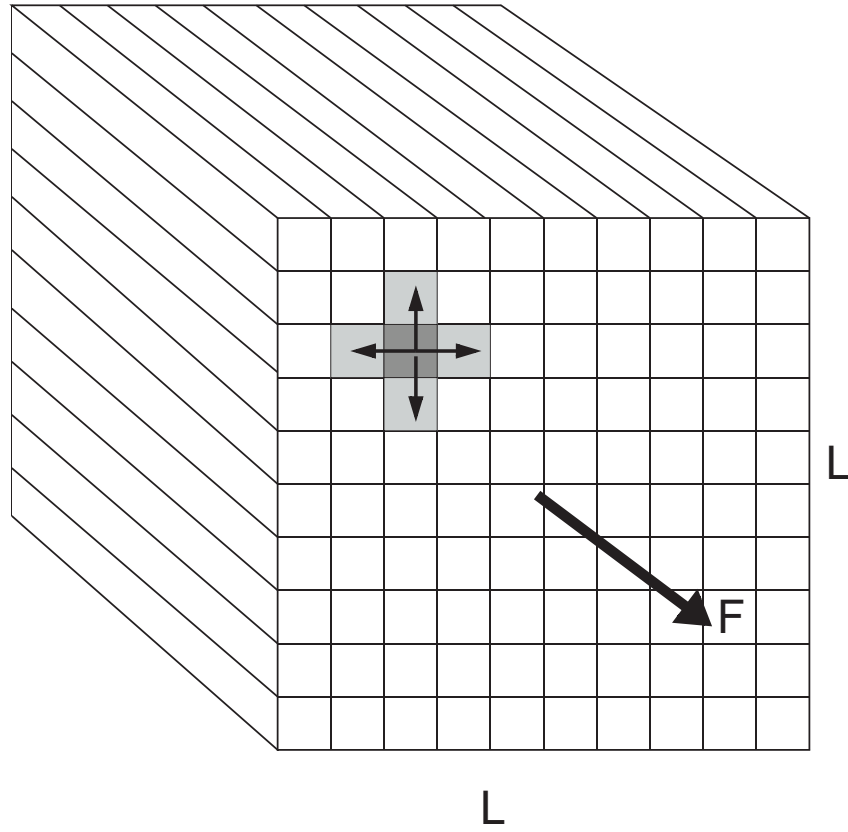


Figure 2.1: Schematic drawing of the classical fibre bundle model setup. The fibres are located on a square lattice of size  $L \times L$ . Loading with a force  $\vec{F}$  is parallel to the fibre direction. Once a fibre fails, its load is either redistributed on the nearest intact neighbors (LLS, see arrows) or the entire set of intact fibres (global load sharing).

For the contrary case of local load sharing (LLS), the load of a failed fibre is shared equally by the neighborhood of intact fibres, usually only the next neighbors on the lattice are taken into account, as depicted in Fig. 2.1. This load redistribution evokes a high level of stress concentration around failed regions. The accompanying correlations set prohibitive limitations towards an analytical treatment of this problem [78; 22; 79], so typically large scale simulations have to be employed [75; 80; 81; 29]. The experimental image corresponding to this situation is the stretching of a bundle of fibres between plates of finite compliance [67; 42; 43].

The amount of disorder in a material is modeled through assigning randomly distributed failure thresholds  $\sigma_{th}^i$  to the fibres, where the probability density is  $p(\sigma_{th})$  and the distribution function is  $P(\sigma_{th}) = \int_{\sigma_{th}^{min}}^{\sigma_{th}^{max}} p(x)dx$ . It is therefore of crucial importance in modeling heterogeneity and deeply influences the overall response of the model: in fact, it is the only component of the classical FBM that represents material dependent features. Typically, two types of random distributions are employed. The first one is a uniform distribution between 0 and 1 with the density and distribution functions

$$p(\sigma_{th}) = 1, \quad P(\sigma_{th}) = \sigma_{th}, \quad (2.1)$$

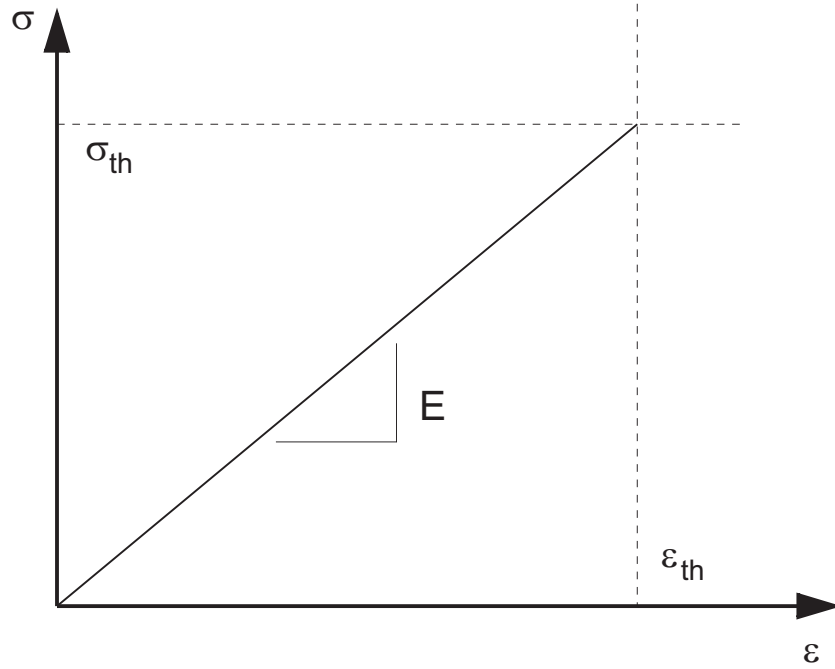


Figure 2.2: Linear elastic loading characteristic of a single fibre, which breaks when its failure load  $\sigma_{th}$  is reached.

which typically serves as a starting point for analytical considerations. A distribution with a much better physical foundation [1; 24] is the Weibull distribution

$$P(\sigma_{th}) = 1 - \exp \left[ - \left( \frac{\sigma_{th}}{\lambda} \right)^m \right], \quad (2.2)$$

where  $m$  and  $\lambda$  denote the Weibull index and scale parameter, respectively. It should be noted that the amount of disorder can easily be controlled by tuning the Weibull index  $m$ .

Some general features of FBMs should be mentioned in the following, as they are shared by most variants and underscore the importance of the models in understanding the breakdown of heterogeneous materials.

Loading of a bundle is usually performed quasi-statically, and can be controlled in two substantially different ways: first, if the deformation  $\varepsilon$  of the bundle is controlled externally, the load on single fibres  $\sigma_i$  at each stage of loading is determined by the externally imposed deformation  $\varepsilon$   $\sigma_i = E\varepsilon$ ; consequently, no load sharing occurs and the fibres break subsequently in the order of the increasing breaking thresholds. Hence, at a given deformation  $\varepsilon$  only those fibres with breaking thresholds  $\sigma_{th}^i < E\varepsilon$  have failed, with the intact fibres sustaining an equal load  $E\varepsilon$ . It follows from this that the macroscopic constitutive behavior of the FBM is

$$\sigma(\varepsilon) = E\varepsilon [1 - P(E\varepsilon)], \quad (2.3)$$

where  $[1 - P(E\varepsilon)]$  is the fraction of intact fibres at the deformation  $\varepsilon$  [47; 77]. For the case of Weibull distributed strength values with  $m = 2$  and  $\lambda = 1$  the constitutive curve is shown in Fig. 2.2 as a representative example.

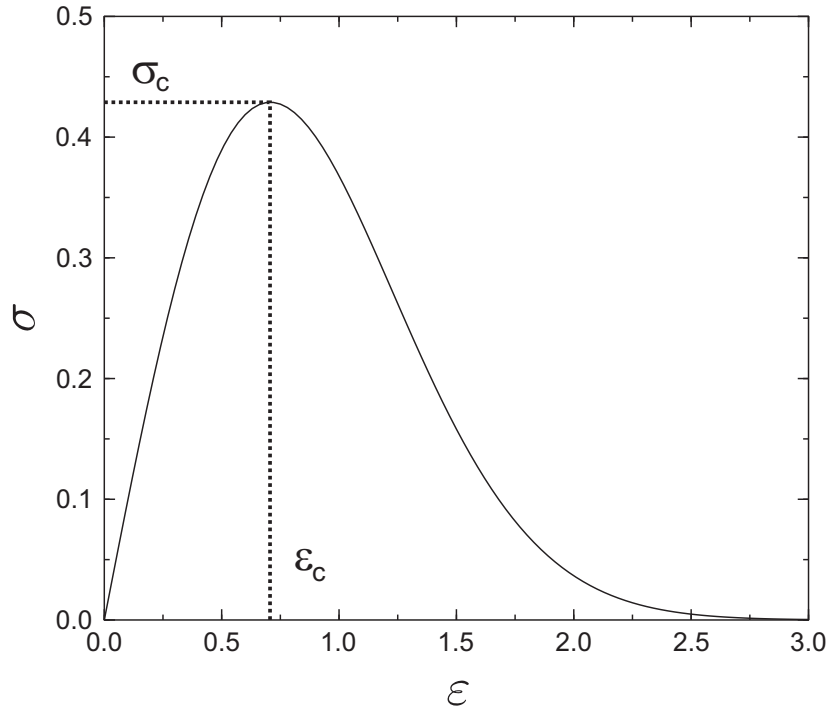


Figure 2.3: Macroscopic constitutive behavior of a fibre bundle with global load sharing Eq. 2.3 using Weibull distributed strength values  $\sigma_{th}$  ( $m = 2$  and  $\lambda = 1$ ).

Secondly, there is the stress controlled case, where the loading is controlled externally. Here the damage process is more complex due to the load redistribution following a fibre breaking. The load received in this way by the remaining fibres —both in the cases of GLS or LLS— can cause secondary fibre breakings. It turns out that consecutive load redistributions after fibre failures can evoke entire avalanche of breakings; these avalanches then can either stop after a certain number of fibre breakings and the integrity of the bundle is preserved, or continue as a catastrophic event resulting in the macroscopic failure of the entire system as all remaining intact fibres are destroyed [6; 68; 56; 30]. This catastrophic event also determines the ending point of the constitutive curve at its maximum, and the subsequent decreasing part of the curve cannot be attained under stress controlled loading.

The existence of a quadratic maximum whose position and value define the critical strain  $\epsilon_c$  and stress  $\sigma_c$  of a bundle has been proven analytically for a broad class of disorder distributions  $P$  under GLS conditions [47; 77]. The global strength  $\sigma_c(N)$  rapidly converges to the finite non-zero strength of the infinite bundle with increasing system size  $N$  [5; 22; 77].

The macroscopic response of the bundle is more brittle under localized load sharing with the constitutive curve  $\sigma(\epsilon)$  of the LLS bundle equating the GLS counterpart, but macroscopic failure occurring at a lower critical stress  $\sigma_c^{LLS} < \sigma_c^{GLS}$ , and with only a weak non-linearity present before failure [29]. It has been revealed through computer simula-

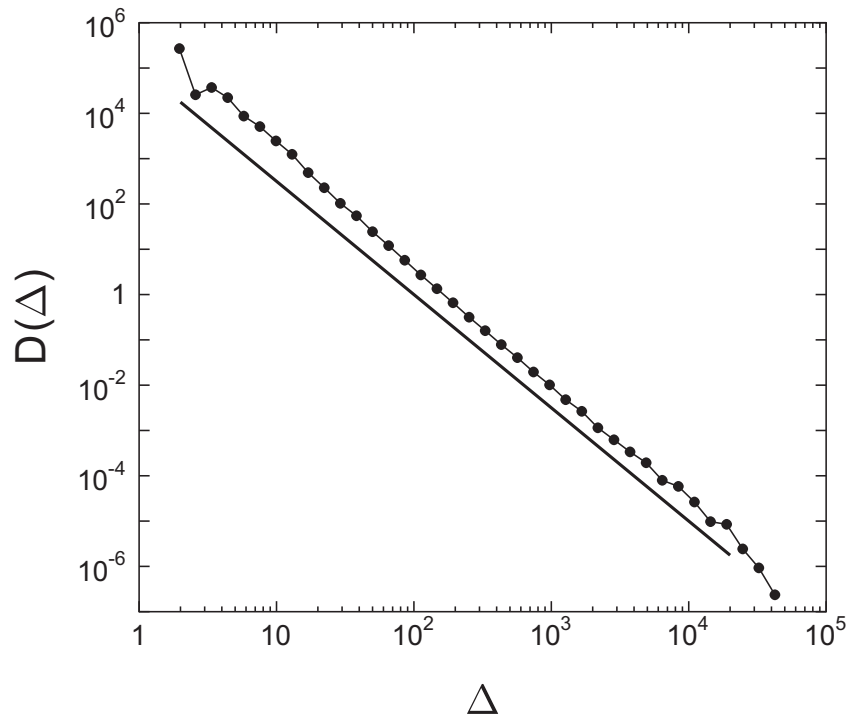


Figure 2.4: Distribution  $D$  of burst sizes  $\Delta$  obtained by computer simulations of a bundle of  $10^7$  fibres. A straight line of slope 2.5 is drawn to guide the eye.

tions that in the thermodynamic limit  $N \rightarrow \infty$  the strength of LLS bundles decreases to zero as  $1/(\ln N)$  [82].

Fibre bundle models exhibit interesting properties on the micro-level, depending on the range of load sharing. Under GLS the spatial distribution of breaking events is completely stochastic, no spatial correlations arise and randomly nucleated clusters of broken fibres appear analogous to percolation. Under stress controlled loading, the cascades of reloading events produce bursts of fibre breakings, and it has been proven analytically that the distribution  $D(\Delta)$  of burst sizes  $\Delta$  has a power law behavior

$$D(\Delta) \sim \Delta^{-\alpha}, \quad (2.4)$$

if recorded over the entire course of loading. The exponent  $\alpha = 5/2$  is universal and independent of the disorder distribution  $P$  [6; 68; 71]. Using simulation results for a large fibre bundle, this generic behavior is illustrated in Fig. 2.4.

A power law distribution has also been found for more complicated long range interactions, e.g. in the fuse model, which is another model system for studying material breakdown [83; 84]). For localized load sharing in the FBM, however, studies found a rapid decrease of  $D(\Delta)$  and a dependence on the specific form of disorder  $P$  [75].



# Chapter 3

## A Simple Beam Model for the Shear Failure of Interfaces

In this chapter we study the shear failure of the glued interface connecting two solid blocks in the framework of a novel type of model. In this model the interface is discretized in terms of elastic beams which can be elongated and bent when exposed to a shear load. The breaking of a beam is caused by two breaking modes, i. e. stretching and bending, characterized by randomly distributed threshold values. The two breaking modes can be either independent or combined in terms of a von Mises type breaking criterion [85]. Assuming long range interaction among the beams, the full analytic solution of the model for the macroscopic response of the interface, and for the microscopic process of failure is found. It will be shown that the presence of two breaking modes lowers the critical stress and strain of the material without changing the statistics of bursts of simultaneously failing elements with respect to the case of a single breaking mode. The coupling of breaking modes results in further reduction of the strength of the interface. We demonstrate that the macroscopic response of the interface can be tuned over a broad range by varying the relative importance of the two breaking modes. The limiting case of very localized interaction of beams is also considered. We determine the constitutive behavior and the distribution of avalanches of breaking beams for the case when beams interact solely with their nearest and next-nearest neighbors in a square lattice. An effective simulation technique is worked out which makes it possible to study large systems, and an account of the research has been published in [86].

### 3.1 Properties of the model

In the model the glued interface of two solid blocks is represented as an ensemble of parallel beams connecting the two surfaces. First, we derive an analytical description of a single beam of quadratic cross section clamped at both ends and sheared by an external force  $f$ , see Fig. 3.1(a). The shearing is exerted in such a way that the distance  $l$  between the two clamping planes is kept constant. Consequently, the beam experiences not only a

torque  $m$ , but also a normal force  $t$  due to the elongation  $\Delta l$ , which is characterized by the longitudinal strain  $\epsilon = \Delta l/l$ .



Figure 3.1: (a) Shearing of a single beam between two rigid plates. Since the distance  $l$  between the plates is kept constant, the beam experiences stretching and bending deformation, with longitudinal  $t$  and shear  $f$  forces. (b) Shearing of an array of beams, with the corresponding forces. In the case shown, one beam is broken.

We derive the form of the deflection curve of the beam, as well as the magnitude of the tension force. It is necessary to introduce some approximations, so the model can be incorporated into the simulation code in a sensible way. Following the procedure outlined e. g. in [87], we solve the differential equation for the beam deflection  $\zeta(z)$  under the influence of the lateral force  $f$  and a given stretching force  $t$ . We then solve self-consistently for  $t(f)$ , with  $t$  being the result of the longitudinal elongation.

The governing differential equation for the bending situation depicted in Fig. 3.1(a) can be cast in the form

$$\zeta'''(z) - \frac{t}{EI}\zeta'(z) = -\frac{f}{EI}, \quad (3.1)$$

with boundary conditions

$$\begin{aligned} \zeta(0) &= 0, \\ \zeta'(0) &= 0, \\ \zeta''(l/2) &= 0. \end{aligned} \quad (3.2)$$

Here,  $E$  denotes the modulus of elasticity, and  $I$  is the moment of inertia for bending of the beam. For a beam of rectangular cross-section, we have  $I = d^4/12$ , where  $d$  is the side length. Let us briefly motivate this ansatz by stating that the second derivative  $\zeta''(z)$  is proportional to the torque on the beam, so consequently it needs to vanish at the beam half-length  $l/2$ . Accordingly, the third derivative  $\zeta'''(z)$  is proportional to the shearing force exerted on the beam, hence, it constitutes a term of the balance equation, Eq. (3.1).



The first derivative term with  $\zeta'(z)$  denotes the projection of the tension force  $t$ . Due to the clamping, the deflection and its first derivative must vanish at the end  $z = 0$ . The formula for the bending moment  $m$  is

$$m = -EI\zeta''(z). \quad (3.3)$$

The solution  $\zeta(z)$  for vanishing  $t$  can be obtained as [88]

$$\zeta(z) = \frac{fz^2}{12EI} (3l - 2z), \quad (3.4)$$

from which we can calculate the elongation

$$\Delta l = \int_0^l dz \sqrt{1 + \zeta'^2(z)} - l \approx \frac{1}{2} \int_0^l \zeta'^2 dz. \quad (3.5)$$

It follows from the above equation

$$t = ES \frac{\Delta l}{l} = ES\epsilon, \quad (3.6)$$

where  $S = d^2$  is the beam cross-section area. The first order solution for  $t(f)$  reads as

$$t \approx \frac{l^4 S}{240EI^2} f^2. \quad (3.7)$$

From a computational point of view, a formulation of bending and stretching in terms of the longitudinal strain  $\epsilon$  is more suitable than using the lateral force  $f$ . For that, we only need to replace  $m(f)$  by  $m(\epsilon)$ , which yields

$$m(\epsilon) \approx \frac{fl}{2} = \sqrt{\frac{5}{12}} \frac{Ed^4}{l} \sqrt{\epsilon}, \quad (3.8)$$

with

$$\epsilon = \frac{t}{ES} = \frac{3l^4}{5E^2 d^8} f^2. \quad (3.9)$$

Using  $\epsilon$  as an independent variable enables us to make comparisons to the simple case of fibre bundle models [5; 77; 89; 69; 29; 30] where the elements can have solely stretching deformation. In the model we represent the interface as an ensemble of parallel beams connecting the surface of two rigid blocks (see Fig. 3.1(b)). The beams are assumed to have identical geometrical extensions (length  $l$  and side length  $d$ ) and linearly elastic behaviour characterized by the Young modulus  $E$ . In order to capture the failure of the interface in the model, the beams are assumed to break when their deformation exceeds a certain threshold value. As it has been shown above, under shear loading of the interface beams suffer stretching and bending deformation resulting in two modes of breaking, which can act independently or in combination. The strength of beams is characterized by the two threshold values of stretching  $\epsilon_1$  and bending  $\epsilon_2$  a beam can withstand. The breaking thresholds are assumed to be randomly distributed variables of the joint probability distribution (PDF)  $p(\epsilon_1, \epsilon_2)$ . The randomness of the breaking thresholds is supposed to represent the disorder of the interface material.

After breaking of a beam the excess load has to be redistributed over the remaining intact elements. Coupling to the rigid plates ensures that all the beams have the same deformation giving rise to global load sharing, i. e. the load is equally shared by all the elements, stress concentration in the vicinity of failed beams cannot occur. If one of the interfaces has a certain compliance, the load redistribution following breaking of beams becomes localized. This case has recently been studied for the external load imposed perpendicular to the interface [46].

In the present study we are mainly interested in the macroscopic response of the interface under shear loading and the process of progressive failure of interface elements. The global load sharing of beams enables us to obtain closed analytic results for the constitutive behaviour of the system for both independent and coupled breaking modes. We examine by computer simulations the statistics of simultaneously failing elements. The limiting case of the very localized interaction of interface elements is explored by computer simulations.

## 3.2 Constitutive behaviour

Assuming global load sharing for the redistribution of load after the failure of beams, the most important characteristic quantities of the interface can be obtained in closed analytic form.

Breaking of the beam is caused by two breaking modes, i. e. stretching and bending which can be either independent or coupled by an empirical breaking criterion. Assuming that the two breaking modes are independent, a beam breaks if either the longitudinal stress  $t$  or the bending moment  $m$  exceeds the corresponding breaking threshold. Since the longitudinal stress  $t$  and the bending moment  $m$  acting on a beam can easily be expressed as functions of the longitudinal deformation  $\epsilon$ , the breaking conditions can be formulated in a transparent way in terms of  $\epsilon$ . To describe the relative importance of the breaking modes, we assign to each beam two breaking thresholds  $\epsilon_1^i, \epsilon_2^i$ ,  $i = 1, \dots, N$ , where  $N$  denotes the number of beams. The threshold values  $\epsilon_1$  and  $\epsilon_2$  are randomly distributed according to a joint probability density function  $p(\epsilon_1, \epsilon_2)$  between lower and upper bounds  $\epsilon_1^{\min}, \epsilon_1^{\max}$  and  $\epsilon_2^{\min}, \epsilon_2^{\max}$ , respectively. The density function needs to obey the normalization condition

$$\int_{\epsilon_2^{\min}}^{\epsilon_2^{\max}} d\epsilon_2 \int_{\epsilon_1^{\min}}^{\epsilon_1^{\max}} d\epsilon_1 p(\epsilon_1, \epsilon_2) = 1. \quad (3.10)$$

### 3.2.1 OR breaking rule

First, we provide a general formulation of the failure of a bundle of beams. We allow for two independent breaking modes of a beam that are functions  $f$  and  $g$  of the longitudinal deformation  $\epsilon$ . This case will be called the *OR* breaking rule, since a single beam breaks

if either its stretching or bending deformation exceed the respective breaking threshold  $\epsilon_1$  or  $\epsilon_2$ , i.e. failure occurs if

$$\frac{f(\epsilon)}{\epsilon_1} \geq 1 \text{ or} \quad (3.11)$$

$$\frac{g(\epsilon)}{\epsilon_2} \geq 1, \quad (3.12)$$

where Eqs. (3.11,3.12) describe the stretching and bending breaking modes, respectively. The functions  $f(\epsilon)$  and  $g(\epsilon)$  are called failure functions, for which the only restriction is that they be monotonic functions of  $\epsilon$ . For our specific case of elastic beams the failure functions can be determined from Eqs. (3.6,3.8) as

$$f(\epsilon) = \epsilon, \quad g(\epsilon) = a\sqrt{\epsilon}, \quad (3.13)$$

where  $a$  is a constant and the value of the Young modulus  $E$  is set to 1.

In the plane of breaking thresholds each point  $(\epsilon_1, \epsilon_2)$  represents a beam. For each value of  $\epsilon$  those beams which survived the externally imposed deformation are situated in the area  $f(\epsilon) \leq \epsilon_1 \leq \epsilon_1^{\max}$  and  $g(\epsilon) \leq \epsilon_2 \leq \epsilon_2^{\max}$ , as it is illustrated in Fig. 3.2. Hence, the fraction of intact beams  $N_{\text{intact}}/N$  at a given value of  $\epsilon$  can be obtained by integrating the density function over the shaded area in Fig. 3.2

$$\frac{N_{\text{intact}}}{N} = \int_{g(\epsilon)}^{\epsilon_2^{\max}} d\epsilon_2 \int_{f(\epsilon)}^{\epsilon_1^{\max}} d\epsilon_1 p(\epsilon_1, \epsilon_2). \quad (3.14)$$

Due to the global load sharing, deformation and stress of the beams are the same every-

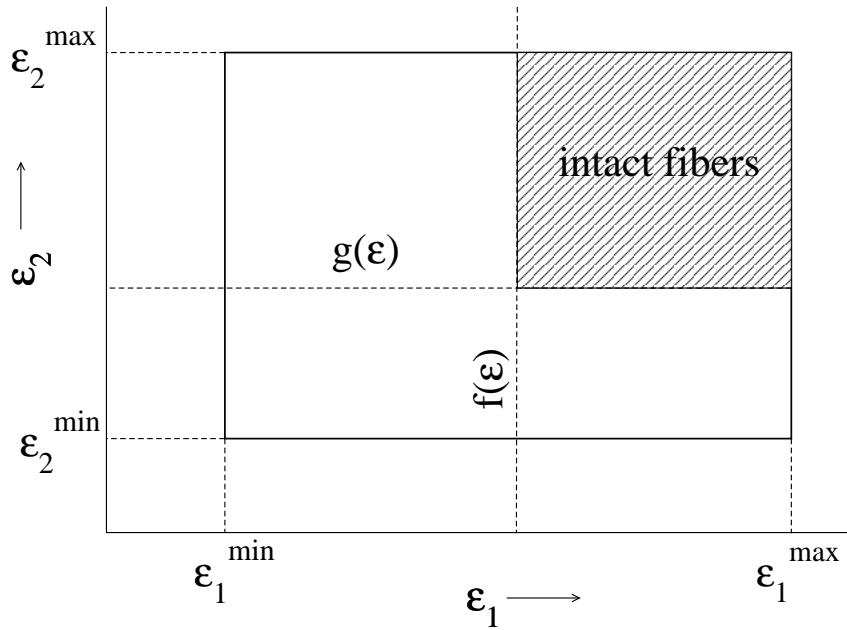


Figure 3.2: Plane of breaking thresholds  $(\epsilon_1, \epsilon_2)$ . The point of intersection of  $f(\epsilon)$  and  $g(\epsilon)$  determines the fraction of remaining beams.

where along the interface. Consequently, the macroscopic elastic behaviour of the system can be obtained by multiplying the load of a single beam,  $\sigma^{(1)} = \epsilon$  ( $E = 1$  is taken), by the fraction of intact elements Eq. (3.14)

$$\sigma = \epsilon \int_{g(\epsilon)}^{\epsilon_2^{\max}} d\epsilon_2 \int_{f(\epsilon)}^{\epsilon_1^{\max}} d\epsilon_1 p(\epsilon_1, \epsilon_2). \quad (3.15)$$

Assuming that the breaking thresholds, characterizing the relative importance of the two breaking modes, are independently distributed, the joint PDF can be factorized as

$$p(\epsilon_1, \epsilon_2) = p_1(\epsilon_1) \cdot p_2(\epsilon_2). \quad (3.16)$$

Introducing the cumulative distribution functions (CDFs) as

$$P_1(\epsilon_1) = \int_{\epsilon_1^{\min}}^{\epsilon_1} p_1(\epsilon'_1) d\epsilon'_1, \text{ and } P_2(\epsilon_2) = \int_{\epsilon_2^{\min}}^{\epsilon_2} p_2(\epsilon'_2) d\epsilon'_2, \quad (3.17)$$

we can rewrite Eq. (3.15) as

$$\begin{aligned} \sigma &= \epsilon \int_{g(\epsilon)}^{\epsilon_2^{\max}} d\epsilon_2 p_2(\epsilon_2) \int_{f(\epsilon)}^{\epsilon_1^{\max}} d\epsilon_1 p_1(\epsilon_1) \\ &= \epsilon [1 - P_2(g(\epsilon))] [1 - P_1(f(\epsilon))]. \end{aligned} \quad (3.18)$$

This is the general formula for the constitutive behaviour of a beam bundle with two breaking modes applying the *OR* criterion. In the constitutive equation  $1 - P_1(f(\epsilon))$  and  $1 - P_2(g(\epsilon))$  are the fraction of those beams whose threshold value for bending and stretching is larger than  $g(\epsilon)$  and  $f(\epsilon)$ , respectively. It follows from the structure of Eq. (3.18) that the existence of two breaking modes leads to a reduction of the strength of the material, both the critical stress and strain take smaller values compared to the case of a single breaking mode applied in simple fibre bundle models [5; 77; 6; 29; 30; 65; 70; 63].

Considering the special case of two uniform distributions for the breaking thresholds in the intervals  $[\epsilon_1^{\min}, \epsilon_1^{\max}]$  and  $[\epsilon_2^{\min}, \epsilon_2^{\max}]$ , respectively, we can derive the specific form of Eq. (3.18) by noting that

$$p(\epsilon_1) = \frac{1}{\epsilon_1^{\max} - \epsilon_1^{\min}}, \quad p(\epsilon_2) = \frac{1}{\epsilon_2^{\max} - \epsilon_2^{\min}} \quad (3.19)$$

After calculating the cumulative distributions, the final result follows as

$$\sigma = \epsilon \frac{[\epsilon_1^{\max} - f(\epsilon)][\epsilon_2^{\max} - g(\epsilon)]}{[\epsilon_1^{\max} - \epsilon_1^{\min}][\epsilon_2^{\max} - \epsilon_2^{\min}]}. \quad (3.20)$$

More specifically, if the distributions have equal boundaries  $[0, 1]$ , and substituting the failure functions  $f$  and  $g$  from Eq. (3.13), the constitutive equation takes the form

$$\sigma = \epsilon [1 - \epsilon] [1 - a\sqrt{\epsilon}]. \quad (3.21)$$

### 3.2.2 Von Mises type breaking rule

We now address the more complicated case that the two breaking modes are coupled by a von Mises type breaking criterion: a single beam breaks if its strain  $\epsilon$  fulfills the condition [85]

$$\left(\frac{f(\epsilon)}{\epsilon_1}\right)^2 + \frac{g(\epsilon)}{\epsilon_2} \geq 1. \quad (3.22)$$

This algebraic condition can be geometrically represented as it is illustrated in Fig. 3.3. In the plane of the failure thresholds  $\epsilon_1, \epsilon_2$ , the beams that survive a load  $\epsilon$  are bounded by the maximum values  $\epsilon_1^{\max}, \epsilon_2^{\max}$  and the hyperbola-like curve defined by Eq. (3.22). Calculating the intersection points  $a$  and  $b$  defined in Fig. 3.3, which are found to be

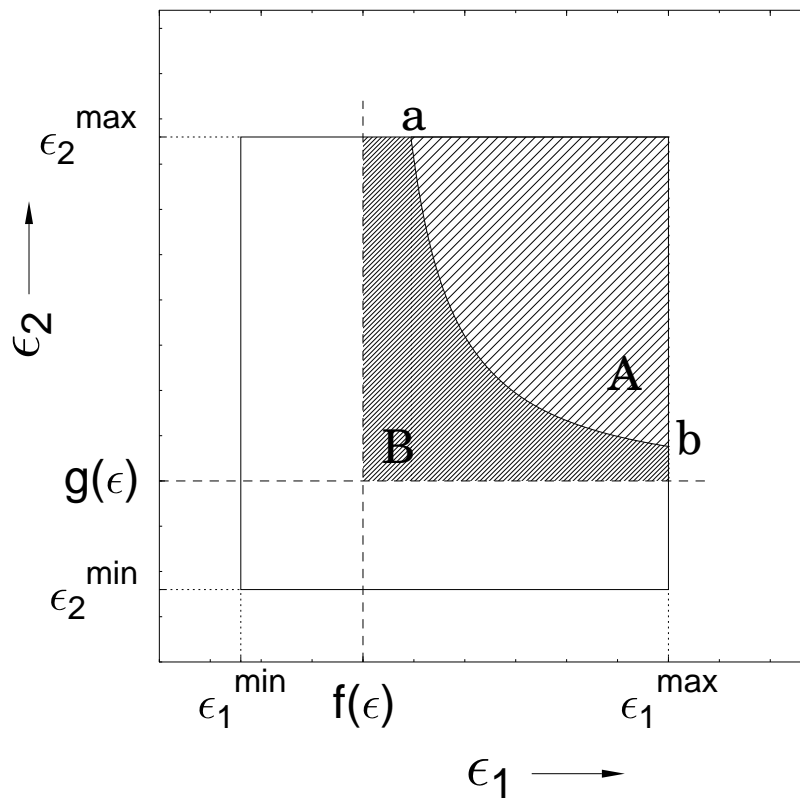


Figure 3.3: Intact beams in the plane of the failure thresholds  $\epsilon_1, \epsilon_2$  for a given strain  $\epsilon$ , if breaking is determined by the von Mises criterion. The shaded region labeled  $A$  denotes the intact beams; the shaded region  $B$  represents the additionally failing beams that would be intact in the case of the *OR*-criterion. The values  $a$  and  $b$  are defined as the intersections between the curve of the breaking condition Eq. (3.22) and the maximum values  $\epsilon_1^{\max}, \epsilon_2^{\max}$ , respectively.

$$\begin{aligned}
a &= f(\epsilon) \left( \frac{\epsilon_2^{\max}}{\epsilon_2^{\max} - g(\epsilon)} \right)^{1/2} \quad \text{and} \\
b &= \frac{g(\epsilon)(\epsilon_1^{\max})^2}{(\epsilon_1^{\max})^2 - f^2(\epsilon)}, \tag{3.23}
\end{aligned}$$

the fraction of surviving beams can be expressed as

$$\frac{N_{\text{intact}}}{N} = \int_a^{\epsilon_1^{\max}} d\epsilon_1 \int_{\tilde{\epsilon}_2(\epsilon_1, \epsilon)}^{\epsilon_2^{\max}} d\epsilon_2 p(\epsilon_1, \epsilon_2) \tag{3.24}$$

with the integration limit

$$\tilde{\epsilon}_2(\epsilon_1, \epsilon) = \frac{\epsilon_1^2 g(\epsilon)}{\epsilon_1^2 - f^2(\epsilon)}. \tag{3.25}$$

The constitutive behaviour in this case is therefore given by

$$\sigma = \epsilon \int_a^{\epsilon_1^{\max}} d\epsilon_1 \int_{\tilde{\epsilon}_2(\epsilon_1, \epsilon)}^{\epsilon_2^{\max}} d\epsilon_2 p(\epsilon_1, \epsilon_2). \tag{3.26}$$

We would like to emphasize that assuming independence of the breaking thresholds the joint distribution factorizes  $p(\epsilon_1, \epsilon_2) = p_1(\epsilon_1) \cdot p_2(\epsilon_2)$ , but the integrals in Eq. (3.26) over the two variables cannot be performed independently. Still, the integral in Eq. (3.26) can be evaluated analytically for a broad class of disorder distributions. As an example, we again consider two homogeneous distributions Eq. (3.19) over the interval  $[0, 1]$  along with the failure functions Eq. (3.13). Setting the Young modulus and the parameter  $E = 1 = a$ , the integrals yield

$$\begin{aligned}
\sigma &= \epsilon \cdot \frac{1}{2} \left[ \left( 2 - 2\sqrt{\epsilon} + \epsilon^{\frac{3}{2}} \log \frac{1+\epsilon}{1-\epsilon} \right) \right. \\
&\quad \left. - \epsilon^{3/2} \left( 2\sqrt{\frac{1-\sqrt{\epsilon}}{\epsilon}} + \log \frac{1+\sqrt{1-\sqrt{\epsilon}}}{1-\sqrt{1-\sqrt{\epsilon}}} \right) \right]. \tag{3.27}
\end{aligned}$$

Even for the simplest case of uniformly distributed breaking thresholds, the constitutive equation takes a rather complex form. It is important to note that the coupling of the two breaking modes gives rise to a higher amount of broken beams compared to the *OR* criterion. In Fig. 3.3 the beams which break due to the coupling of the two breaking modes fall in the area labeled by *B*.

### 3.3 Computer simulations

In order to determine the behaviour of the system for complicated disorder distributions and explore the microscopic failure process of the sheared interface, it is necessary to work out a computer simulation technique. In the model we consider an ensemble of  $N$  beams arranged on a square lattice. Two breaking thresholds  $\epsilon_1^i, \epsilon_2^i$  are assigned to each beam  $i$  ( $i = 1, \dots, N$ ) of the bundle from the joint probability distribution  $p(\epsilon_1, \epsilon_2)$ . For

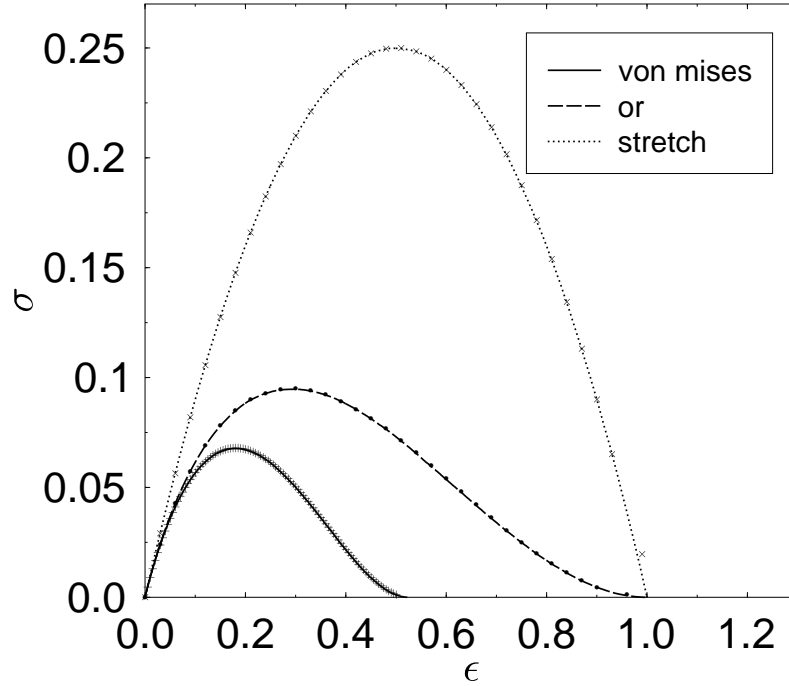


Figure 3.4: Constitutive behaviour of a bundle of beams with two breaking modes in a strain-controlled simulation of  $N = 4 \cdot 10^5$  beams, under the *OR* (dashed line), *von Mises type* (solid line), and a pure stretching breaking criterion (dotted line). The random failure thresholds for the breaking modes of each beam are sampled from uniform distribution between  $[0, 1]$ . The points marked with ‘·’, ‘+’ and ‘×’ denote the respective theoretical results, Eqs. (3.21, 3.27), and  $\sigma = \epsilon(1 - \epsilon)$  for the pure stretching case. The constants  $E$  and  $a$  are set to unity here.

the *OR* breaking rule, the failure of a beam is caused either by stretching or bending depending on which one of the conditions Eqs. (3.11,3.12) is fulfilled at a lower value of the external load. This way an effective breaking threshold  $\epsilon_c^i$  can be defined for the beams as

$$\epsilon_c^i = \min(f^{-1}(\epsilon_1^i), g^{-1}(\epsilon_2^i)), \quad i = 1, \dots, N, \quad (3.28)$$

where  $f^{-1}$  and  $g^{-1}$  denote the inverse of  $f, g$ , respectively. A beam  $i$  breaks during the loading process of the interface when the load on it exceeds its effective breaking threshold  $\epsilon_c^i$ . For the case of the von Mises type breaking criterion Eq. (3.22), the effective breaking threshold  $\epsilon_c^i$  of beam  $i$  can be obtained as the solution of the algebraic equation

$$\left(\frac{f(\epsilon_c^i)}{\epsilon_1^i}\right)^2 + \frac{g(\epsilon_c^i)}{\epsilon_2^i} = 1, \quad i = 1, \dots, N. \quad (3.29)$$

Although for the specific case of the functions  $f, g$  given by Eqs. (3.11,3.12) the above equation can be converted to a 4th order polynomial and solved analytically, this solution turns out to be impractical, especially since the numerical evaluation of the solution is too slow. We therefore solve Eq. (3.29) numerically by means of a modified Newton root finding scheme, where we make use of the fact that the solution has the lower bound 0.

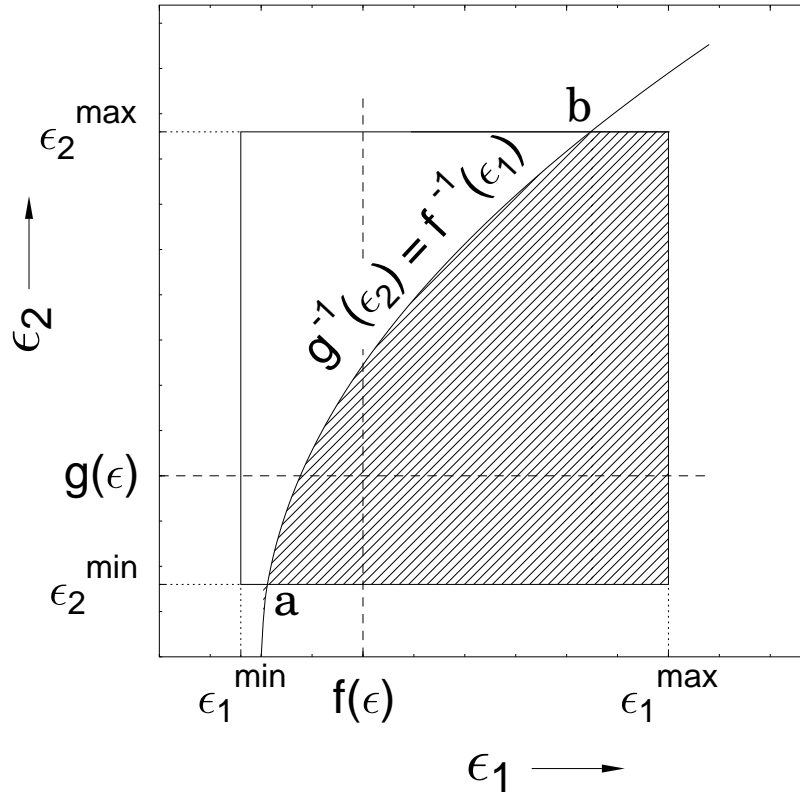


Figure 3.5: The beams that break due to mode  $g$  fall in the shaded region. The labels  $a$  and  $b$  mark the abscissae of the intersection points of the curve  $g^{-1}(\epsilon_2) = f^{-1}(\epsilon_1)$  with the lines  $\epsilon_2 = \epsilon_2^{\min}$  and  $\epsilon_2 = \epsilon_2^{\max}$ , respectively.

In the case of global load sharing, the load and deformation of beams is everywhere the same along the interface, which implies that beams break in the increasing order of their effective breaking thresholds. In the simulation, after determining  $\epsilon_c^i$  for each beam, they are sorted in increasing order. Quasi-static loading of the beam bundle is performed by increasing the external load to break only a single element. Due to the subsequent load redistribution on the intact beams, the failure of a beam may trigger an avalanche of breaking beams. This process has to be iterated until the avalanche stops, or it leads to catastrophic failure at the critical stress and strain. Under strain controlled loading conditions, however, the load of the beams is always determined by their deformation so that there is no load redistribution and avalanche activity.

In Fig. 3.4 the analytic results on the constitutive behaviour Eqs. (3.21, 3.27) are compared to the corresponding results of computer simulations. As a reference, we also plotted the constitutive behaviour of a bundle of fibres where the fibres fail solely due to simple stretching [5; 77; 6; 29; 30; 65; 70; 63]. It can be seen in the figure that the simulation results are in perfect agreement with the analytical predictions. It is important to note that the presence of two breaking modes substantially reduces the critical stress  $\sigma_c$  and strain  $\epsilon_c$  ( $\sigma$  and  $\epsilon$  value of the maximum of the constitutive curves) with respect to the case when



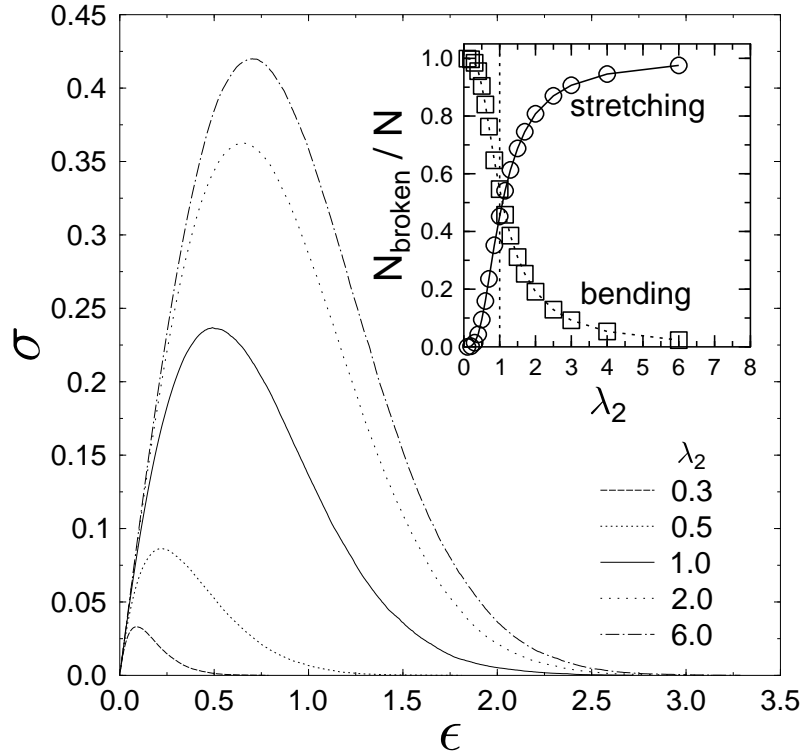


Figure 3.6: Constitutive behaviour of a bundle of  $N = 90000$  beams using the *OR* criterion. The parameter values  $\lambda_1 = 1.0$  (stretching),  $m_1 = m_2 = 2$  were fixed, while  $\lambda_2$  corresponding to the bending mode was shifted. Inset: Fraction of beams breaking by stretching and bending as a function of  $\lambda_2$ .

failure of elements occurs solely under stretching. Since one of the failure functions  $g(\epsilon)$  is non-linear, the shape of the constitutive curve  $\sigma(\epsilon)$  also changes, especially in the post-peak regime. The coupling of the two breaking modes in the form of the von Mises criterion gives rise to further reduction of the strength of the interface.

### 3.4 Progressive failure of the interface

During the quasi-static loading process of an interface, avalanches of simultaneously failing beams occur. Inside an avalanche, however, the beams can break under different breaking modes when the *OR* criterion is considered, or the breaking can be dominated by one of the breaking modes in the coupled case of the von Mises type criterion. Hence, it is an important question how the fraction of beams breaking due to a specific breaking mode (stretching or bending) varies during the course of loading of the interface.

For the *OR* criterion, those beams break, for instance, under bending, i. e. under mode  $g$

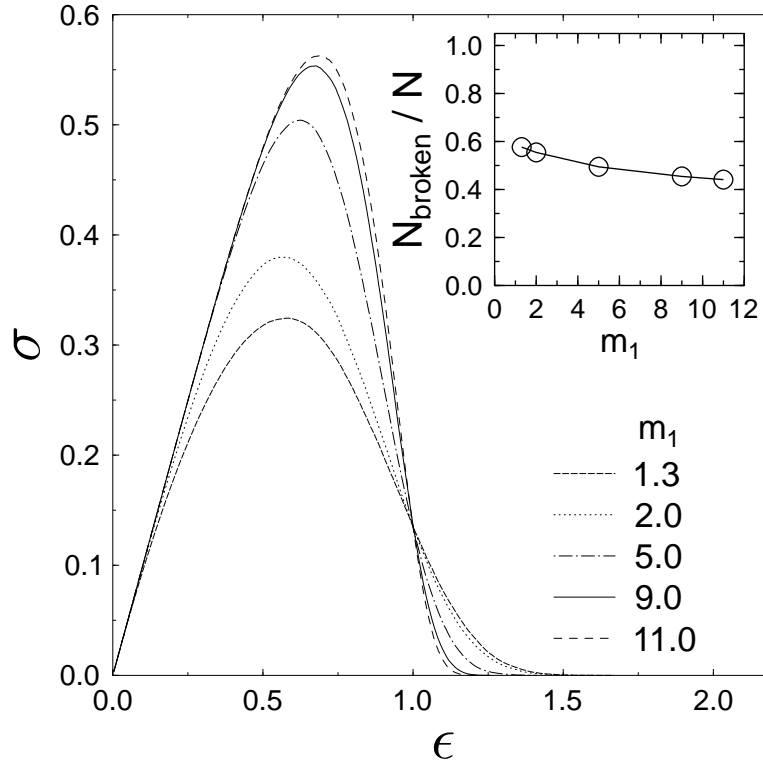


Figure 3.7: Constitutive behaviour for different values of the shape parameter  $m_1$  of stretching. Strain controlled simulation of  $N = 90000$  beams with failure due to the *OR*-criterion, fixing the parameters  $\lambda_1 = \lambda_2 = 1.0$  and  $m_2 = 2$ . Inset: total fraction of beams broken under mode  $g$  during the course of loading.

defined by Eq. (3.12), whose effective breaking threshold  $\epsilon_c^i$  is determined by  $g^{-1}(\epsilon_2^i)$  in Eq. (3.28) so that the inequality holds

$$g^{-1}(\epsilon_2^i) < f^{-1}(\epsilon_1^i). \quad (3.30)$$

In the plane of breaking thresholds  $\{\epsilon_1, \epsilon_2\}$  the region of beams which fulfill the above condition is indicated by shading in Fig. 3.5. The fraction of beams  $\mathcal{B}_g(\epsilon)$  breaking under mode  $g$  up to the macroscopically imposed deformation  $\epsilon$  can be obtained by integrating the probability distribution  $p(\epsilon_1, \epsilon_2)$  over the shaded area in Fig. 3.5. Taking into account the fact that the intersection points  $a, b$  defined in Fig. 3.5 may in general lie outside the rectangle  $(\epsilon_1^{\min}, \epsilon_1^{\max}, \epsilon_2^{\max}, \epsilon_2^{\min})$  and adjusting the integral limits accordingly, we arrive at the following formula for the fraction of fibres breaking under mode  $g$  as a function of the

deformation  $\epsilon$

$$\begin{aligned}
\mathcal{B}_g(\epsilon) = & \int_{\max(\epsilon_1^{\min}, a)}^{\min(f(\epsilon), b)} d\epsilon_1 \int_{\epsilon_2^{\min}}^{g(f^{-1}(\epsilon_1))} d\epsilon_2 p(\epsilon_1, \epsilon_2) \\
& + \int_{\min(f(\epsilon), b)}^{f(\epsilon)} d\epsilon_1 \int_{\epsilon_2^{\min}}^{\epsilon_2^{\max}} d\epsilon_2 p(\epsilon_1, \epsilon_2) \\
& + \int_{f(\epsilon)}^{\epsilon_1^{\max}} d\epsilon_1 \int_{\epsilon_2^{\min}}^{g(\epsilon)} d\epsilon_2 p(\epsilon_1, \epsilon_2). \tag{3.31}
\end{aligned}$$

It should be noted that the second integral vanishes unless  $b < \epsilon_1^{\max}$ . The total fraction of beams breaking under mode  $g$  during the entire course of the loading can be obtained by substituting  $\epsilon = \epsilon^{\max}$  in the above formulas, where  $\epsilon^{\max}$  denotes the deformation at the breaking of the last beam.

In order to study the effect of the disorder distribution  $p(\epsilon_1, \epsilon_2)$  of beams on the relative importance of the two breaking modes and on the progressive failure of the interface, we considered independently distributed breaking thresholds  $\epsilon_1, \epsilon_2$  both with a Weibull distribution

$$p_b(\epsilon_b) = \frac{m_b}{\lambda_b} \left( \frac{\epsilon_b}{\lambda_b} \right)^{m_b-1} \exp \left[ - \left( \frac{\epsilon_b}{\lambda_b} \right)^{m_b} \right], \tag{3.32}$$

where index  $b$  can take values 1 and 2. The exponents  $m_1, m_2$  determine the amount of disorder in the system for stretching and bending, respectively, i. e. the width of the distributions Eq. (3.32), while the values of  $\lambda_1, \lambda_2$  set the average strength of beams for the two breaking modes. Computer simulations were performed in the framework of global load sharing by setting equal values for the shape parameters  $m_1 = m_2$  and fixing the value of  $\lambda_1 = 1$  of the stretching mode, while varying  $\lambda_2$  of the bending mode.

The total fraction of beams breaking by stretching and bending using the *OR* breaking rule is presented in Fig. 3.6. Increasing  $\lambda_2$  of the bending mode, the beams become more resistant against bending so that the stretching mode starts to dominate the breaking of beams, which is indicated by the increasing fraction of stretching failure in the figure. In the limiting case of  $\lambda_2 \gg \lambda_1$  the beams solely break under stretching. Decreasing  $\lambda_2$  has the opposite effect, more and more beams fail due to bending, while the fraction of beams breaking by the stretching mode tends to zero. It is interesting to note that varying the relative importance of the two failure modes gives also rise to a change of the macroscopic constitutive behaviour of the system. Fig. 3.6 illustrates that shifting the strength distributions of beams the functional form of the constitutive behaviour remains the same, however, the value of the critical stress and strain vary in a relatively broad range.

The same analysis can also be performed by fixing the values  $\lambda_1$  and  $\lambda_2$  and changing the relative width of the two distributions by varying one of the Weibull shape parameters

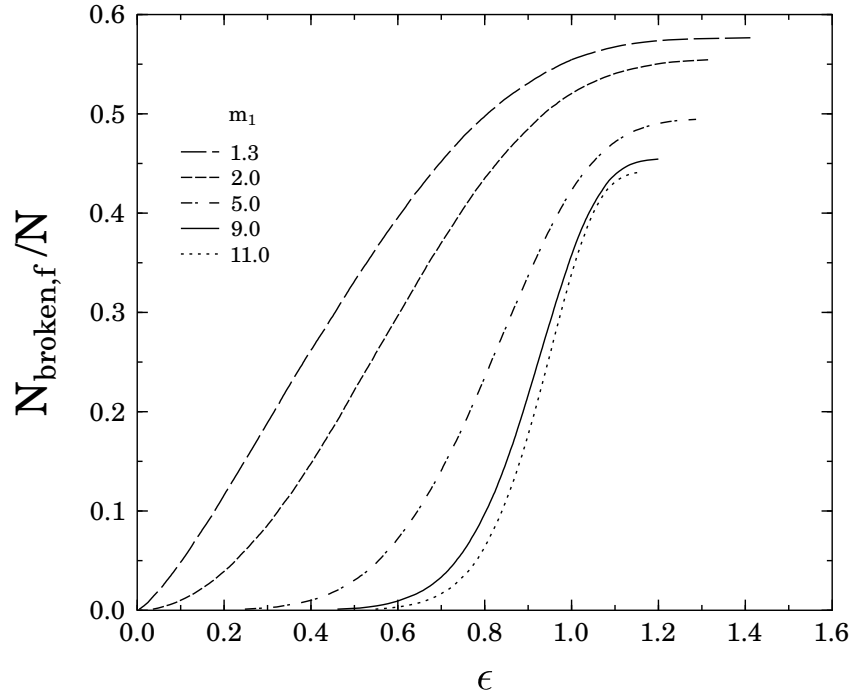


Figure 3.8: Fraction of fibres broken by the stretching mode as a function of  $\epsilon$  for different values of the corresponding shape parameter  $m_1$ . Strain controlled simulation with failure due to the *OR*-criterion,  $N = 90000$ ,  $\lambda_1 = \lambda_2 = 1.0$ ,  $m_2 = 9$ .

$m$ . We find it convenient to shift  $m_1$ , the shape parameter of the stretching mode instead of  $m_2$ . It can be observed in Fig. 3.7 that for this choice of the scale parameters  $\lambda$ , the value of the critical strain hardly changes, however the critical stress nearly doubles as compared to Fig. 3.6.

Although the effect on the final fraction of beams broken by each mode, see inset of Fig. 3.7, is not as pronounced as for shifting  $\lambda$ , we should also consider the fraction of fibres broken up to a value of  $\epsilon$  during the loading process (Fig. 3.8). It should be noted that the end points of the respective curves in Fig. 3.8 are just the final fraction numbers in Fig. 3.7, but the curves show a strong spread for intermediate values of  $\epsilon$ . This demonstrates that changing the amount of disorder in the breaking thresholds strongly influences the process of damaging of the interface.

We apply the methods outlined in the previous paragraphs to the von Mises case. Obviously, Eq. (3.22) does not allow for a strict separation of the two modes. However, the breaking of a beam at a certain value  $\epsilon_c$  is dominated by stretching if

$$\left( \frac{f(\epsilon)}{\epsilon_1} \right)^2 > \frac{g(\epsilon)}{\epsilon_2}. \quad (3.33)$$

With the previous prescriptions for the failure functions Eqs. (3.13), we again find a massive influence on the constitutive behaviour and the final number of broken beams, see

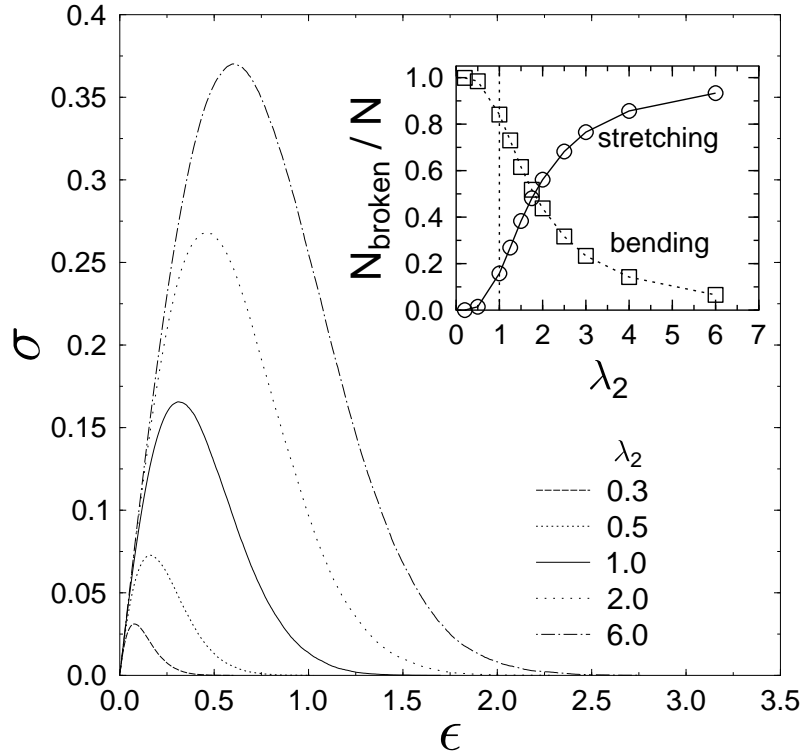


Figure 3.9: Constitutive behaviour for different values of the bending scale parameter  $\lambda_2$ . Strain controlled simulation with the von Mises criterion,  $N = 90000$ ,  $\lambda_1 = 1.0$ ,  $m_1 = m_2 = 2$ . The inset presents the fraction of beams whose failure was dominated by the stretching or bending mode.

Fig. 3.9. The inset of Fig. 3.9 demonstrates that a crossover between stretching and bending preponderance occurs also in the von Mises case.

### 3.5 Avalanche statistics

The stress controlled loading of the glued interface is accompanied by avalanches of simultaneously failing elements. The avalanche activity can be characterized by the distribution  $D(\Delta)$  of burst sizes  $\Delta$  defined as the number of beam breakings triggered by the failure of a single beam. In the framework of simple fibre bundle models, it has been shown analytically that global load sharing gives rise to a power law distribution of avalanche sizes for a very broad class of disorder distributions of materials strength [68; 6]

$$D(\Delta) \propto \Delta^{-\delta} \quad (3.34)$$

with an universal exponent  $\delta = 5/2$ .

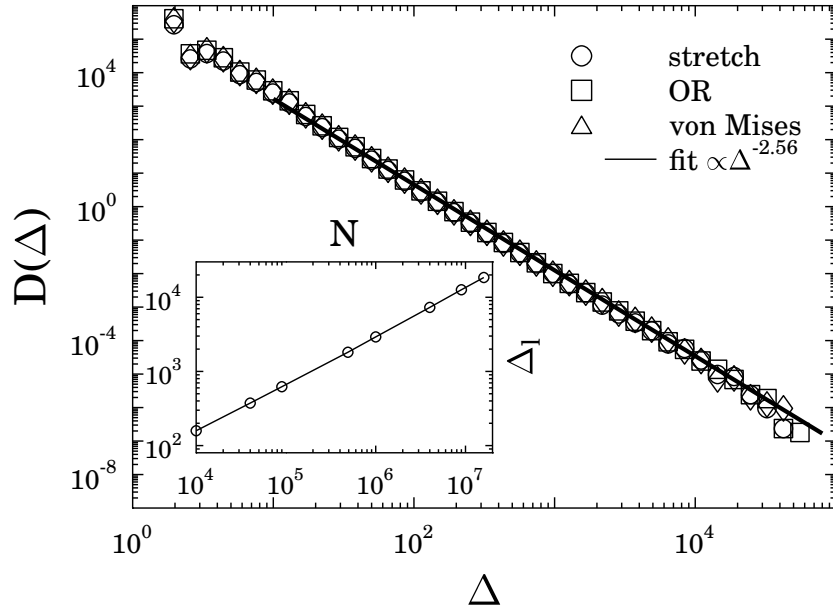


Figure 3.10: Avalanche size distribution  $D(\Delta)$  for pure stretching of a fibre bundle, and the two beam breaking conditions for system sizes  $N = 16 \cdot 10^6$ , averaged over 100 runs. A fit with the best result  $D \propto \Delta^{-2.56}$  over almost four decades is provided. The inset shows the dependency of the largest avalanche  $\Delta_1$  on the system size for the three cases. Again, no difference is found.

In the previous sections we have shown that in our model the interplay of the two breaking modes results in a complex failure mechanism on the microscopic level, which is strongly affected by the distributions of the breaking thresholds. In order to investigate the bursts of breaking beams we performed stress controlled simulations on large systems ( $N = 10^4 \dots 16 \cdot 10^6$ ) with both the *OR* and von Mises type breaking criterion. In Figure 3.10 the simulation results are compared to the avalanche size distribution of a simple fibre bundle model where failure occurs solely due to stretching [68; 6; 29; 30; 65]. In all the cases the avalanche size distributions can be fitted by a power law over three orders of magnitude. The best fit exponent of  $\delta = 2.56 \pm 0.08$  was derived from the system of size  $N = 16 \cdot 10^6$  beams, with an average taken over 100 samples. The size of the largest avalanche in the inset of Fig. 3.10 proved to be proportional to the system size. It can be concluded that the beam model belongs to the same universality class as the fibre bundle model [68; 6; 29; 30; 65].

### 3.6 Local load sharing

During the failure of interfaces, stress localization is known to occur in the vicinity of failed regions, which results in correlated growth and coalescence of cracks. In our model this effect can be captured by localized interaction of the interface elements, which naturally occurs when the two solid blocks are not perfectly rigid [42]. For simplicity, in our model solely the extremal case of very localized interactions is considered, i. e. after

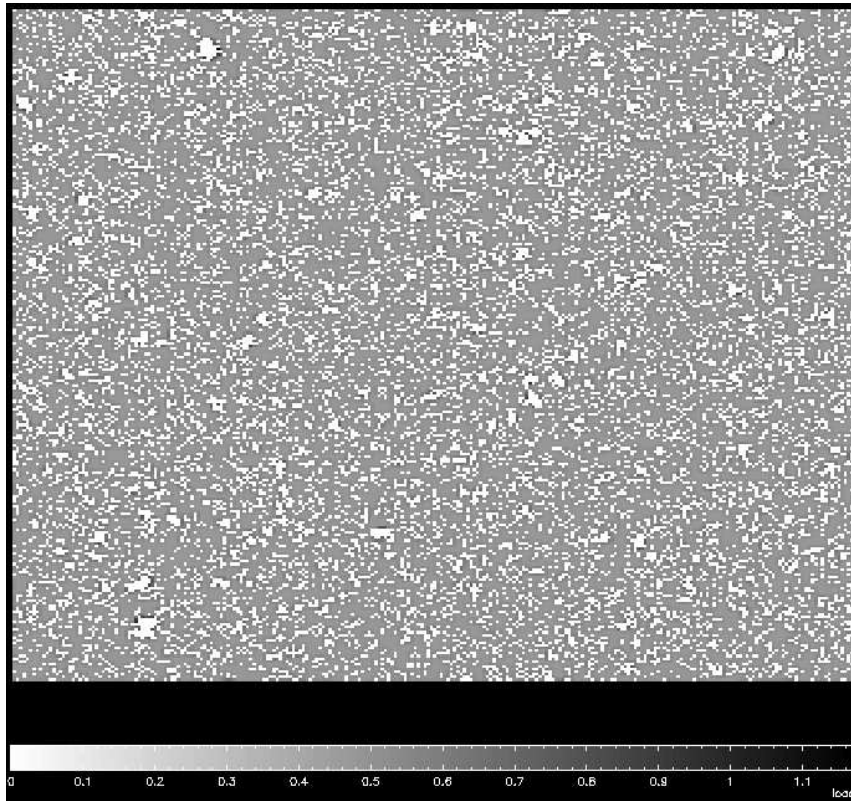


Figure 3.11: Snapshot of a LLS system at the last stable configuration. The color coding represents the load per beam, with broken beams carrying a vanishing load. The system size is  $L = 100$ .

breaking of a beam in the square lattice, the load is redistributed equally on its nearest and next-nearest intact neighbors. This localized load sharing (LLS) results in growing failed regions (cracks) with high stress concentration along their perimeter [42; 29; 75]. Figure 3.11 shows the last stable configuration of a beam lattice preceding global failure, which was obtained using the *OR* criterion for beam breaking. Due to the stress concentration around cracks, the onset of a catastrophic avalanche occurs at lower external loads making the macroscopic response of the interface more brittle compared to the case of global load sharing [42; 29; 75].

As for global load sharing, we shift the relative importance of the two breaking modes by changing their threshold distributions, and record the influence on micro- and macroscopic system properties. We consider here the *OR*-criterion, and use two Weibull distributions with parameters  $\lambda_1, \lambda_2$  and  $m_1, m_2$ , where the indices 1 and 2 denote the stretching and bending mode, respectively. Varying  $\lambda_2$  for a fixed  $\lambda_1$ , we find a considerable influence on the constitutive properties, as Fig. 3.12 illustrates.

We investigated also the distribution of avalanche sizes for LLS, Fig. 3.13, where we vary the scale parameter  $\lambda_2$  of the bending mode  $g$ . We find merely a shifting to different amplitudes, but no considerable effect on the shape of the distribution function, which is similar to the one reported in [29]. In comparison to the GLS case, we should note that large avalanches cannot occur, and the functional form of the curves can be approximated

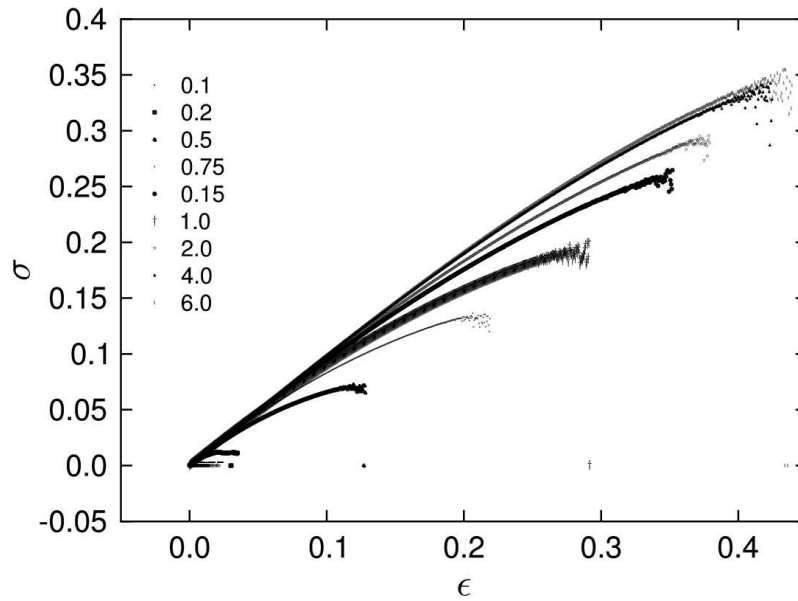


Figure 3.12: Constitutive curves in the LLS case, shifting  $\lambda_2$  (legend) and keeping the parameters  $\lambda_1 = 1.0$  and  $m_1 = m_2 = 2$  fixed. Stress controlled simulation of  $N = 10000$  fibres averaged over 300 runs.

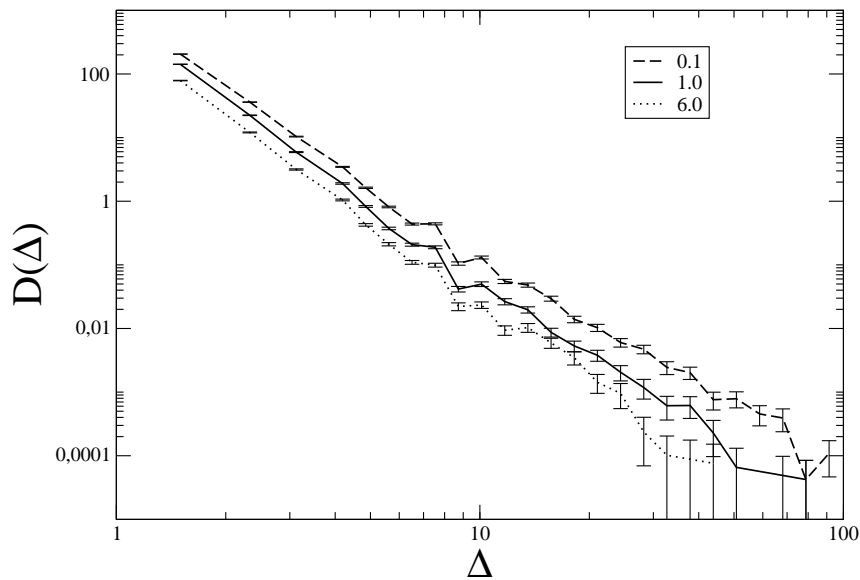


Figure 3.13: Distribution of avalanche sizes for LLS for three values of  $\lambda_2$  (legend), with  $\lambda_1 = 1$  and  $m_1 = m_2 = 2$  fixed. Simulations were performed using the *OR* criterion for a bundle of 10000 beams averaged over 300 runs.

by a power law with an exponent higher than for GLS in agreement with Refs. [68; 6; 75].



### 3.7 Concluding remarks

Fibre bundle models have been applied to describe various aspects of the failure of heterogeneous interfaces. However, fibres can sustain solely elongation, and hence cannot account for more complex deformation states of interface elements, which naturally occurs under shear loading. We constructed a novel type of model for the shear failure of the glued interface of two solid blocks. In the model the interface is discretized in terms of elastic beams which experience stretching and bending deformation under shear. Breaking of a beam can be caused by both deformations resulting in two failure modes. The mechanical strength of beam elements is characterized by the two threshold values of stretching and bending the beam can withstand. The beams are assumed to have identical elastic properties, the heterogeneous microstructure is represented by the disorder distribution of the breaking thresholds. In the model we assume that the two solid blocks are perfectly rigid which results in a global load redistribution over the intact beams following the breaking events.

We presented a detailed study of the macroscopic response and the progressive damaging of the interface under quasistatic loading. Making use of the global load sharing of intact beams, we obtained the analytic solution of the model for the constitutive behaviour and the amount of damage during the course of loading. In order to explore the microscopic process of damaging we worked out an efficient simulation technique which enables us to study large systems. We demonstrated that the disorder distribution and the relative importance of the two failure modes have a substantial effect on both the microscopic damage process and the macroscopic constitutive behaviour of the interface. Varying its parameters, the model provides a broad spectrum of material behaviours, where the presence of a second breaking mode reduces the critical stress and strain as compared to the classical FBM. Simulations showed that the failure of the interface proceeds in bursts of simultaneously breaking beams. The distribution of burst sizes follows power law behaviour with an exponent equal to the one of simple fibre bundles. Under stress controlled loading conditions, the macroscopic failure of the interface occurs analogously to phase transitions, where our beam model proved to be in the same universality class as the equal load sharing fibre bundle model [61; 29; 69]. We showed that the localized interaction of beams leads to a more brittle behaviour of the interface, which implies a more abrupt transition at the critical load.

Beam models have been successfully applied to study the fracture of cohesive frictional materials where cracks usually form along the grain-grain interface. Beam elements proved to give a satisfactory description of the interfacial failure of grains and the emerging micro- and macro-behaviour of materials [90]. The beam model presented here provides a more realistic description of the interface of macroscopic solid bodies than the simple fibre bundle model and is applicable to more complex loading situations. Experiments on the shear failure of glued interfaces are rather limited, especially on the microscopic mechanism of the progressive damage, which hinders the direct comparison of our theoretical results to experimental findings. Our work in this direction is in progress.



# Chapter 4

## Failure Process of a Bundle of Plastic Fibres

We present an extension of models of the shear failure of glued interfaces –such as the one presented in Chapter 3— considering that surface elements after failure still can have a certain load bearing capacity. The disordered interface is represented by a parallel set of fibres with random breaking thresholds and linearly elastic behavior until failure. The broken fibres are assumed to carry a constant load which is a fraction  $0 \leq \alpha \leq 1$  of their failure load. Varying the value of  $\alpha$  the model interpolates between the perfectly brittle ( $\alpha = 0$ ) and perfectly plastic ( $\alpha = 1$ ) constitutive behavior of fibres. Based on analytic calculations and computer simulations, we show that the finite load bearing capacity of failed fibres has a substantial effect on both the macroscopic response and microscopic damage process of the fibre bundle. When the load redistribution following fibre failure is short ranged, an interesting phase transition is revealed at a specific value of  $\alpha$ . The results presented here have been published in [91].

### 4.1 Model

In Chapter 3 we presented a detailed study which demonstrated that the beam model of sheared interfaces with two breaking modes can be mapped into a simple fibre bundle model of a single breaking mode by an appropriate transformation of the fibres' strength disorder. For the sake of simplicity, the following account therefore refers to bundles of fibres, where the possible application to the problem of sheared interfaces should be kept in mind.

In the present chapter, we extend fibre and beam models by taking into account that failed surface elements can still carry some external load increasing the load bearing capacity of the damaged interface. A bundle of parallel fibres is considered with breaking thresholds  $\sigma_{th}$  in the interval  $0 \leq \sigma_{th} \leq \sigma_{th}^{max}$  with a probability density  $p(\sigma_{th})$  and distribution function  $P(\sigma_{th}) = \int_0^{\sigma_{th}} p(\sigma'_{th}) d\sigma'_{th}$ . We assume that after the breaking of a fibre at the

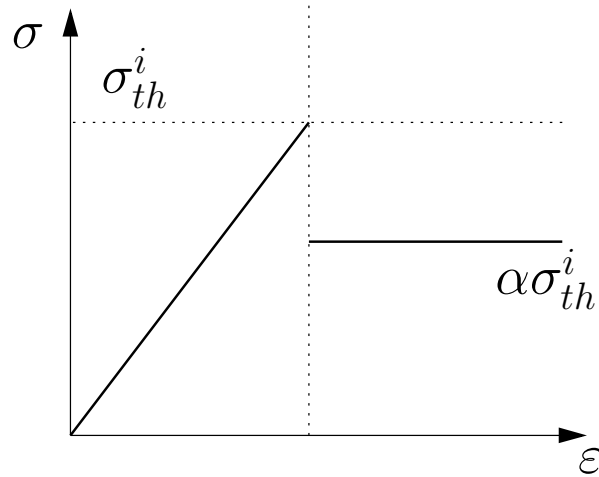


Figure 4.1: Constitutive behaviour of a single fibre: the fibre shows linearly elastic behaviour up to the breaking threshold  $\sigma_{th}^i$ , then it keeps a fraction  $0 \leq \alpha \leq 1$  of the ultimate load  $\alpha\sigma_{th}^i$ .

failure threshold  $\sigma_{th}^i$ , it may retain a fraction  $0 \leq \alpha \leq 1$  of its ultimate load  $\sigma_{th}^i$ , i. e. it will continue to transfer a constant load  $\alpha\sigma_{th}^i$  between the surfaces. This assumption can be interpreted so that at the damaged areas of the interfaces the two solids still remain in contact exerting for instance a friction force which may contribute to the overall load bearing capacity.

In many applications involving glued parts, the glue between two interfaces has disordered properties but its failure characteristics is not perfectly brittle, under shear the glue may also yield. The constitutive behaviour of single fibres is illustrated in Fig. 4.1. Note that the load carried by the broken fibres is independent of the external load, furthermore, it is a random variable due to the randomness of the breaking thresholds. Varying the value of  $\alpha$ , the model interpolates between the perfectly brittle failure ( $\alpha = 0$ ) and perfectly plastic ( $\alpha = 1$ ) behaviour of fibres. The load stored by the failed fibres reduces the load increment redistributed over the intact fibres, which strongly affects the process of gradual failure occurring under quasi-static loading of the interface. In the following we present a detailed study of the model system varying the strength of plasticity  $\alpha$ . For the range of load sharing the two limiting cases of global and local load redistributions will be considered after failure events.

## 4.2 Transition to perfect plasticity

Assuming global load sharing (GLS) after fibre breaking, the constitutive equation of the interface can be cast into a closed form. At an externally imposed deformation  $\varepsilon$  the interface is a mixture of intact and broken fibres, which both contribute to the load bearing capacity of the interface. Since the broken fibres retain a fraction  $\alpha$  of their failure load, at the instant of fibre breaking only the reduced load  $(1-\alpha)\sigma_{th}^i$  is redistributed over the intact

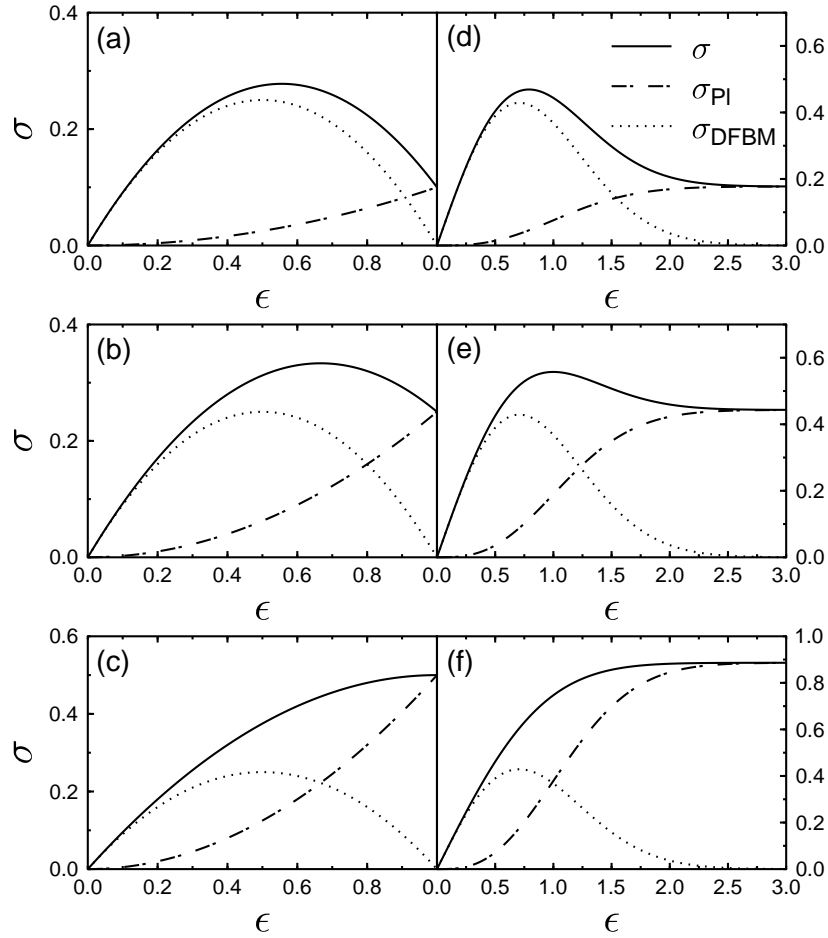


Figure 4.2: Constitutive behaviour  $\sigma(\varepsilon)$  of the plastic fibre bundle for uniform (a, b, c) and Weibull distribution with  $m = 2$  (d, e, f) at  $\alpha = 0.2$  (a, d),  $\alpha = 0.5$  (b, e) and  $\alpha = 1.0$  (c, f). The contribution of intact  $\sigma_{\text{DFBM}}$  and failed fibres  $\sigma_{\text{PI}}$  are also shown. Note that  $\sigma_{\text{DFBM}}$  is identical with the constitutive curve of simple dry fibre bundle models.

fibres. Since the fraction of fibres having breaking threshold in the interval  $[\varepsilon, \varepsilon + d\varepsilon]$  can be obtained as  $p(\varepsilon)d\varepsilon$ , the constitutive equation  $\sigma(\varepsilon)$  reads as

$$\sigma(\varepsilon) = \underbrace{E\varepsilon(1 - P(\varepsilon))}_{\sigma_{\text{DFBM}}} + \alpha \underbrace{\int_0^\varepsilon E\varepsilon'p(\varepsilon') d\varepsilon'}_{\sigma_{\text{PI}}}, \quad (4.1)$$

where the integration is performed over the entire load history. The first term labeled  $\sigma_{\text{DFBM}}$  provides the load carried by the intact fibres, which corresponds to the classical dry fibre bundle (DFBM) behaviour [5; 6; 77]. The constitutive law of DFBMs is recovered in the limiting case  $\alpha = 0$ , when the complete load of the failed fibre is transferred to the remaining intact fibres of the bundle. In the second term  $\sigma_{\text{PI}}$ , which accounts for the load carried by the broken fibres, the integral is calculated over the entire load history of the interface up to the macroscopic deformation  $\varepsilon$ . It can be seen in Eq. (4.1) that the value of  $\alpha$  controls the relative importance of the *elastic* and *plastic* terms influencing

the macroscopic response  $\sigma(\varepsilon)$  and also the microscopic damage process of the system. When  $\alpha$  is increased, less load is transferred to the intact fibre and in the limiting case  $\alpha = 1$  failed fibres retain their entire load so no load transfer occurs. In this chapter, we explore the influence of the parameter  $\alpha$  when it is tuned between these two extremal cases. In the following calculations the value of the fibres' Young modulus was set to unity  $E = 1$ .

We note that the plastic fibre bundle model resembles up to some extent to the continuous damage fibre bundle model (CDFBM) worked out in Refs. [21; 30]. The main assumption of the CDFBM is that due to the activation of certain internal degrees of freedom, the fibres undergo a gradual softening process reducing their Young modulus in consecutive partial failure events. The fibres always remain linearly elastic but with a Young modulus  $E(k) = a^k E$ , where the multiplication factor  $0 \leq \alpha \leq 1$  describes the stiffness reduction in a single failure event and  $k$  denotes the number of failures occurred. If the fibres can fail only once ( $k = 1$ ) and keep their stiffness value constant, the constitutive law of the system reads as

$$\sigma(\varepsilon) = E\varepsilon(1 - P(\varepsilon)) + aE\varepsilon P(\varepsilon). \quad (4.2)$$

It was demonstrated in Refs. [21; 30] that increasing the number of times  $k$  the fibres can fail, the CDFBM develops a plastic plateau, however, with a mechanism completely different from the one considered here.

It is instructive to consider two fundamentally different cases of disorder distributions  $P(\varepsilon)$ , namely bounded and unbounded ones, where the largest breaking threshold  $\sigma_{th}^{max}$  takes a finite value or goes to infinity, respectively. In this chapter, we focus on two specific realizations, i. e. a uniform distribution between 0 and  $\sigma_{th}^{max}$

$$P(\sigma_{th}) = \frac{\sigma_{th}}{\sigma_{th}^{max}}, \quad 0 \leq \sigma_{th} \leq \sigma_{th}^{max}, \quad (4.3)$$

and distributions of the Weibull type

$$P(\sigma_{th}) = 1 - e^{-(\sigma_{th}/\lambda)^m}, \quad (4.4)$$

are considered where  $\lambda$  and  $m$  denote the characteristics strength and Weibull modulus of the distribution, respectively. For our study the Weibull distribution has the advantage that the amount of disorder in the failure thresholds can easily be controlled by the value of  $m$ .

The functional form of the constitutive behaviour  $\sigma(\varepsilon)$  is shown in Fig. 4.2 for both disorder distributions Eqs. (4.3),(4.4). It is interesting to note that for  $\alpha < 1$  there always exists a maximum of  $\sigma(\varepsilon)$ , just as in the case of DFBM. Under stress controlled loading conditions, macroscopic failure occurs at the maximum of  $\sigma(\varepsilon)$  so that the position and value of the maximum define the critical stress  $\sigma_c$  and strain  $\varepsilon_c$  of the bundle, respectively. It can be observed in Fig. 4.2 that the value of  $\sigma_c$  and  $\varepsilon_c$  are both higher than the corresponding values of DFBM indicating that the presence of plastic fibres increases the macroscopic strength of the bundle. The decreasing part and the plateau of  $\sigma(\varepsilon)$  can be realized under strain controlled loading conditions gradually increasing  $\varepsilon$ . Under strain control the local load on the fibres is determined by the externally imposed deformation so that there is no

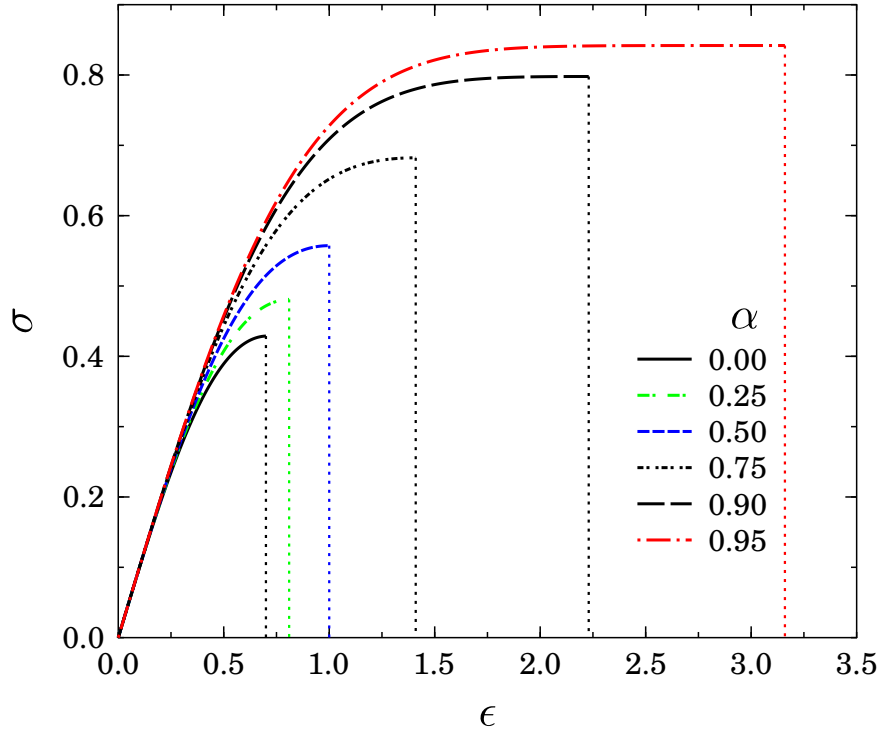


Figure 4.3: Simulations of stress controlled loading of a bundle of  $N = 1.6 \times 10^6$  fibres with Weibull distributed breaking thresholds ( $\lambda = 1, m = 2$ ). For clarity, the occurrence of macroscopic failure is indicated by vertical lines. Increasing  $\alpha$  the constitutive behaviour becomes perfectly plastic, i. e. a horizontal plateau with vanishing slope appears.

load redistribution after fibre failure. The fibres break one-by-one in the increasing order of their failure thresholds  $\sigma_{th}^i = E\varepsilon_{th}^i$ . When the deformation  $\varepsilon$  approaches the maximum value of the breaking thresholds  $\varepsilon_{th}^{max} = \sigma_{th}^{max}/E$ , all fibres must fail gradually so that the load of intact fibres  $\sigma_{DFBM}$  tends to zero, while that of the broken fibres  $\sigma_{PI}$  takes a finite asymptotic value

$$\sigma_{PI} \rightarrow \tilde{\sigma} = \alpha E \int_0^\infty \varepsilon' p(\varepsilon') d\varepsilon' = \alpha \langle \sigma_{th} \rangle, \quad (4.5)$$

where the integral is equal to the average fibre strength  $\langle \sigma_{th} \rangle$ . When the strength of plasticity  $\alpha$  is increased, the critical strain  $\varepsilon_c$  and stress  $\sigma_c$ , furthermore, the asymptotic stress of the plateau  $\tilde{\sigma}$  increase. The value of the critical deformation  $\varepsilon_c$  can be obtained by differentiating Eq. (4.1) with respect to  $\varepsilon$  and calculating the root [77]

$$1 - P(\varepsilon_c) - \varepsilon_c p(\varepsilon_c) [1 - \alpha] = 0, \quad (4.6)$$

from which the critical stress follows as  $\sigma_c = \sigma(\varepsilon_c)$ . Eq. (4.6) implies that in the limiting case of  $\alpha \rightarrow 1$  the critical strain  $\varepsilon_c$  tends to the maximum of the breaking thresholds  $\varepsilon_{th}^{max}$ , where  $P(\varepsilon_{th}^{max}) = 1$ . For the uniform distribution Eq. (4.3) we obtain

$$\varepsilon_c = \frac{\varepsilon_c^0}{1 - \alpha/2}, \quad \text{hence,} \quad \varepsilon_c \xrightarrow{\alpha \rightarrow 1} 2\varepsilon_c^0 = \varepsilon_{th}^{max}. \quad (4.7)$$

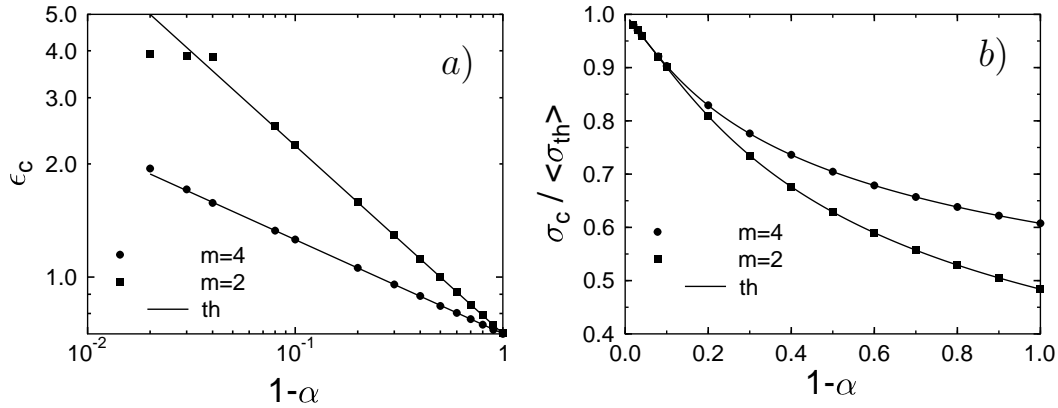


Figure 4.4: Critical strain  $\epsilon_c$  (a), and critical stress  $\sigma_c$  (b) as a function of  $1 - \alpha$  for a Weibull distribution with  $\lambda = 1, m = 2$ ; symbols: simulation results, solid lines: analytical expressions Eqs. (4.8),(4.9),(4.10).

Here  $\epsilon_c^0$  denotes the critical strain of DFBM  $\epsilon_c^0 = \epsilon_{th}^{max}/2$ , which can be obtained by setting  $\alpha = 0$  in Eq. (4.6). It follows that for unbounded threshold distributions like the Weibull distribution,  $\epsilon_c$  diverges so that perfect plasticity is only reached in the limit  $\epsilon_c \rightarrow \infty$ . The functional form of the divergence is not universal, due to the structure of the third term on the left hand side of Eq. (4.6),  $\epsilon_c$  depends on the specific form of  $p(\epsilon)$ . For the Weibull distribution,  $\epsilon_c$  as a function of  $\alpha$  reads as

$$\epsilon_c = \epsilon_c^0 (1 - \alpha)^{-1/m}, \quad \text{where} \quad \epsilon_c^0 = \lambda \left( \frac{1}{m} \right)^{1/m} \quad (4.8)$$

for any Weibull exponent  $m$ . Parallel to this, the decreasing part and the plateau of the constitutive curve  $\sigma(\epsilon)$  disappear so that  $\sigma_c$  and  $\tilde{\sigma}$  converge to the same finite value, which is the average fibre strength  $\langle \sigma_{th} \rangle$

$$\tilde{\sigma} \rightarrow \langle \sigma_{th} \rangle \quad \text{and} \quad \sigma_c \rightarrow \langle \sigma_{th} \rangle. \quad (4.9)$$

The average fibre strength  $\langle \sigma_{th} \rangle$  can be determined as

$$\langle \sigma_{th} \rangle = \frac{\sigma_{th}^{max}}{2} \quad \text{and} \quad \langle \sigma_{th} \rangle = \frac{1}{m} \Gamma \left( \frac{1}{m} \right) \quad (4.10)$$

for the uniform and Weibull distributions, respectively. Here  $\Gamma$  denotes the Gamma function.

In order to illustrate this behaviour, Fig. 4.3 presents constitutive curves for Weibull distributed fibre strength obtained by computer simulations of stress controlled loading up to the critical point with  $\lambda = 1$  and  $m = 2$ . It is apparent that in the limiting case of  $\alpha \rightarrow 1$  the constitutive curve  $\sigma(\epsilon)$  reaches a plateau, indicating a perfectly plastic macroscopic state of the system. The position of the maximum  $\epsilon_c$  of the constitutive curves, i. e. the ending point of the curves, rapidly increases as  $\alpha$  approaches 1, while the value of the



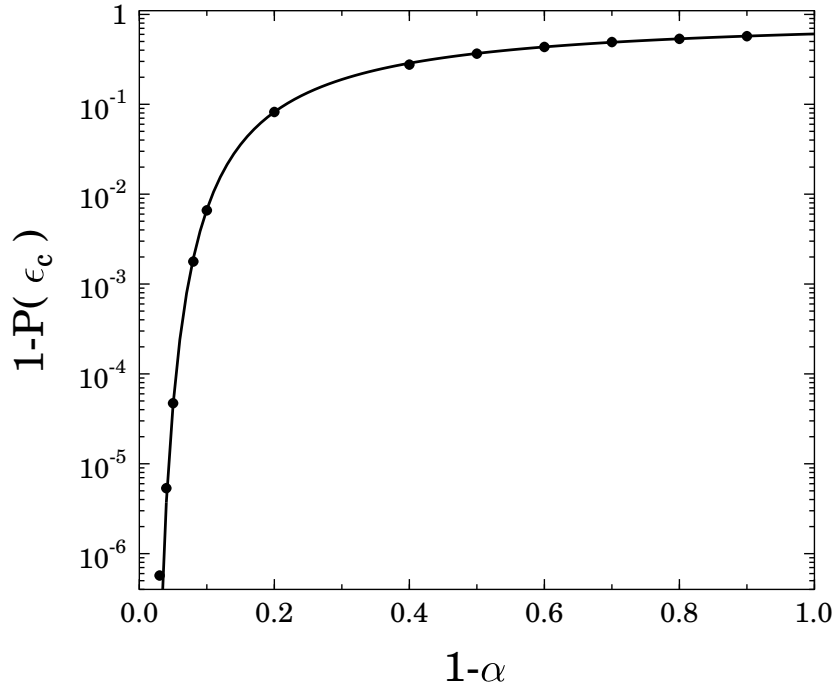


Figure 4.5: Fraction of intact fibres  $\phi = 1 - P(\epsilon_c(\alpha))$  at the point of macroscopic failure  $\epsilon_c$  vs.  $1 - \alpha$  for a Weibull distribution of  $\lambda = 1, m = 2$ ; circles: GLS simulation results, solid line: analytical solution Eq. (4.11).

maximum  $\sigma_c$  tends to a finite value. In agreement with the analytic predictions Eq. (4.8), simulations confirmed that  $\epsilon_c$  diverges as a power law whose exponent depends on the parameters of the strength distribution (see Fig. 4.4).

Controlling the external stress, the constitutive curve of the system Fig. 4.3 can only be realized up to the maximum, since at the critical load  $\sigma_c$  abrupt failure of the bundle occurs breaking all the surviving intact fibres in a large burst. The fraction  $\phi$  of fibres which break in the final burst causing global failure can be determined as  $\phi = 1 - P(\epsilon_c(\alpha))$ , which is illustrated in Fig. 4.5 as a function of  $1 - \alpha$  for the specific case of a Weibull distribution

$$\phi(\alpha) = e^{-1/m(1-\alpha)}. \quad (4.11)$$

It can be observed that as the system approaches the state of perfect plasticity  $\alpha \rightarrow 1$ ,  $\phi$  tends to zero. This demonstrates that more and more fibres break before global failure occurs, and perfect plasticity is obtained when the strongest fibre fails at the maximum of  $\sigma(\epsilon)$  (compare also to Fig. 4.3). This argument also implies that for  $\alpha \rightarrow 1$ , the difference of the microscopic damage process under stress and strain controlled loading disappears, the fibres break one-by-one without triggering avalanches of breakings.

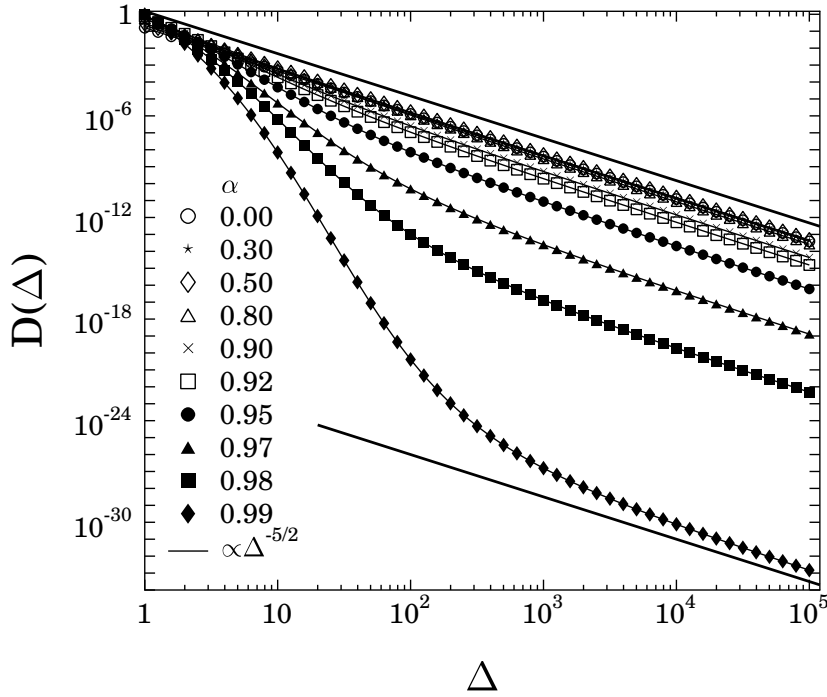


Figure 4.6: Analytic solution of the avalanche size distribution  $D(\Delta)$  at various different values of  $\alpha$ . For  $\alpha \rightarrow 0$  the usual power law distribution is recovered, whereas for  $\alpha \rightarrow 1$  an exponential decay of  $D(\Delta)$  is obtained. For the specific calculations a Weibull distribution was used with  $m = 2$ .

### 4.3 Avalanches of fibre breakings

Under stress controlled loading of the fibre bundle, the load dropped by a breaking fibre is redistributed over the intact ones. This load increment can give rise to further breakings which then may trigger an entire avalanche of failure events. The distribution  $D(\Delta)$  of avalanche sizes  $\Delta$  is an important quantity for the dynamical description of the loaded system. For the case of classical DFBMs ( $\alpha = 0$ ) under GLS conditions the avalanche size distribution  $D(\Delta)$  can be obtained analytically [68; 6] as an integral, from which the asymptotic form of the distribution for large avalanches proved to be a power law

$$D(\Delta) \propto \Delta^{-5/2}, \quad \Delta \rightarrow \infty. \quad (4.12)$$

The value of the exponent  $5/2$  is universal, it does not depend on the details of the disorder distribution of the failure thresholds [68; 6].

In order to obtain the analytical solution for the avalanche distribution in the presence of plastic fibres  $\alpha \neq 0$ , we can follow the derivation of Refs. [68; 6], taking into account that the average number of fibres  $a(\varepsilon, \alpha)d\varepsilon$  which break as a consequence of the load increment caused by a fibre breaking at the deformation  $\varepsilon$ , is reduced by a factor of  $(1 - \alpha)$

$$a(\varepsilon, \alpha)d\varepsilon = \frac{\varepsilon p(\varepsilon)(1 - \alpha)}{1 - P(\varepsilon)}d\varepsilon. \quad (4.13)$$

Taking into account that the critical deformation  $\varepsilon_c$  where macroscopic failure occurs also depends on  $\alpha$ , the avalanche size distribution  $D(\Delta)$  can be cast in the form

$$\frac{D(\Delta)}{N} = \frac{\Delta^{\Delta-1}}{\Delta!} \int_0^{\varepsilon_c(\alpha)} a(\varepsilon, \alpha)^{\Delta-1} e^{-a(\varepsilon, \alpha)\Delta} \times [1 - a(\varepsilon, \alpha)] p(\varepsilon) d\varepsilon. \quad (4.14)$$

For the specific case of the Weibull distribution with an arbitrary modulus  $m$  the general equation Eq. (4.14) can be written in the form

$$D(\Delta, \alpha) = \frac{\Delta^{\Delta-1}}{\Delta! (m(1-\alpha))^2 \Delta_c^{\Delta+1}} [\gamma(\Delta, \Delta_c) + \Delta_c^\Delta m(1-\alpha) e^{-\Delta_c}] , \quad (4.15)$$

where  $\Delta_c$  depends on the amount of disorder  $m$  and on the strength of plasticity  $\alpha$

$$\Delta_c = \Delta + \frac{1}{m(1-\alpha)}. \quad (4.16)$$

In Eq. (4.15)  $\gamma$  denotes the incomplete Gamma function<sup>1</sup>. Two limiting cases can be distinguished in the solution: first, for  $\alpha \rightarrow 0$  the classical power law dependence Eq. (4.12) is recovered. This analytic solution is illustrated in Fig. 4.6 for a Weibull distribution with  $m = 2$ , where a power law of  $D(\Delta)$  is apparent for  $\alpha < 0.9$ . However, for the limiting case of  $\alpha \rightarrow 1$ , we have to consider the behaviour of the argument  $\Delta_c$  of the analytic solution Eq. (4.15). For  $\alpha \approx 1$ , there will be a regime of  $\Delta$  values where the term  $1/(m(1-\alpha))$  dominates over  $\Delta$  resulting in a faster decay of the distribution  $D(\Delta)$  than any power. Still, for any values of  $\alpha$  in the limiting case  $\Delta \gg \Delta_c(\alpha)$ , the usual mean field power law behaviour Eq. (4.12) is asymptotically recovered. Avalanche size distributions  $D(\Delta)$  obtained from computer simulations at various different values of  $\alpha$  are presented in Fig. 4.7. In a good quantitative agreement with the analytic predictions, the numerical results can be well fitted by a power law of exponent  $5/2$  for moderate values of  $\alpha$ . However, for  $\alpha > 0.9$  strong deviations from the power law Eq. (4.12) can be observed for intermediate avalanche sizes  $1 \leq \Delta \leq 10^3$ , which appears to be an exponential decay. Although in the analytical solution the asymptotic power law behaviour is still visible for very large  $\Delta$ , see Fig. 4.6, computer simulations in Fig. 4.7 show solely a very steep decrease. It can be seen in the analytic solution in Fig. 4.6 that the relative frequency of avalanches of size  $\Delta > \mathcal{O}(10^3)$  is  $D = \mathcal{O}(10^{-30})$  for  $\alpha = 0.99$ , so it would require extremely large systems to count any such events. The size of the largest avalanche  $\Delta_{max}$  is plotted in Fig. 4.8 as a function of  $\alpha$ . Obviously,  $\Delta_{max}$  is a monotonically decreasing function of  $\alpha$  whose decrease gets faster in the regime where the distribution  $D(\Delta)$  exhibits the crossover to the faster decaying form.

An important consequence of the analytic solution Eqs. (4.15),(4.16) is that the characteristic avalanche size where the crossover occurs from a power law to a faster decaying exponential form also depends on the amount of disorder, i. e. the stronger the disorder is, the larger the crossover size gets at a given  $\alpha$ .

<sup>1</sup>There are several definitions of the incomplete Gamma function, we use  $\gamma(a, x) = \int_0^x e^{-t} t^{a-1} dt$ .

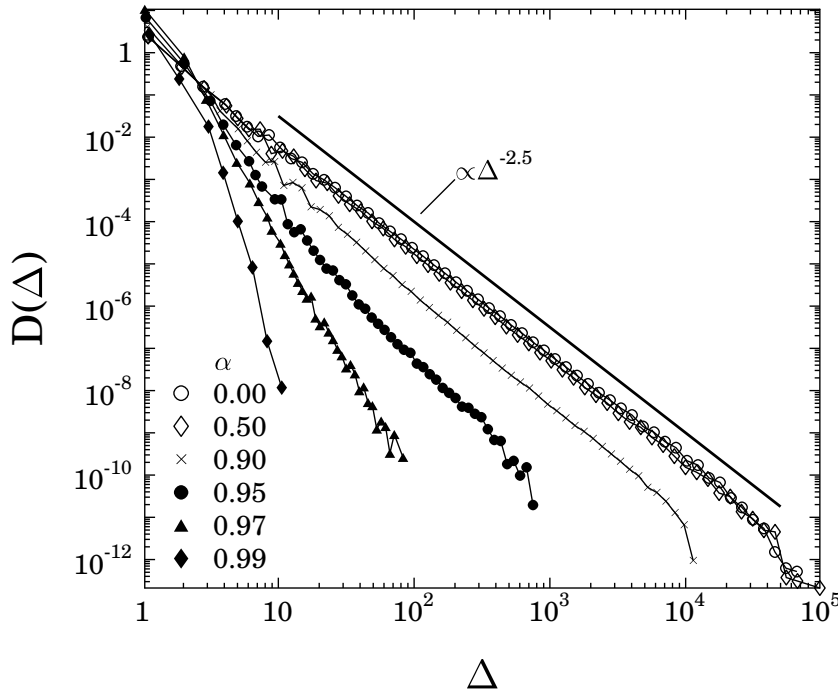


Figure 4.7: Distribution  $D(\Delta)$  of avalanches of size  $\Delta$  for various values of  $\alpha$  obtained by computer simulations for a system of  $N = 1.6 \cdot 10^7$  fibres with Weibull distributed failure thresholds  $m = 2$ . Satisfactory agreement is obtained with the analytic results presented in Fig. 4.6.

## 4.4 Local load sharing

From experimental and theoretical point of view, it is very important to study the behaviour of the plastic bundle when the interaction of fibres is localized. In the case of local load sharing (LLS) under stress controlled external loading conditions, the load dropped by the broken fibre is redistributed in a local neighborhood of the fibre giving rise to high stress concentration in the vicinity of failed regions. Stress concentration leads to correlated growth of clusters of broken fibres (cracks), which plays a crucial role in the final breakdown of the system, i. e. macroscopic failure of the bundle occurs due to the instability of a broken cluster which then triggers an avalanche of failure events where all the remaining intact fibres break. This effect typically leads to a more brittle constitutive behaviour of the system and the appearance of non-trivial spatial and temporal correlations in the damage process [75; 42; 29; 21].

In the plastic bundle, after a fibre breaks it still retains a fraction  $\alpha$  of its failure load  $\sigma_{th}$  so that only the amount  $(1 - \alpha)\sigma_{th}$  is redistributed over the intact fibres in the neighborhood. It implies that the load bearing broken fibres reduce the stress concentration around failed regions giving rise to stabilization which also affects the temporal and spatial evolution of damage during the loading process.

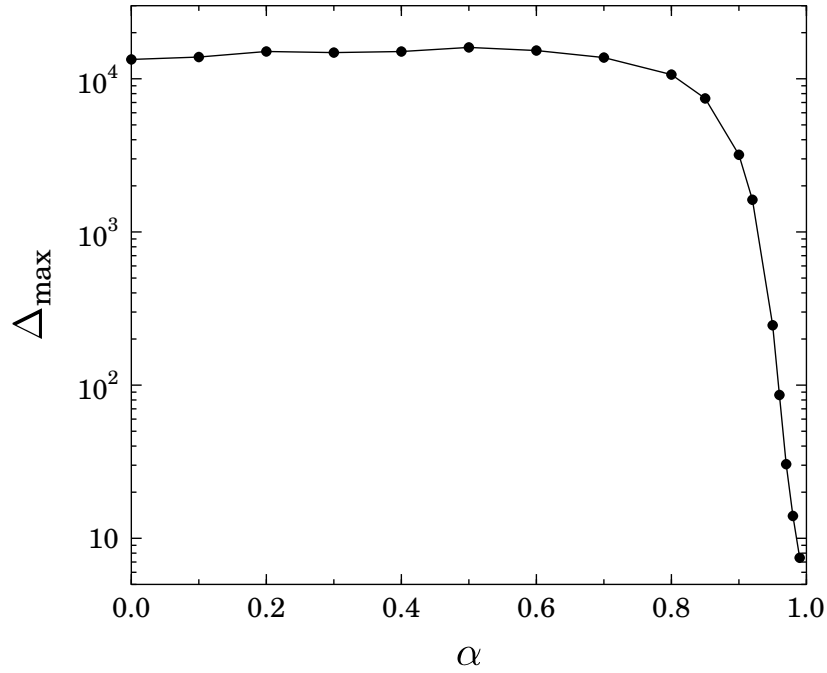


Figure 4.8: Size of the largest avalanche in a GLS simulation with a Weibull distribution of  $m = 2$ .

In the following we consider a bundle of  $N$  fibres organized on a square lattice of size  $L \times L$  with periodic boundary conditions. The fibres are assumed to have Weibull distributed strength Eq. (4.4), where the value of  $\lambda$  is always set to unity and for the Weibull modulus two different values are considered:  $m = 2$  (large disorder) and  $m = 4$  (smaller disorder). After a failure event the load dropped by the broken fibre  $(1 - \alpha)\sigma_{th}^i$  is equally redistributed over the nearest and next-nearest intact neighbors in the square lattice, i. e. the local neighborhood of a broken fibre contains at most 8 intact sites. Stress controlled simulations have been carried out for system sizes ranging from  $L = 33$  to  $L = 801$  varying the strength of plasticity  $0 \leq \alpha \leq 1$ .

#### 4.4.1 Macroscopic response

It has been shown for DFBMs where broken fibres carry no load, that the macroscopic response of the bundle when the interaction of fibres is localized follows the constitutive law of the corresponding GLS system with a reduced critical strain and stress, i. e. the *LLS* bundle behaves macroscopically in a more brittle way than its GLS counterpart [75; 21; 29]. Figure 4.9 shows the constitutive curve of a plastic bundle of size  $L = 401$  for several different values of  $\alpha$ . It can be observed that for  $\alpha \approx 0$  the constitutive curve exhibits the usual *LLS* behaviour, i. e. the macroscopic failure is preceded by a relatively short non-linear regime and global failure occurs in an abrupt manner. The position of the macroscopic failure defines the value of the critical strain  $\varepsilon_c^{LLS}$  and stress  $\sigma_c^{LLS}$ . It is very interesting to note that when  $\alpha$  is increased, the *LLS* constitutive curves practically

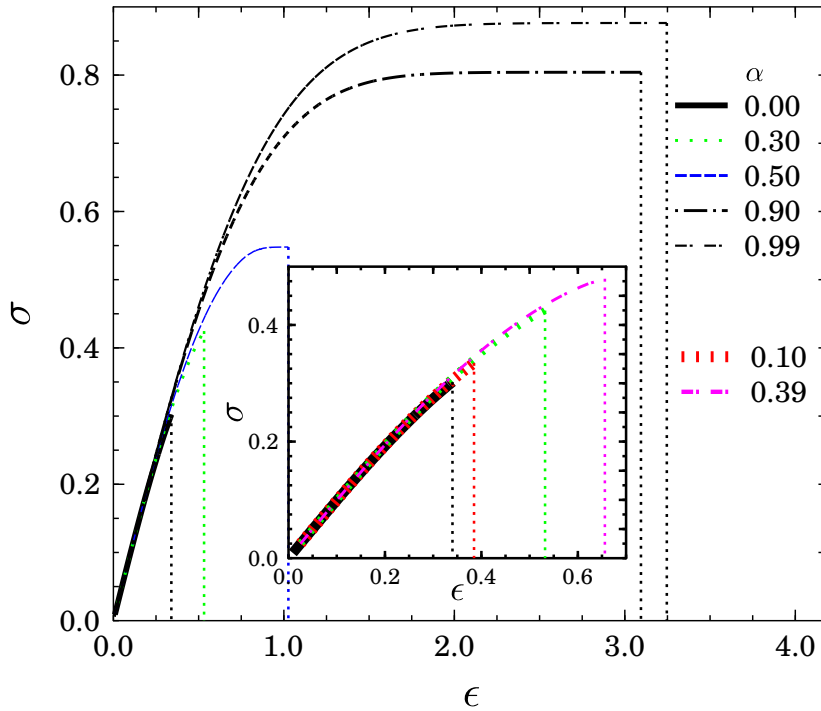


Figure 4.9: Constitutive law  $\sigma(\varepsilon)$  of the LLS bundle obtained by computer simulations of a system of size  $L = 401$  for several different values of  $\alpha$ . The inset shows a magnified view of  $\sigma(\varepsilon)$  for the regime  $\alpha < 0.4$ . For clarity, vertical lines indicate the location of macroscopic failure. For the breaking thresholds a Weibull distribution was used with  $m = 2$ .

recover the behaviour of the corresponding GLS system, i. e. for  $\alpha \geq 0.4$  the macroscopic failure occurs when reaching the plateau of  $\sigma(\varepsilon)$ .

The convergence of the LLS system to the GLS macroscopic behaviour is better seen in Fig. 4.10 where the relative difference of the critical stresses  $\sigma_c^{GLS}(\alpha)$  and  $\sigma_c^{LLS}(\alpha)$  of the global and local load sharing bundles is presented. It can be seen in the figure that there exists a threshold value  $\alpha_c$  of  $\alpha$  above which the macroscopic response of the LLS bundle becomes very close to the corresponding GLS system, while below  $\alpha_c$  the constitutive behaviour of the bundle changes continuously from the usual LLS response with a high degree of brittleness ( $\alpha = 0$ ) to the global load sharing behaviour. It seems that at  $\alpha_c$  a continuous transition occurs between the two regimes. The transition indicates that as a consequence of the reduction of stress concentration around failed fibres, the bundle can sustain higher external loads and is able to keep its integrity until the maximum of  $\sigma(\varepsilon)$  is reached.

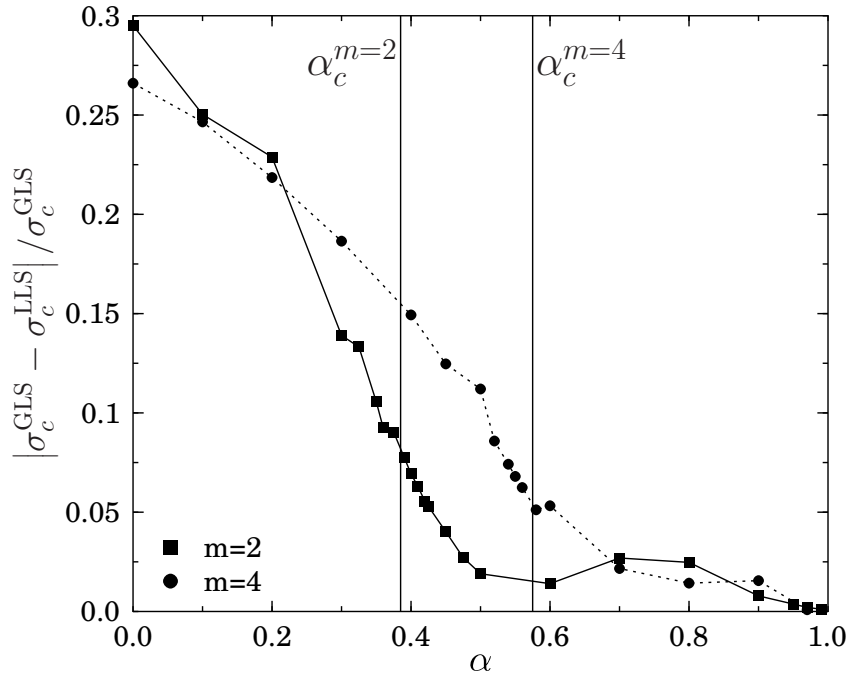


Figure 4.10: The relative difference of the critical stresses  $\sigma_c^{GLS}$  and  $\sigma_c^{LLS}$  of global and local load sharing systems as a function of  $\alpha$  for two different values of the Weibull modulus  $m$ . The vertical lines indicate the critical values of  $\alpha$ , which were obtained in Sec. 4.4.3.

#### 4.4.2 Bursts of fibre breakings

The evolution of the macroscopic response of the system with increasing  $\alpha$  is accompanied by interesting changes of the damage process on the micro-level, characterized by the avalanches of fibre breakings and the cluster structure of failed regions. The avalanche statistics presented in Fig. 4.11 shows remarkable features. For  $\alpha \approx 0$ , due to the high stress concentration around failed fibres, the LLS bundle can only tolerate small avalanches so that the avalanche size distribution  $D(\Delta)$  decays rapidly. With increasing  $\alpha$  the higher amount of load kept by broken fibres can stabilize the bundle even after larger bursts, hence, the cut-off of the distributions moves to higher values. It is interesting to note that also the functional form of the distribution  $D(\Delta)$  changes, i. e. when  $\alpha$  approaches  $\alpha_c$  the exponential cut-off disappears and the distribution becomes a power law

$$D(\Delta) \sim \Delta^{-\mu} \quad (4.17)$$

for large avalanches. The exponent  $\mu$  of the power law was determined numerically as  $\mu^{LLS} = 1.5 \pm 0.07$ , which is significantly lower than the mean field value  $\mu^{GLS} = 2.5$  [6]. Increasing  $\alpha$  above the critical point an exponential cut-off occurs and the power law regime of large avalanches gradually disappears. Comparing Fig. 4.11 to the corresponding GLS results presented in Fig. 4.7, it is apparent that above  $\alpha_c$  the LLS distributions  $D(\Delta)$  have the same functional form and follow the same tendency with increasing  $\alpha$  as

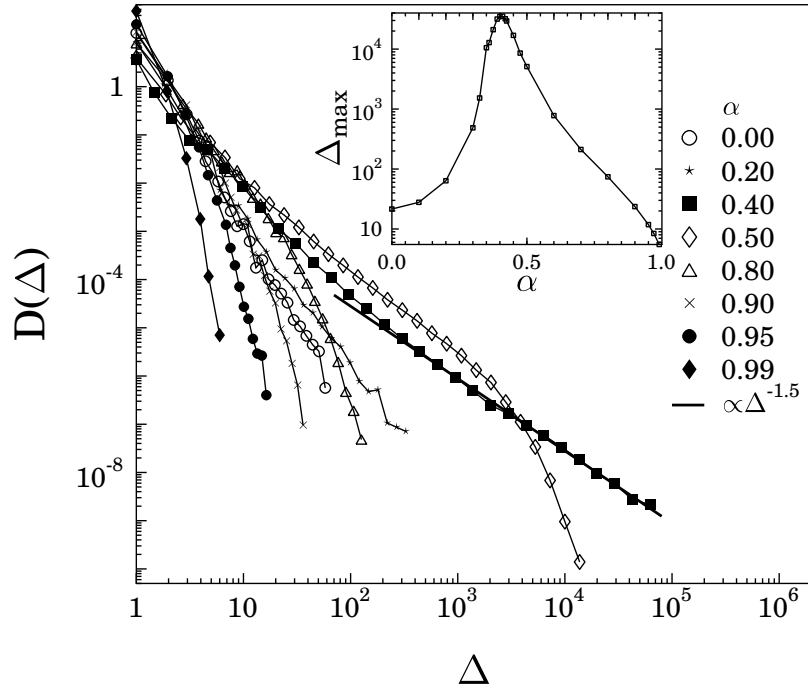


Figure 4.11: Avalanche size distributions  $D(\Delta)$  obtained by computer simulations for the system size  $L = 401$  with local load sharing, using Weibull distributed failure thresholds  $m = 2$ . The power law fit is demonstrated for  $\alpha = 0.4$ . In the inset the size of the largest avalanche  $\Delta_{max}$  is plotted versus  $\alpha$ .

the mean field results. It can be concluded that the avalanche statistics presents the same transitional behaviour between the local load sharing and mean field regimes as observed for the macroscopic response. The same value of  $\mu^{LLS}$  was obtained numerically for  $m = 4$ , indicating the universality of the exponent with respect to the strength of disorder. The transition is more evident in the inset of Fig. 4.11, where the size of the largest avalanche  $\Delta_{max}$  is plotted as a function of  $\alpha$ . The sharp peak indicates the transition point whose position defines  $\alpha_c$ , while in GLS the size of the largest avalanche  $\Delta_{max}$  was a monotonically decreasing smooth function (compare to Fig. 4.8).

### 4.4.3 Spatial structure of damage

Gradually increasing the external load in the fibre bundle, the weakest fibres break first in an uncorrelated manner. Since the load is redistributed solely over the intact neighbors of the broken fibre, the chance of fibre breakings increases in the vicinity of damage regions. This effect can result in correlated growth of clusters of broken fibres with a high stress concentration around their boundaries. The larger the cluster is, the higher stress concentration arises. Global failure of the bundle occurs when, due to an external load increment, one of the clusters becomes unstable and grows until all fibres break. The spatial structure of the damage emerging when the interaction of fibres is localized can be



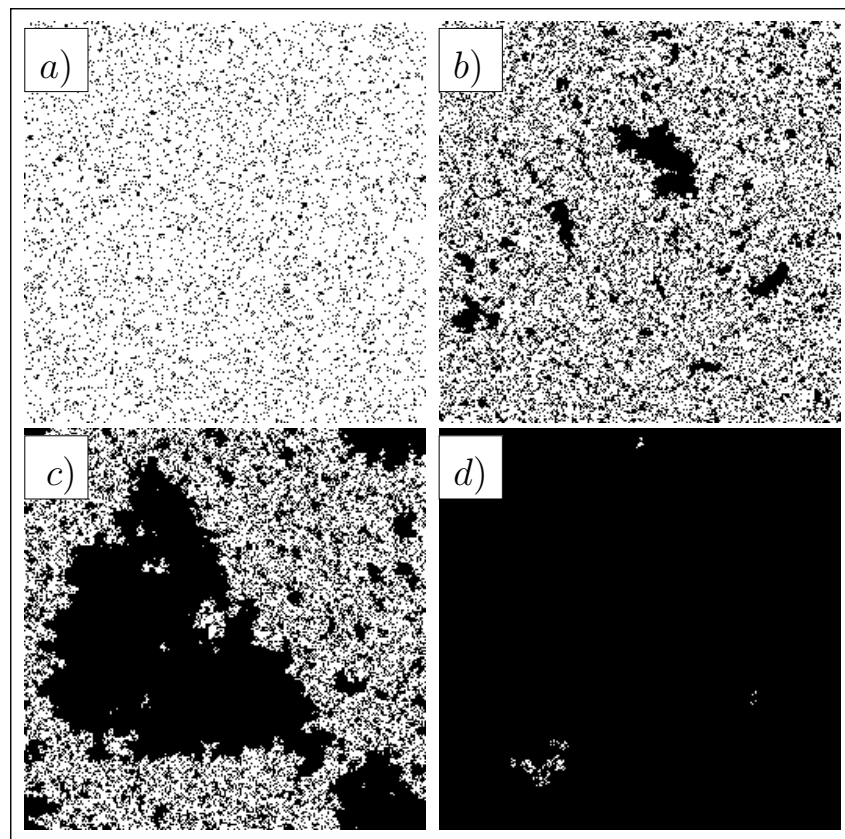


Figure 4.12: Latest stable configuration in LLS simulations of a system of size  $L = 401$ , with a Weibull strength distribution  $m = 2$  at different values of the control parameter  $\alpha$  (a) 0.0, (b) 0.35, (c) 0.4, (d) 0.6. The strength of the largest cluster  $P_\infty$  in the lattices are (a) 0.003, (b) 0.097, (c) 0.517, (d) 0.999. Broken and intact fibres are indicated by black and white, respectively.

characterized by studying the statistics and structure of clusters of broken fibres. Former studies of the limiting case of very localized interactions have revealed that the size of the largest cluster in the system is rather limited, furthermore, it is independent of the system size. Since the clusters are relatively small, merging of neighboring clusters does not occur frequently. The clusters themselves are found to be compact objects dispersed homogeneously over the cross section of the bundle [72; 48; 21].

In Fig. 4.12 the latest stable configuration of the bundle is presented just before catastrophic failure occurs at the critical load  $\sigma_c^{LLS}$  for several different values of  $\alpha$ . For  $\alpha \approx 0$  we note only small clusters of broken fibres as it is expected for LLS bundles (Fig. 4.12a). With increasing  $\alpha$ , these clusters grow and adjacent clusters can even merge further increasing the typical cluster size (Fig. 4.12b). Around the critical value of  $\alpha \approx 0.4$ , a *spanning cluster* of broken fibres seems to appear (Fig. 4.12c), whereas for higher values of  $\alpha > 0.4$  almost all fibres have failed (Fig. 4.12d) already by the time the critical stress is reached. The existence of very large clusters is the direct consequence of the increased load bearing capacity of broken fibres.

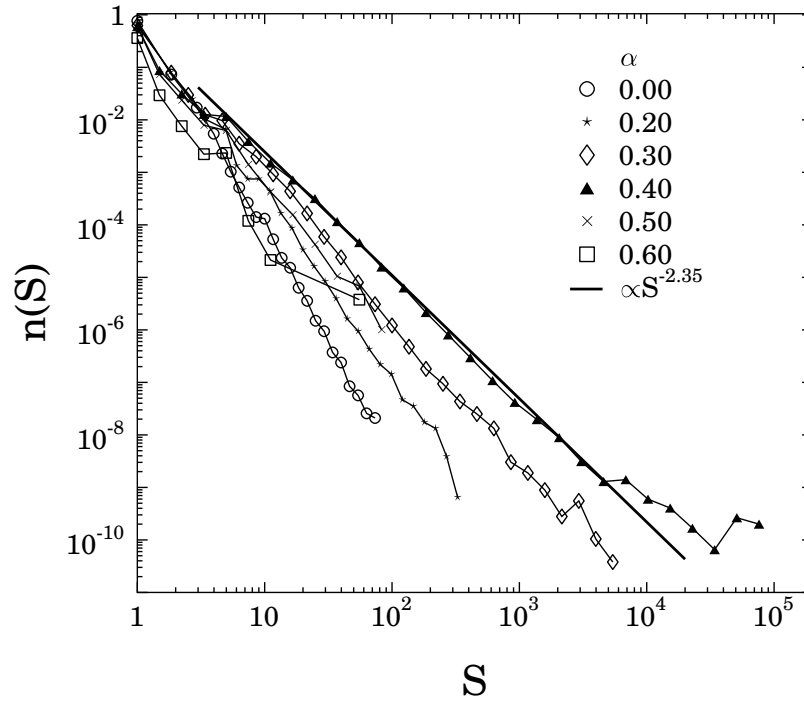


Figure 4.13: Distribution  $n$  of the size  $S$  of broken clusters in LLS simulations with a Weibull distribution  $m = 2$ , for different values of  $\alpha$ . The spanning clusters were excluded from the distributions for  $\alpha \geq 0.4$ .

Clusters of broken fibres were identified in the square lattice using the Hoshen-Kopelman algorithm. We evaluated the distribution of cluster sizes  $n(S)$  in the last stable configuration just before macroscopic failure occurs. The behaviour of  $n(S)$  shows again the transitional nature we have observed for other quantities. It can be seen again in Fig. 4.13 that a well defined  $\alpha_c$  exists which separates two regimes: for  $\alpha < \alpha_c$  the clusters are small and  $n(S)$  has a steep decrease. Approaching  $\alpha_c$ , the cluster size distribution  $n(S)$  tends to a power law

$$n(S) \sim S^{-\tau}, \quad (4.18)$$

where the value of the exponent was obtained as  $\tau = 2.35 \pm 0.08$  which is higher than the corresponding exponent of 2d-percolation on a square lattice  $\tau = 187/91 \approx 2.0549$  [92]. Note that in the regime where spanning clusters exist ( $\alpha \geq 0.4$ ), the distribution  $n(S)$  contains only the finite clusters.

In order to characterize the evolution of the cluster structure when  $\alpha$  is changed and to reveal the nature of the transition occurring at  $\alpha_c$ , we calculated the average cluster size  $S_{av}$  as the ratio of the second and first moments of the cluster size distribution

$$S_{av} = \frac{m_2}{m_1}. \quad (4.19)$$

The  $k$ -th moment  $m_k$  of the distribution  $n(S)$  is defined as

$$m_k = \sum_S S^k n(S) - S_{max}^k, \quad (4.20)$$

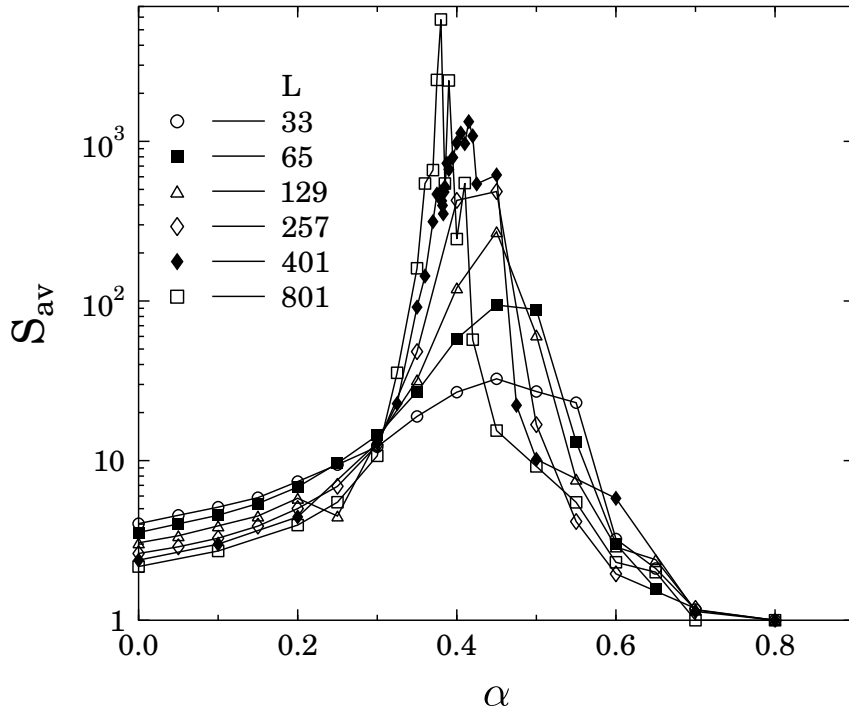


Figure 4.14: Average cluster size  $S_{av} = m_2/m_1$  as a function of  $\alpha$  for different system sizes  $L$ . Simulation results were obtained with a Weibull distribution  $m = 2$ .

where the largest cluster is excluded from the summation. Figure 4.14 presents  $S_{av}$  as a function of  $\alpha$  for different system sizes ranging from  $L = 33$  to  $L = 801$ . It can be seen in the figure that for each value of  $L$  the average cluster size  $S_{av}$  has a maximum at a well defined value of  $\alpha$ , which becomes a sharp peak with increasing  $L$ , i. e. the peak becomes higher and narrower for larger systems. The observed behaviour is typical for continuous phase transitions, where the position of the maximum defines the critical point of the finite size system. Based on the analogy to critical phenomena we tested the validity of the scaling law  $S_{av} \sim L^{\gamma/\nu} \phi((\alpha - \alpha_c)L^{1/\nu})$ , where  $\phi$  denotes the scaling function of  $S_{av}$  [93; 92]. The results presented in Fig. 4.15 were obtained by varying the values of the critical point  $\alpha_c$  and of the critical exponent of the susceptibility  $\gamma$ , and correlation length  $\nu$  until the best data collapse was reached. It can be observed in Fig. 4.15 that in the vicinity of the critical point  $\alpha_c$  a good quality data collapse is obtained using the values  $\alpha_c = 0.385 \pm 0.01$ ,  $\gamma = 2.0 \pm 0.15$ , and  $\nu = 1.0 \pm 0.1$ , where the critical exponents are only slightly different from the percolation exponents of  $\gamma = 43/18 \approx 2.389$  and  $\nu = 4/3 \approx 1.33$  in 2d [92].

At the critical point a spanning cluster of broken fibres occurs which is much larger than the other clusters. In order to characterize the strength of the spanning cluster we calculated the probability  $P_\infty(\alpha)$  that a failed fibre belongs to the largest cluster. For percolation the quantity  $P_\infty$  plays the role of the order parameter whose value distinguishes the phases of the system. Similarly to percolation lattices, we find numerically a sharp rise from  $P_\infty = 0$  to  $P_\infty = 1$  at  $\alpha_c \approx 0.4$ , see Fig. 4.16. When the system size  $L$  is increased

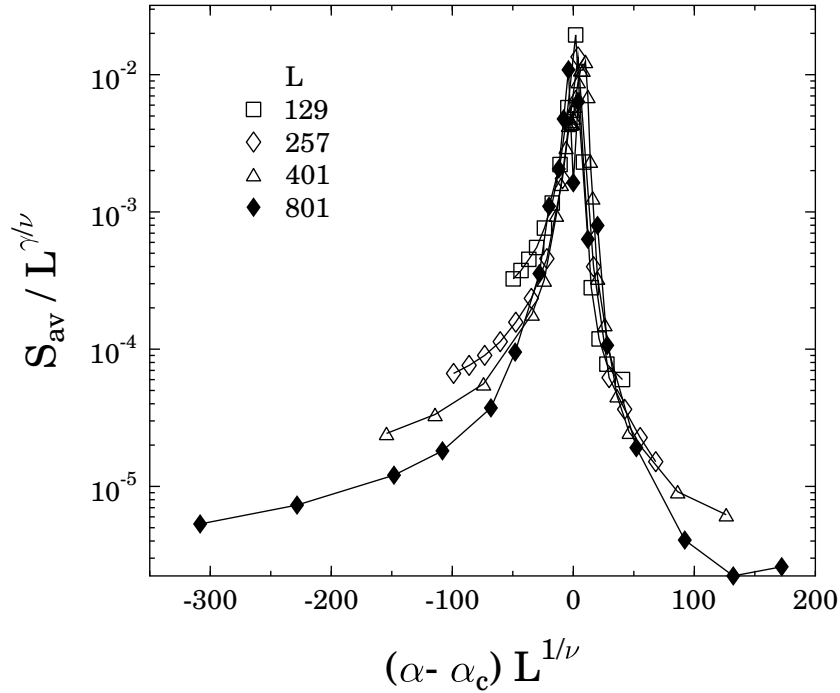


Figure 4.15: Finite size scaling of the average cluster size  $S_{av}$  presented in Fig. 4.14. The collapse of the curves enables us to determine the value of the critical exponents  $\gamma$  and  $\nu$  with a relatively good precision.

$P_\infty$  tends to a step function indicating that the transition becomes sharper. Assuming the scaling law  $P_\infty \sim L^{-\beta/\nu} \psi((\alpha - \alpha_c) L^{1/\nu})$  of the order parameter for finite size systems, where  $\psi$  denotes the scaling function and  $\beta$  is the order parameter exponent [93; 92], we re-plotted the data in Fig. 4.17. The good quality of the data collapse was obtained with the parameter values  $\alpha_c = 0.33 \pm 0.01$ ,  $\beta = 0.15 \pm 0.06$ , and  $\nu = 0.95 \pm 0.1$ . Note that the value of  $\nu$  agrees well with the one determined by the finite size scaling of the average cluster size  $S_{av}$ , larger deviations occur only for the critical point  $\alpha_c$ . The order parameter exponent  $\beta$  is compatible with the percolation value  $\beta = 5/36 \approx 0.13$

#### 4.4.4 Random crack nucleation versus crack growth

The failure mechanism of disordered materials and its relation to the amount of disorder has long been discussed in the literature [1; 24; 21; 84; 48; 62; 94; 83]. When the material has a low degree of disorder only a small amount (if any) of damage occurs prior to macroscopic failure. In this case even the nucleation of a single microcrack can lead to localization and abrupt failure of the system. Increasing the amount of disorder, the macroscopic failure is preceded by a larger and larger precursory activity, i. e. a large amount of damage accumulates and local breakings can trigger bursts of breaking events [6]. Since cracks nucleate randomly, the process of damage before localization resembles

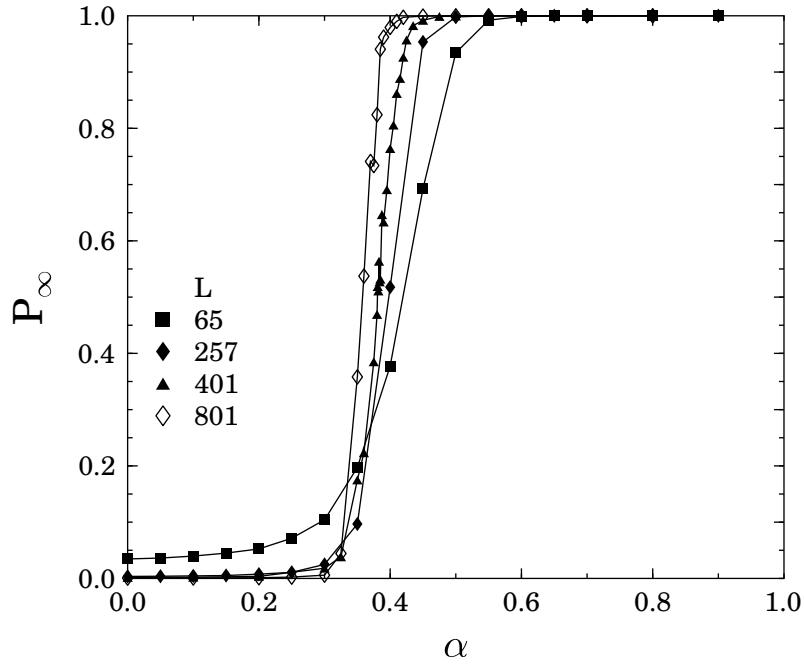


Figure 4.16: Order parameter  $P_\infty$  vs.  $\alpha$  for several system sizes  $L$  with the Weibull index  $m = 2$ .

percolation up to some extent. Stress concentration builds up around failed regions which might lead to correlated growth of the nucleated cracks [95; 21; 84; 61]. Increasing the strength of disorder, correlation effects become less dominating and in the limit of infinite disorder the damage accumulation process can be mapped to percolation [96].

We have shown above that in the plastic fibre bundle model (PFBM), the load bearing capacity of broken fibres has a substantial effect on the process of failure when the load redistribution is localized due to the reduction of the stress concentration along cracks. In order to give a quantitative characterization of damage accumulation in our model, we determined the fraction of broken fibres  $p_b$  at global failure  $\sigma_c$  as a function of the strength of plasticity  $\alpha$ . The quantity  $p_b$  can also be interpreted as the probability  $0 \leq p_b \leq 1$  that a randomly chosen fibre in the bundle is broken which makes it possible to compare the spatial structure of damage to percolation lattices [92] generated with the occupation probability  $p = p_b$  [1; 24; 29; 96]. The results are presented in Fig. 4.18 for the system size  $L = 401$  and Weibull parameters  $m = 2$  and  $m = 4$  plotting also the corresponding GLS results for comparison. In the case of local load sharing, when the failure load of fibres is almost entirely redistributed locally ( $\alpha \approx 0$ ) only a small damage can accumulate up to global failure  $p_b^{LLS} \approx 0.1 - 0.2$  keeping the integrity of the system. Comparing the curves of different Weibull indices  $m$  it follows that the stronger the disorder is, the larger amount of damage the system can tolerate at the same value of  $\alpha$ . In the vicinity of the respective  $\alpha_c$ , the breaking fraction  $p_b^{LLS}$  rapidly increases and converges to the maximum value  $p_b^{LLS} \approx 1$ , which implies that in the regime  $\alpha > \alpha_c$  practically no

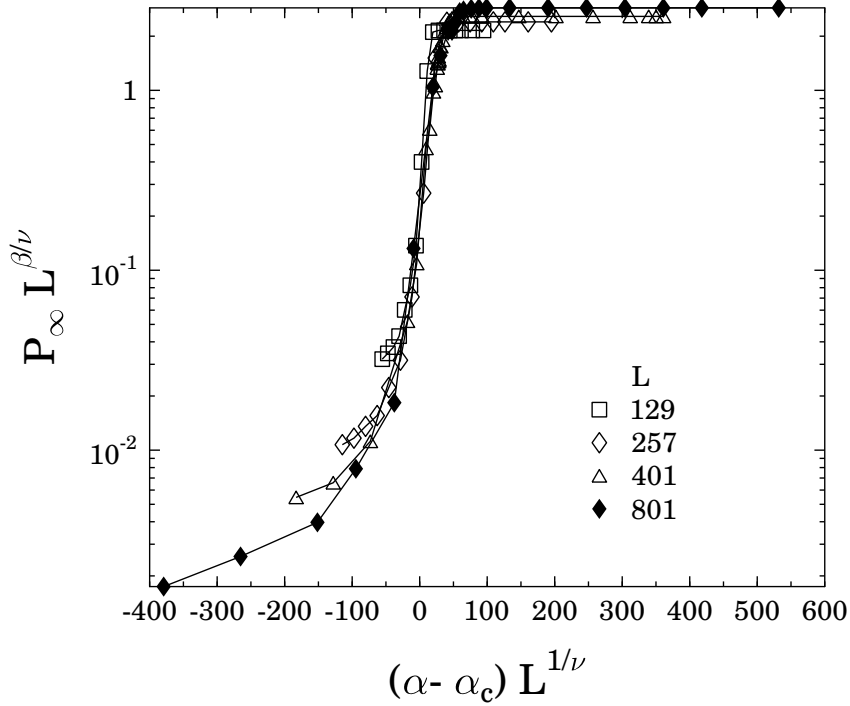


Figure 4.17: Finite size scaling of the order parameter  $P_\infty$  presented in Fig. 4.16. The parameter values used to obtain the best quality data collapse agree well with the ones determined by the finite size scaling of  $S_{av}$ .

localization occurs, the bundle can remain stable until almost all fibres break.

It is instructive to compare this behaviour to the case of GLS, where those fibres break up to the critical point whose breaking threshold falls below  $\sigma_c$ , hence,  $p_b^{GLS}(\alpha)$  can simply be obtained as  $p_b^{GLS} = P(\sigma_c(\alpha))$ . In Fig. 4.18 it can be seen that under global load sharing for  $\alpha \approx 0$  a significantly larger fraction of fibres fails without destroying the system than in the LLS bundle. The breaking fraction  $p_b$  is a monotonically increasing function of  $\alpha$  irrespective of the range of load sharing, however, in the vicinity of the critical point of LLS bundles  $p_b^{LLS}$  exceeds the smoothly rising GLS curves  $p_b^{GLS}$ . Note that depending on the threshold distribution  $P$  of fibres, even at  $\alpha = 0$  the value of  $p_b^{GLS}$  can be smaller or larger than the critical percolation probability  $p_c$  of the corresponding lattice type, since (contrary to fuse networks [83; 84] or discrete element models [90]) fracture in fibre bundles is not related to the appearance of a spanning cluster of failed elements. Varying  $\alpha$  as a control parameter, formally the GLS results could be perfectly mapped onto a percolation problem: at the critical value of the control parameter  $\alpha_c^{GLS}$  defined as  $P(\sigma_c(\alpha_c^{GLS})) = p_c$  a spanning cluster occurs, which has a fractal structure, the average size of finite clusters has a maximum at the critical point and the cluster size distribution exhibits gap scaling [92]. However, this percolation is not related to the point of failure of the GLS bundle, the analogy to percolation is based purely on geometrical properties without any physical relevance.

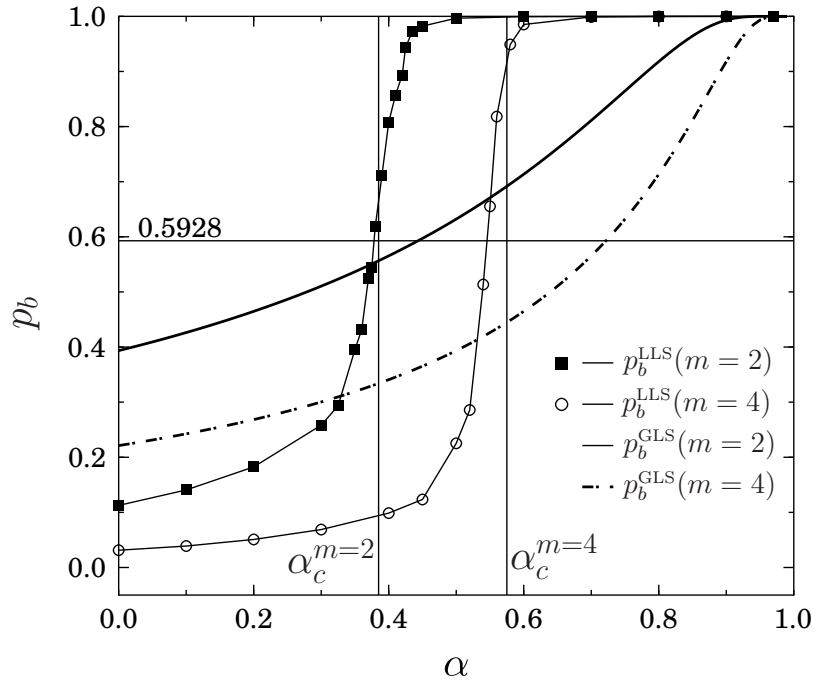


Figure 4.18: The fraction of broken fibres  $p_b$  at  $\sigma_c$  as a function of  $\alpha$  for fibre bundles of LLS and GLS with different strength of disorder  $m = 2$  and  $m = 4$ . The vertical line indicates the critical point obtained as the position of the maximum of the average cluster size (see Fig. 4.14). The critical probability of percolation  $p_c$  on the square lattice is indicated by the horizontal line. Note that for both disorder distributions in LLS, the location where  $p_b^{LLS}$  exceeds  $p_c$  practically coincides with the corresponding critical point  $\alpha_c$ , indicating the percolation nature of the transition.

Figure 4.18 shows that for localized load sharing the phase transition occurs when the damage fraction  $p_b^{LLS}$  reaches the critical percolation probability  $p_c$  of the corresponding lattice type. Due to the very localized load sharing, only short range correlations arise in the system which are further moderated by the finite load bearing capacity of broken fibres. Hence, in the vicinity of the transition point  $p_b^{LLS}(\alpha_c) \approx p_c$  holds and the evolution of the microstructure of damage shows strong analogy to percolation lattices. It can be seen in Table 4.1 that the critical exponents of the plastic fibre bundle model are slightly different from the corresponding exponents of percolation, furthermore, the usual scaling relations of percolation critical exponents [92] are not fulfilled within the error bars. It has been shown for percolation that correlated occupation probabilities lead to the same critical behaviour as random percolation when the correlations are short ranged [97; 98], however, long range correlations result in changes of the critical exponents [97]. It is interesting to note that the value of the correlation length exponent  $\nu$  of PFBM is smaller than the value of random percolation which is consistent with the presence of relevant correlations [97]. We would like to emphasize that contrary to global load sharing, this percolation like transition has important physical consequences on the behaviour of the fibre bundle. The failure process of the bundle is dominated by the competition of fibre breaking by local stress enhancement due to load redistribution and by local weakness

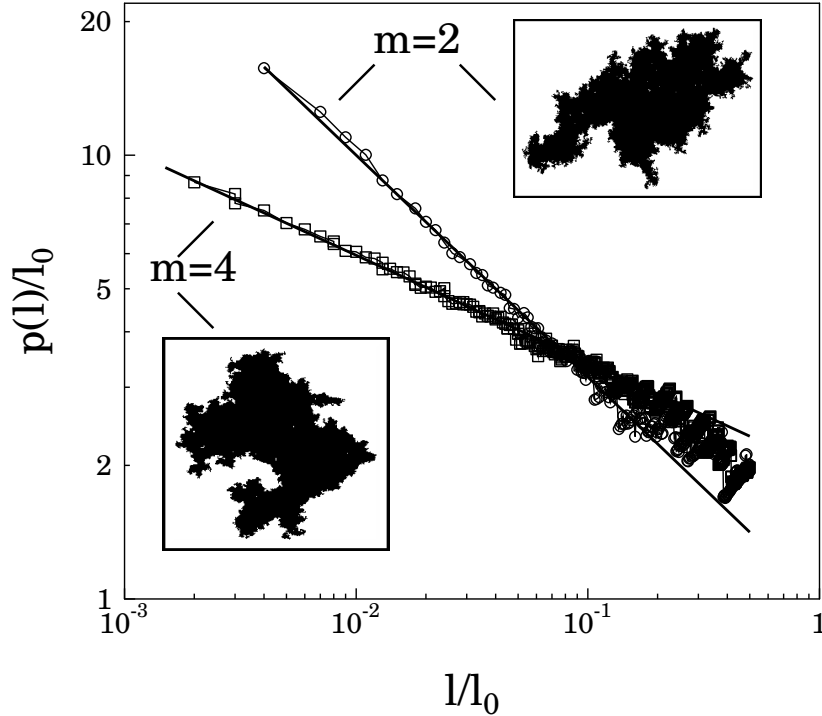


Figure 4.19: Structure of the spanning cluster at two different disorder strengths in a lattice of size  $L = 401$ . The perimeter length  $p(l)$  of the cluster is plotted as function of the length  $l$  of the yardstick normalized by the side length  $l_0$  of the inscribing square. The insets present the clusters analyzed.

due to disorder. Our detailed analysis revealed that the relative importance of the two effects is controlled by the parameter  $\alpha$ . Below the critical point  $\alpha < \alpha_c$  high stress concentration can develop around cracks so that the failure of the bundle occurs due to localization. Above the critical point  $\alpha \geq \alpha_c$  the macroscopic response of the LLS bundle becomes practically identical with the GLS constitutive behaviour showing the dominance of disorder. It is important to note that the size distribution of bursts of simultaneously failing fibres becomes a power law at the critical point  $\alpha_c$  with an exponent  $\mu$  equal to the value recently predicted for GLS bundles of so-called critical failure threshold distributions [56; 57], which is discussed for LLS systems in Chapter 5. This can be explained such that the large avalanches of power law distribution occurring in the plastic fibre bundle model at  $\alpha_c$  (see Fig. 4.11) are dominated by the strong fibres of the bundle whose strength distribution is close to critical [56; 57].

The structure of the spanning cluster of the LLS bundle formed at the critical point  $\alpha_c$  has also remarkable features different from the spanning cluster of percolation [92]. The insets of Fig. 4.19 present representative examples of the spanning cluster of a system of size  $L = 401$  at two different disorder strengths. It can be observed that the clusters are compact, they practically do not have holes, there are no islands of unbroken fibres in the interior of the cluster. This structure is a direct consequence of the merging of growing



Critical exponents	PFBM	Percolation
$\beta$	$0.15 \pm 0.06$	$5/36 \approx 0.13$
$\gamma$	$2.0 \pm 0.15$	$43/18 \approx 2.38$
$\tau$	$2.35 \pm 0.08$	$187/91 \approx 2.05$
$\nu$	$1.0 \pm 0.1$	$4/3 \approx 1.33$
$D$	2.0	$D = 91/48 \approx 1.896$
$D_p$	1.0 – 2.0	$7/4 = 1.75$
$\mu$ (Bursts)	$1.5 \pm 0.07$	–

Table 4.1: Summary of the critical exponents of the plastic fibre bundle model with local load sharing. For comparison the value of the corresponding critical exponents of percolation are also shown. For the perimeter fractal dimension  $D_p$  of PFBM, which depends on the amount of disorder, a range is given.

compact clusters where especially large stress concentrations arise between the cluster surfaces breaking the fibres and filling the holes in the spanning cluster. We note that in the limiting case of very strong disorder a small amount of intact fibres may survive dispersed over the spanning cluster. The result implies that the fractal dimension of the spanning cluster of the LLS bundle is 2, which should be compared to the corresponding value of random percolation  $D = 91/48 \approx 1.896$  where a finite amount of holes exists [92] even for short range correlated occupation probabilities [98]. The perimeter of the spanning cluster, however, has a fine structure, i. e. it has a large number of peninsulas and valleys of all sizes. To reveal the structure of the perimeter, we measured its length  $p(l)$  as a function of the length of the yardstick  $l$ . It can be seen in Fig. 4.19 that  $p(l)$  shows a power law dependence on  $l$  over almost two decades

$$p(l) \sim l^{-\delta_p}, \quad (4.21)$$

where the value of the exponent proved to be  $\delta_p = 0.5 \pm 0.03$  for a Weibull distribution of fibre strength with  $m = 2$ . The power law Eq. (4.21) indicates that the perimeter line is a fractal with a dimension  $D_p = 1 + \delta_p = 1.5 \pm 0.03$ . The upper bound of the scaling range in Fig. 4.19 can be attributed to the characteristic size of peninsulas of the spanning cluster, over which the rough structure of the perimeter disappears. Numerical calculations revealed that the fractal dimension of the cluster surface  $D_p$  is not universal, i. e. it depends on the strength of disorder of the breaking thresholds. The insets of Fig. 4.19 illustrate that a lower amount of disorder gives rise to a more regular, smoother cluster surface characterized by a lower value of  $D_p$ . For the Weibull index  $m = 4$  we obtained  $D_p = 1.24 \pm 0.05$ , which is significantly smaller than the corresponding value of  $m = 2$ . The surface of damage clusters should be compared to the hull of the spanning cluster of percolation with the fractal dimension  $D_p = 7/4 = 1.75$  [99] (see also Table 4.1).

## 4.5 Summary

We introduced a fibre bundle model where failed fibres retain a fraction  $0 \leq \alpha \leq 1$  of their failure load. The value of the parameter  $\alpha$  interpolates between the perfectly rigid failure  $\alpha = 0$  and perfect plasticity  $\alpha = 1$  of fibres. We carried out a detailed study of the effect of the finite load bearing capacity of fibres on the microscopic damage process and macroscopic response of fibre bundles considering both global and local load sharing for the load redistribution after fibre failure. Analytic calculations and computer simulations revealed that under global load sharing the macroscopic constitutive behaviour of the interface shows a transition to perfect plasticity when  $\alpha \rightarrow 1$ , where the yield stress proved to be the average fibre strength. Approaching the state of perfect plasticity, the size distribution of bursts has a crossover from the mean field power law form of exponent 2.5 to a faster exponential decay.

When the load sharing is localized it is found that the load carried by the broken fibres has a stabilizing effect on the bundle, i. e. it lowers the stress concentration around clusters of failed fibres which has important consequences on the microscopic process of fracture and on the macroscopic response of the bundle. Extensive numerical calculations showed that at a specific value  $\alpha_c$  a very interesting transition occurs from a phase where macroscopic failure emerges due to stress enhancement around failed regions leading to localization, to another phase where the disordered fibre strength plays the dominating role in the damage process.

On the macro-level, below the critical point  $\alpha < \alpha_c$  the fibre bundle shows a brittle response, i. e. the macroscopic failure is preceded by a weak non-linearity, while for  $\alpha \geq \alpha_c$  the constitutive behaviour of the LLS bundle becomes practically identical with the GLS counterpart. Analyzing the evolution of the micro-structure of damage with increasing  $\alpha$ , the transition proved to be continuous analogous to percolation. Computer simulations revealed that the avalanche size distribution of fibre breakings becomes a power law at the critical point with an universal exponent equal to the mean field exponent of bundles with critical strength distributions. The spanning cluster of failed fibres formed at the transition point proved to be compact with a fractal boundary whose dimension increases with the amount of disorder. The critical value  $\alpha_c$  is not universal, besides the lattice structure, it also depends on the strength of disorder.

The plastic fibre bundle model can be relevant for the shear failure of interfaces where failed surface elements can remain in contact still transmitting load. As an important application, a realization of glued interfaces is found in fibre composites. The finite load bearing capacity of failed elements of the model can account for the frictional contact of debonded fibre-matrix interfaces and also for plastic behaviour of the components.

## Chapter 5

# Local Load Sharing Fibre Bundles with a Lower Cutoff of Strength Disorder

In this chapter, we study the failure properties of fibre bundles with a finite lower cutoff of the strength disorder varying the range of interaction between the limiting cases of completely global and completely local load sharing. Computer simulations are employed to prove that at any range of load redistribution there exists a critical cutoff strength where the macroscopic response of the bundle becomes perfectly brittle, i. e. linearly elastic behaviour is obtained up to global failure, which occurs catastrophically after the breaking of a small number of fibres. As an extension of recent mean field studies [56], we demonstrate that approaching the critical cutoff, the size distribution of bursts of breaking fibres shows a crossover to a universal power law form with an exponent  $3/2$  independent of the range of interaction. A physically based analog of this cutoff is present in other types of FBM, where also a crossover appears, as in Sec. 4.4.2 of Chapter 4 and Sec. 6.3 of Chapter 6. The results in this chapter have been published in [100].

### 5.1 Critical Failure Threshold Distributions

For global load sharing it has recently been pointed out that the distribution of burst sizes significantly changes if the weak fibres are removed from the bundle: if the strength distribution of fibres has a finite lower cutoff, or analogously, if the recording of avalanches starts after the breaking of the weak elements, the burst size distribution is found to show a crossover to another power law with a significantly lower exponent  $3/2$  [56; 57]. The effective range of interaction in real materials may have large variations [29], therefore, in order to use the crossover effect of burst sizes in forecasting of imminent failure, its robustness with respect to the range of interaction has to be explored.

In the present discussion we extend recent mean field studies of the effect of the lower cutoff of fibre strength on the failure process of fibre bundle models [56; 57] by continuously varying the range of load sharing between the limiting cases of completely global load

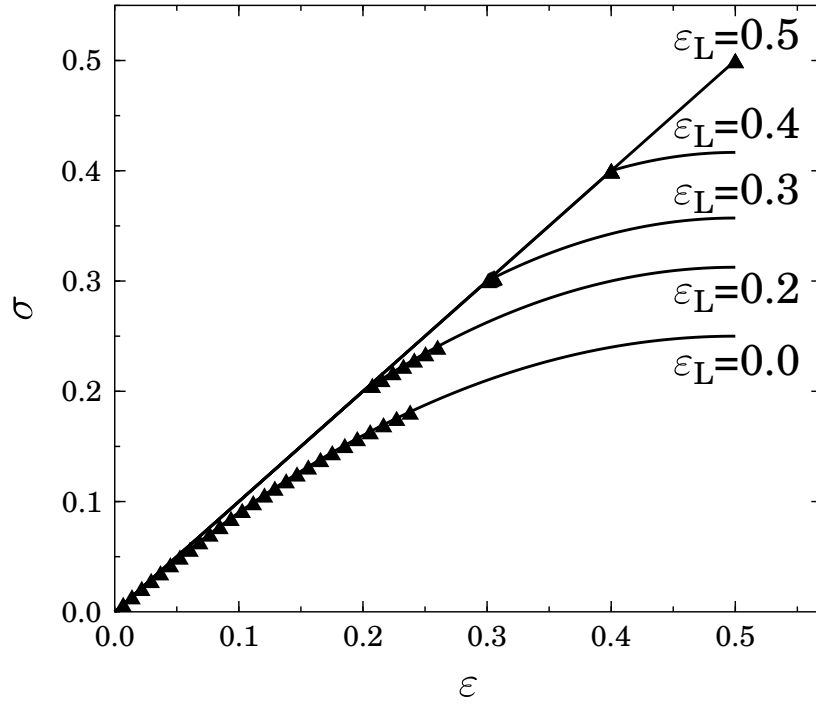


Figure 5.1: Constitutive curves for GLS  $\gamma = 0$  (lines) compared to the case of  $\gamma = 5$  (triangles) at different values of  $\varepsilon_L$ .

sharing and the very localized one [29]. We show that at any range of interaction there exists a critical value of the cutoff strength above which the global response of the bundle becomes perfectly brittle, as in the GLS case [61]. We demonstrate that the crossover of the avalanche size distribution to a power law of an exponent  $3/2$ , when approaching the critical cutoff strength, is independent of the range of interaction. Our results support the usage of the crossover phenomenon of burst sizes in forecasting techniques of imminent failure.

We consider a parallel bundle of fibres organized on a square lattice of size  $L \times L$ . The fibres are assumed to have linearly elastic behaviour with identical Young modulus  $E$  up to a randomly distributed breaking threshold. For simplicity, the failure thresholds  $\sigma_{th}$  are assumed to have a uniform distribution between a lower cutoff strength  $\sigma_L$  and one with the probability density function  $p(\sigma_{th})$  [101]

$$p(\sigma_{th}) = \begin{cases} \frac{1}{1-\sigma_L}, & \text{for } \sigma_L \leq \sigma_{th} \leq 1 \\ 0, & \text{otherwise.} \end{cases} \quad (5.1)$$

Under an increasing external load the fibres break when the load on them exceeds the local threshold value  $\sigma_{th}^i$ , where  $i = 1, \dots, N$  and  $N = L^2$  denotes the number of fibres. Due to the linearly elastic behaviour, the failure thresholds  $\sigma_{th}^i$  can also be expressed in terms of deformation  $\varepsilon_{th}^i = \sigma_{th}^i/E$  with the cutoff strength  $\varepsilon_L = \sigma_L/E$ . After a failure event, the remaining intact fibres have to take over the load of the failed one. In order to give a realistic description of the load redistribution in FBMs, we recently introduced a

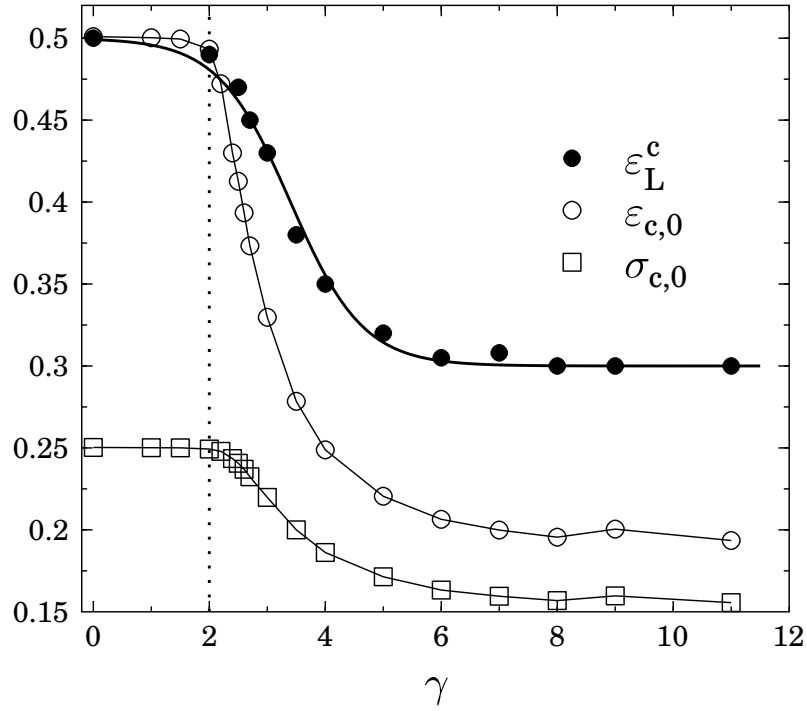


Figure 5.2: Failure stress  $\sigma_c$  and strain  $\epsilon_c$  of the fibre bundle model at zero cutoff  $\epsilon_L = 0$  compared to the critical cutoff  $\epsilon_L^c$  as a function of  $\gamma$ .

load transfer function of the form

$$\sigma_{add} = \frac{1}{Z} r_{ij}^{-\gamma}, \quad (5.2)$$

where  $\sigma_{add}$  denotes the additional load fibre  $i$  receives after the breaking of fibre  $j$  [29]. The load increment  $\sigma_{add}$  decreases as a power law of the distance  $r_{ij}$  from the failed fibre, where the exponent  $\gamma$  is considered to be a free parameter of the model. The exponent  $\gamma$  can take any values between 0 and  $\infty$  controlling the effective range of load redistribution between the limiting cases of completely global  $\gamma = 0$  and completely localized load redistribution  $\gamma \rightarrow \infty$  [29].

Under perfectly global load sharing  $\gamma = 0$  the macroscopic constitutive equation of the system can be cast in a simple analytic form

$$\sigma(\epsilon) = \begin{cases} E\epsilon & \text{for } E\epsilon \leq \sigma_L \\ E\epsilon \frac{1-E\epsilon}{1-E\epsilon_L}, & \text{for } \sigma_L \leq E\epsilon \leq 1, \end{cases} \quad (5.3)$$

where in the following, the value of the Young modulus of fibres will be set to unity  $E = 1$ . The constitutive behaviour Eq. (5.3) of the bundle is perfectly linear up to the deformation  $\epsilon_L$  since no fibres break in this regime (see also Fig. 5.1). Due to the breaking of fibres above  $\epsilon_L$ , the constitutive curve  $\sigma(\epsilon)$  becomes non-linear and develops a maximum whose value  $\sigma_c^{GLS}$  and position  $\epsilon_c^{GLS}$  define the failure stress and strain of the bundle, respectively. It follows from Eq. (5.3) that the critical strain is constant  $\epsilon_c^{GLS} = 1/2$  and

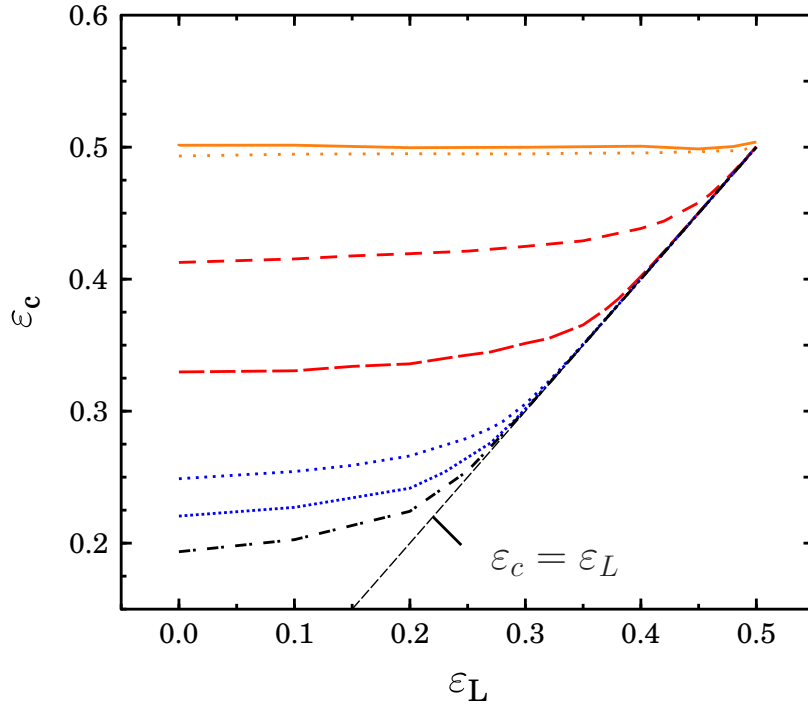


Figure 5.3: Critical deformation  $\varepsilon_c$  as a function of the cutoff value of failure strength  $\varepsilon_L$  for different values of the effective range of load sharing  $\gamma$  (see legend of Fig. 5.6 for the values of  $\gamma$ ).

does not depend on the cutoff strength  $\varepsilon_L$ , while  $\sigma_c^{GLS}$  increases due to the missing weak fibres [101]

$$\sigma_c^{GLS} = \frac{1}{4(1 - \varepsilon_L)}. \quad (5.4)$$

Increasing the external load quasi-statically, the breaking fibres trigger avalanches of failure events which either stop after a finite fraction of fibres failed, or become unstable and destroy the entire system. As a consequence, the cutoff strength  $\varepsilon_L$  can take meaningful values in the interval  $0 \leq \varepsilon_L \leq \varepsilon_c^{GLS}$ , since for  $\varepsilon_L \geq \varepsilon_c^{GLS}$  the breaking of the first weakest fibre results in an immediate catastrophic failure of the bundle.

We explore the effect of the finite cutoff strength  $\varepsilon_L$  on the failure process of FBMs with short ranged load sharing by means of computer simulations, redistributing the load of broken fibres according to the load transfer function Eq. (5.2). Stress controlled simulations were carried out on a square lattice of size  $L = 257$  with periodic boundary conditions varying the cutoff strength  $\varepsilon_L$  of the disorder distribution Eq. (5.1) in the interval  $[0, 0.5]$  at several different values of the effective range of interaction  $\gamma$  between 0 and 11. To characterize the failure process of the bundle at the macro and micro level, we determined the critical stress  $\sigma_c$  and strain  $\varepsilon_c$ , the distribution  $D$  of avalanche sizes  $\Delta$ , the average avalanche size  $\langle \Delta \rangle$ , and the average value of the largest avalanche  $\langle \Delta_{max} \rangle$ . For clarity, we first characterize the behaviour of the system in the specific case of zero

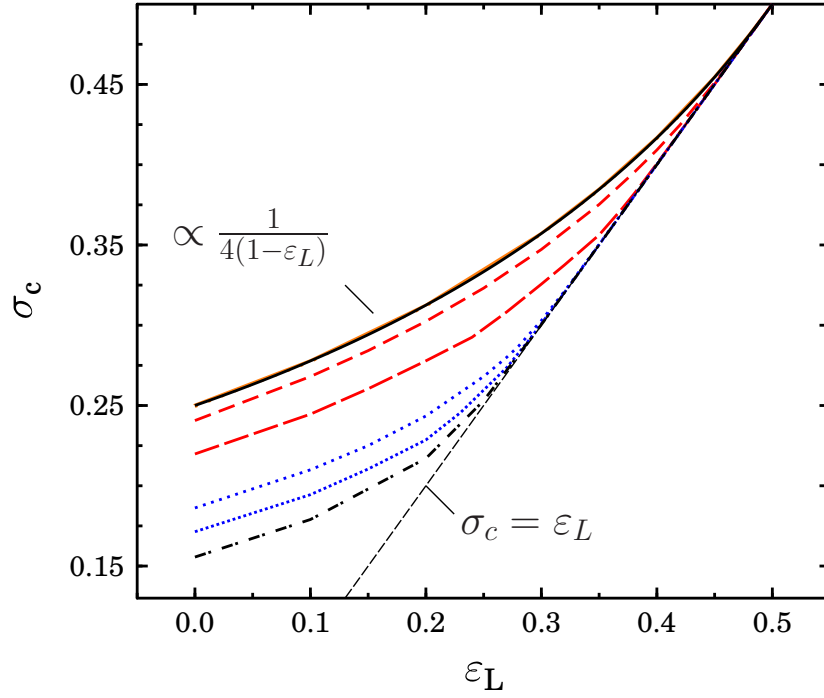


Figure 5.4: Critical stress  $\sigma_c$  as a function of the cutoff value of failure strength  $\varepsilon_L$  for different values of the effective range of load sharing  $\gamma$  (see legend of Fig. 5.6 for the values of  $\gamma$ ).

cutoff  $\varepsilon_L = 0$  by studying the critical stress  $\sigma_c$  and strain  $\varepsilon_c$  of the bundle as a function of  $\gamma$ , see Fig. 5.2. Based on the numerical results, three regimes of the failure of FBM can be distinguished in Fig. 5.2 depending on the range of load sharing: for  $\gamma \leq 2$  the range of interaction is infinite in the two dimensional embedding space, hence both  $\sigma_c$  and  $\varepsilon_c$  take their GLS values  $\sigma_c = 0.25$  and  $\varepsilon_c = 0.5$  independent of  $\gamma$  (see Eq. (5.4) at  $\varepsilon_L = 0$ ). Increasing the value of  $\gamma \geq 2$  the effective range of interaction gradually decreases which lowers the macroscopic strength  $\varepsilon_c$  and  $\sigma_c$  of the bundle. In the limiting case of  $\gamma \rightarrow \infty$  the model recovers the very localized load sharing, where  $\varepsilon_c$  and  $\sigma_c$  take again constant values. According to the numerical results, the perfectly localized limit is practically reached for  $\gamma \geq 6$ , so that in the interval  $2 \leq \gamma \leq 6$  a transition occurs between the completely global and completely local behaviour [29]. Fig. 5.1 demonstrates that for  $\gamma \leq 2$  (i. e. GLS) the macroscopic failure of the bundle is preceded by a strong non-linearity of the constitutive curve  $\sigma(\varepsilon)$ . At any wider range of load sharing,  $\gamma > 2$ , the  $\sigma(\varepsilon)$  curves follow the GLS solution Eq. (5.3), but with lower strength values which implies a more brittle macroscopic response for short ranged interactions.

Varying the cutoff strength  $\varepsilon_L$  at different values of  $\gamma$ , it can be seen in Figs. 5.3,5.4 that in the long range regime  $\gamma \leq 2$  both  $\varepsilon_c$  and  $\sigma_c$  agree well with the analytic predictions Eq. (5.4), i. e.  $\varepsilon_c = 1/2$  is constant while  $\sigma_c$  increases with increasing cutoff  $\varepsilon_L$ . When the load sharing becomes short ranged  $\gamma > 2$ , the increasing macroscopic brittleness has the consequence that the curves of  $\varepsilon_c(\varepsilon_L)$  and  $\sigma_c(\varepsilon_L)$  shift downwards as  $\gamma$  increases and

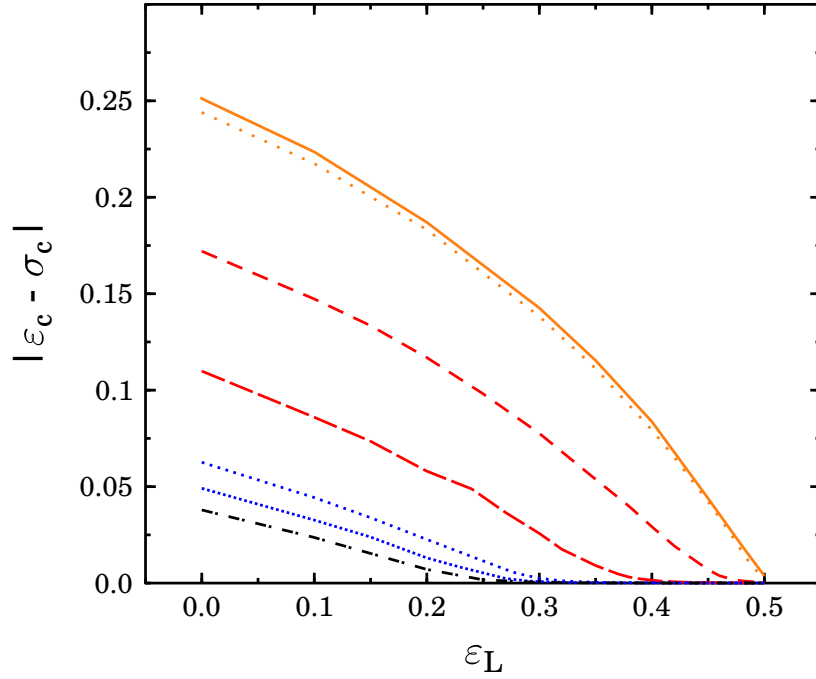


Figure 5.5: Difference  $|\varepsilon_c - \sigma_c|$  as a function of the cutoff value of failure strength  $\varepsilon_L$  for different values of the effective range of load sharing  $\gamma$  (see legend of Fig. 5.6 for the values of  $\gamma$ ).

tend to a limit curve when the interaction becomes completely localized for  $\gamma \geq 6$ . It is interesting to note that for short range interaction of fibres  $\gamma > 2$ , not only the failure stress  $\sigma_c$  but also the failure strain  $\varepsilon_c$  is an increasing function of  $\varepsilon_L$ . It is important to emphasize that at each  $\gamma$  there exists a critical value of the cutoff strength  $\varepsilon_L^c < \varepsilon_c^{GLS}$  where the failure stress  $\sigma_c$  and strain  $\varepsilon_c$  of the system become equal to the cutoff strength, i. e. at  $\varepsilon_L^c$  holds  $\varepsilon_c(\varepsilon_L^c) = \sigma_c(\varepsilon_L^c) = \varepsilon_L^c$ . At this point the macroscopic response of the bundle becomes perfectly brittle, i. e. under gradual loading of the system the macroscopic constitutive behaviour is linear up to  $\sigma_c$ , where the breaking of the weakest fibre gives rise to the collapse of the entire system (Fig. 5.1). This transition is better illustrated by Fig. 5.5 where the difference  $\delta = |\varepsilon_c(\varepsilon_L) - \sigma_c(\varepsilon_L)|$  is plotted versus  $\varepsilon_L$ . It can be observed that  $\delta$  monotonically decreases and becomes practically zero at  $\varepsilon_L^c$  of the given  $\gamma$ . Since the absence of weak fibres gives rise to a higher macroscopic strength, the value of  $\varepsilon_L^c$  is larger than the strength of the bundle  $\varepsilon_c$  and  $\sigma_c$  at zero cutoff (cf. Fig. 5.2).

On the microlevel, the failure process is characterized by the bursts of fibre breakings, which also show an interesting behaviour when the range of interaction  $\gamma$  and the lower cutoff  $\varepsilon_L$  are varied. In the GLS regime  $\gamma < 2$ , our computer simulations perfectly recover the analytical and numerical results of Refs. [56; 57] (see Fig. 5.7a): for  $\varepsilon_L = 0$  the size distribution of bursts  $D(\Delta)$  follows a power law

$$D(\Delta) \sim \Delta^{-\alpha}, \quad (5.5)$$

with an exponent  $\alpha = 5/2$ . Increasing the value of the cutoff  $\varepsilon_L$ , for small avalanches a



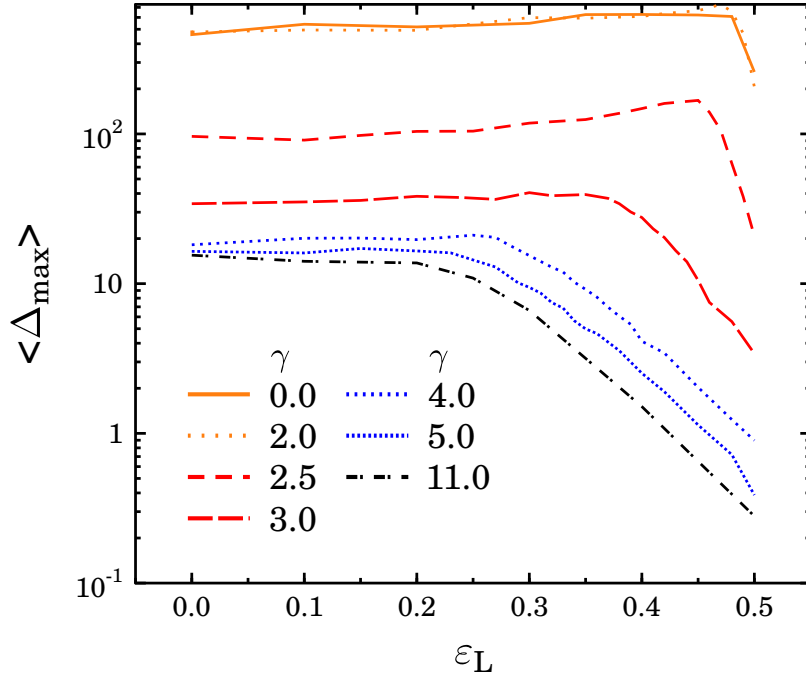


Figure 5.6: Mean size of the largest avalanche  $\Delta_{max}$  as a function of the cutoff value of failure strength  $\varepsilon_L$  for different values of the effective range of load sharing  $\gamma$ .

crossover occurs to a power law of a lower exponent  $\alpha = 3/2$ , while for large avalanches the original power law with  $\alpha = 5/2$  is retained. The crossover to a lower value of the exponent indicates that due to the missing weak fibres the fraction of small avalanches decreases compared to the larger ones. This argument is further supported by Fig. 5.6 and Fig. 5.8 which demonstrate that for  $\gamma \leq 2$  both the average size of the largest avalanche  $\langle \Delta_{max} \rangle$  and the average avalanche size  $\langle \Delta \rangle$  are monotonically increasing functions of the cutoff  $\varepsilon_L$ . However, when the load sharing gets short ranged  $\gamma > 2$ , both  $\langle \Delta_{max} \rangle$  and  $\langle \Delta \rangle$  have a maximum at the critical cutoff strength. The qualitative behaviour of the crossover avalanche size  $\Delta_c$  is equal to that of  $\langle \Delta \rangle$ : for  $\gamma > 2$ ,  $\Delta_c$  has a maximum at  $\varepsilon_L^c$ , and the height of the maximum decreases with increasing  $\gamma$ . It should be noted that the non-vanishing avalanche size above  $\varepsilon_L^c$  arises due to the strength fluctuations of the finite bundle so that above  $\varepsilon_L^c$  the bundle may survive a small number of avalanches instead of collapsing after the breaking of the weakest fibre. It is interesting to note that contrary to GLS, in the transition regime  $2 < \gamma < 6$ , the avalanche size distribution does not show a power law behaviour for small cutoffs  $\varepsilon_L \approx 0$ , however, when  $\varepsilon_L$  approaches the critical value  $\varepsilon_L^c(\gamma)$ , the distribution of burst sizes  $D(\Delta)$  tends again to a power law of an exponent  $\alpha = 3/2$  (Fig. 5.7b, c). For very localized interactions  $\gamma > 6$  an apparent power law of  $D(\Delta)$  is restored for  $\varepsilon_L \approx 0$  with a relatively high exponent  $\alpha \approx 9/2$ , in agreement with Ref. [75] (Fig. 5.7d). The main outcome of our computer simulations is that the crossover behaviour of  $D(\Delta)$  to the universal power law  $D(\Delta) \sim \Delta^{-3/2}$  prevails at any value of the range of interaction  $\gamma$  for the limiting case of  $\varepsilon_L \rightarrow \varepsilon_L^c(\gamma)$ , independently of the original form of  $D(\Delta)$  at zero cutoff  $\varepsilon_L = 0$  (see Fig. 5.7). In spite of the relatively large system size  $L$ , for short range interaction of fibres and  $\varepsilon_L \rightarrow \varepsilon_L^c(\gamma)$  the statistics of avalanche

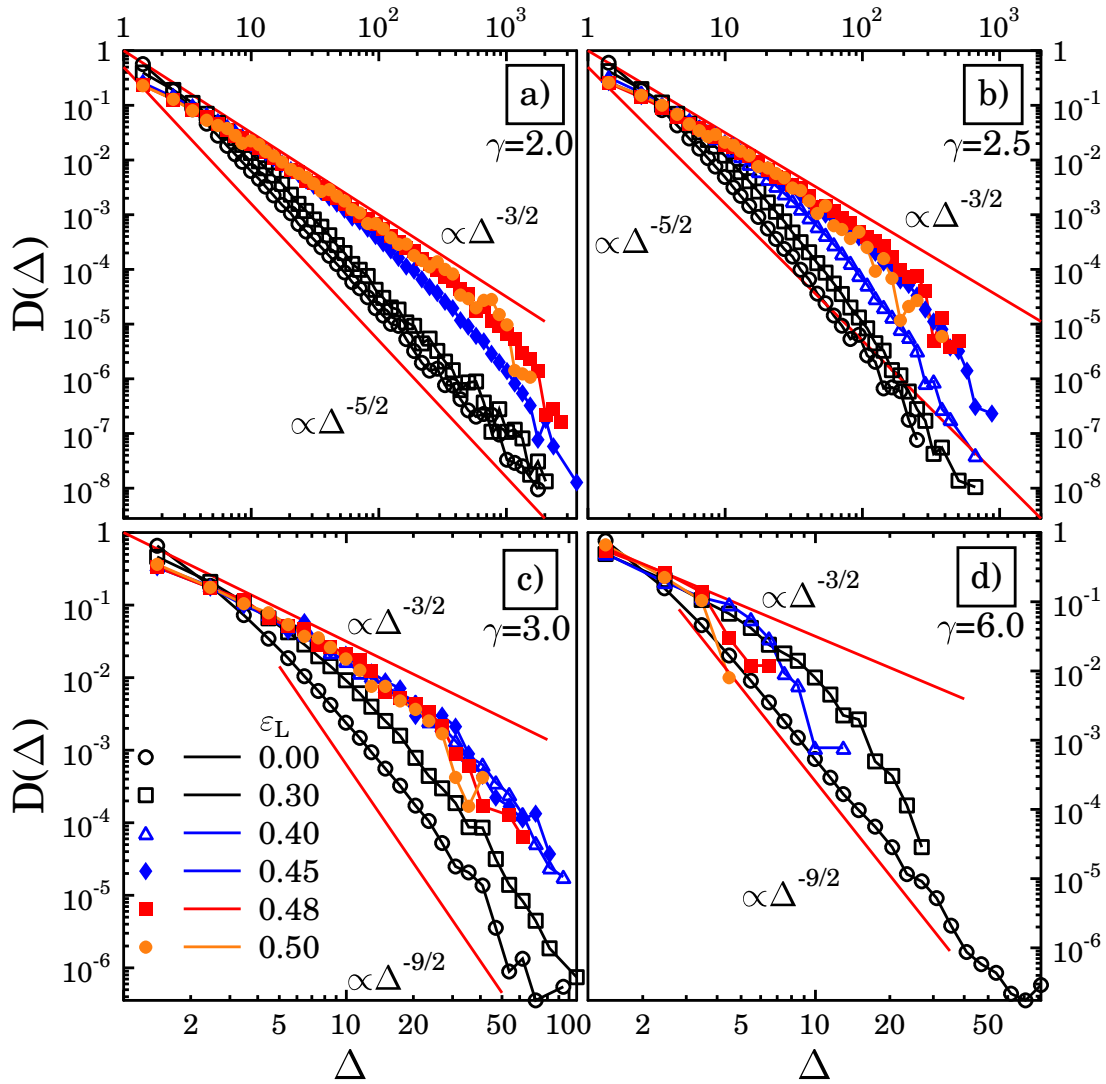


Figure 5.7: Distribution of burst sizes  $D(\Delta)$  varying  $\varepsilon_L$  at different values of  $\gamma$ : a) 2.0, b) 2.5, c) 3.0, d) 6.0. A Crossover behaviour of  $D(\Delta)$  can be observed as  $\varepsilon_L$  approaches the critical cutoff value  $\varepsilon_L^c(\gamma)$ .

sizes is rather poor for large avalanches which hinders us to make a definite conclusion on the shape of  $D(\Delta)$  in this  $\Delta$  regime.

## 5.2 Discussion

An interesting experimental realization of the crossover for crackling noise was very recently found in the magnitude distribution of earthquakes in Japan [102]. Analyzing the local magnitude distribution of earthquakes preceding main shocks, a significant decrease of the Gutenberg-Richter exponent was obtained when the lower bound of the time win-

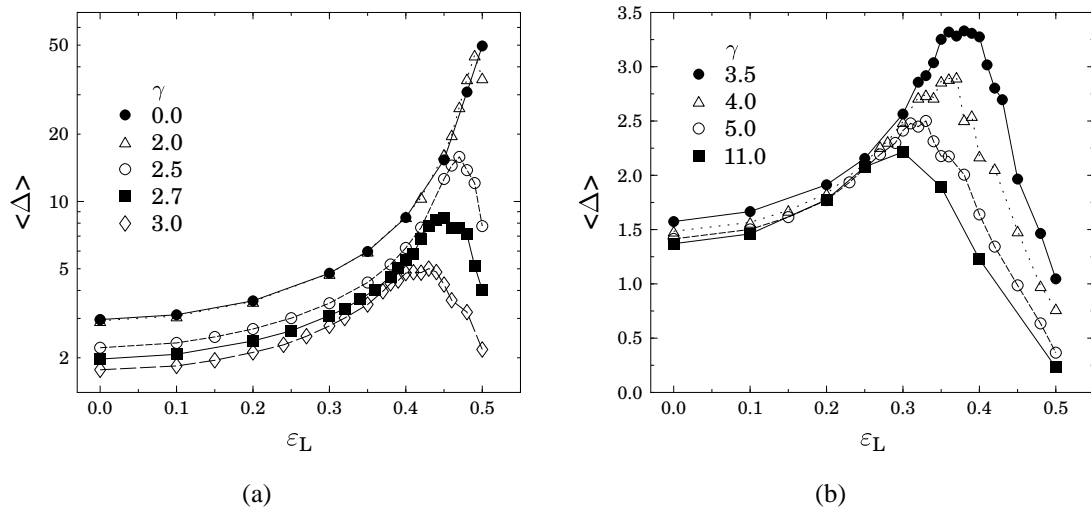


Figure 5.8: The average burst size  $\langle \Delta \rangle$  as a function of  $\varepsilon_L$  for different values of  $\gamma$ . (a)  $\gamma < 2$ , (b)  $\gamma > 2$ . In the short range regime  $\gamma > 2$ , where the average avalanche size  $\langle \Delta \rangle$  has a clear maximum which coincides with the critical cutoff strength  $\varepsilon_L^c$ .

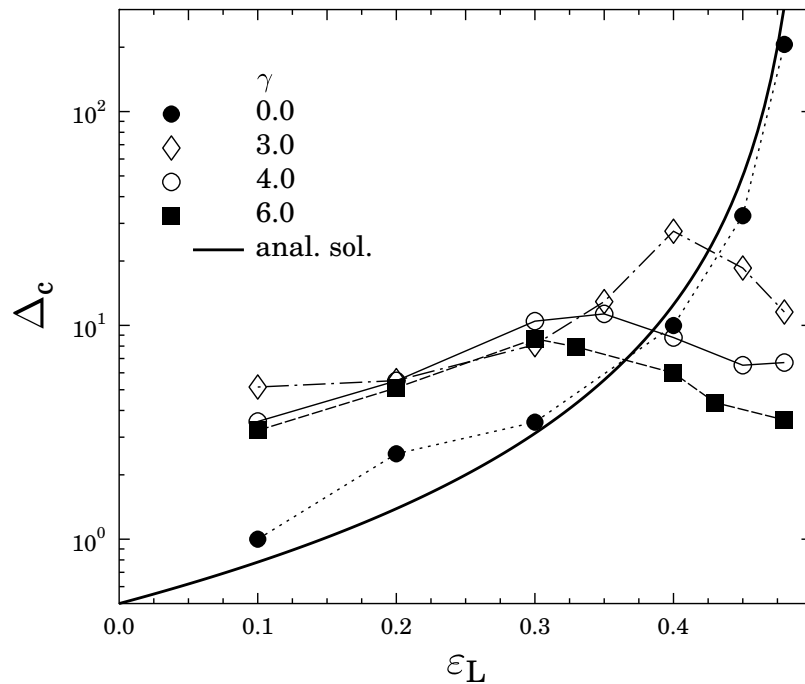


Figure 5.9: The crossover avalanche size  $\Delta_c$  and GLS analytical solution [8] as a function of  $\varepsilon_L$  for different values of  $\gamma$ .

dow of the analysis is shifted towards the catastrophic event [102]. Fracture of ferromagnetic materials is accompanied by changes of the magnetic flux, which can be recorded as magnetic noise and provides information on the dynamics of crack propagation [103]. The amplitude, area and energy of magnetic emission signals have recently been found to

have power law distributions with exponents depending on the type of fracture, i. e. ductile failure where stable crack propagation occurs in a large number of elementary steps is characterized by significantly higher exponents than brittle failure, where the crack propagates in an unstable catastrophic manner breaking the specimen in a few large jumps [103]. Our numerical results suggest that the reduction of non-linearity of the macroscopic response of materials preceding global failure when going from ductile and quasi-brittle to brittle fracture is responsible for the lowering of the crackling noise exponents on the micro-level.

In summary, we carried out computer simulations of the failure process of a bundle of fibres with a finite cutoff of the fibres' strength, continuously varying the range of interaction between the limiting cases of global and local load sharing. We showed that increasing the cutoff strength  $\varepsilon_L$  the macroscopic response of the fibre bundle becomes perfectly brittle when  $\varepsilon_L$  approaches a critical value  $\varepsilon_L^c(\gamma)$ , depending on the range of interaction  $\gamma$ . Our numerical results demonstrate the robustness of the crossover of the avalanche size distribution  $D(\Delta)$  to a universal power law of exponent  $3/2$ , irrespective of the range of interaction between the material elements.

# Chapter 6

## Extensions of the continuous damage model

### 6.1 Introduction

Materials with a highly disordered microstructure exhibit a variety of constitutive characteristics when subjected to an increasing external load—from perfectly brittle to perfectly plastic as well as strain hardening and softening. Experiments have revealed that even if the constituents are brittle, the macroscopic behaviour shows these variations, especially if a hierarchy of length scales can be identified in the specimen. A possible explanation of this observation is the influence of gradual degradation of material elements under loading, such that failure does not occur instantaneously, but after a finite number of degradation steps. The microscopic origin of this mechanism can be the accumulation of damage due to a growing population of nucleating microcracks, or the growth and arrest of a larger crack. A continuous damage fibre bundle model (CDFBM) has been developed in [21; 30], which can account for protracted failure of a single fibre—or constituent—of a material due to the activation of internal degrees of freedom. However, the conventional CDFBM does not capture two experimentally observable effects. First, the number of maximum failures or restructuring events of the material constituents is not a fixed number, but shows strong variations between samples. In fact, this is again an effect of disorder: the number of faults, defects and also particularly failure resistant spots in a material is a random variable, which becomes particularly important if the total number of these defects is small, such as the amount of knotholes in a wood sample. The second aspect that is not addressed so far by the CDFBM is the arrest of cracks: if a sample is stressed, cracks will evolve and propagate, and sometimes develop branches. Since the stress concentration around the tip of the crack increases with the crack length, cracks that grow larger than a certain critical size are unstable. However, cracks can also become arrested at strong locations inside the material. This phenomenon therefore requires the knowledge of the distribution of the strongest points in the sample, an issue that is related to order statistics. If there are subsequent cycles of crack arrest and release in a material under increasing external load, then the increasing stress concentration around the tip

of the growing crack demands that the subsequent arrest locations must have increasing strength; otherwise, they would be destroyed.

In order to address these issues, two additions to the CDFBM model will be discussed in this chapter. Both additions are compatible and can be combined in order to allow for a more realistic description of the experimental findings.

For the first extension, the maximum number of failure events for a single fibre can be a random variable subject to a Poissonian distribution. The constitutive behaviour will be explored by analytical methods, and simulations will be presented for the avalanche size distribution, so that a comparison to the case with a fixed number of maximum failures can be drawn. For the second model, the failure thresholds of subsequent failure events of a single fibre are considered to be random variables, which are however sorted in ascending order. Again, both analytical considerations and numerical calculations will be presented, and the comparison with the conventional CDFBM will produce some intriguing new features.

## 6.2 CDFBM with a randomly distributed number of maximum failures

In the CDFBM [21; 30], the damage law of the classical FBM is supplemented by a gradual degradation of fibre strength in the sequence of failure events. It was shown in [30] that for certain choices of the model parameters a variety of experimental situations can be recovered, i.e. either strain hardening or plasticity can occur. On the micro-scale, the size distribution of avalanche events shows a power law behaviour, but the exponent is different from the ordinary FBM, and for certain choices of parameters an exponential cutoff appears [30].

The CDFBM is constructed as follows: the bundle consists of  $N$  parallel fibres with identical Young-modulus  $E$  and random failure thresholds  $\sigma_{th}^i$ ,  $i = 1, \dots, N$  with a probability density  $p$  and distribution function  $P$ . Under loading, the fibres behave linearly elastic until they reach their respective point of failure and break in a brittle manner, i.e. as soon as the load on a fibre exceeds its breaking threshold  $\sigma_{th}^i$ , the fibre will fail. The failure law of the DFBM is now modified by assuming that at the failure point the stiffness of the fibre is reduced by a factor  $a$ , where  $0 \leq a < 1$ ; consequently the stiffness of the fibre after failure is  $aE$ . The loading of the fibre will then resume in a linear manner with the reduced stiffness until the next breaking threshold is reached. The parameter  $k_{\max}$  determines the maximum number of failures allowed for a single fibre. The damage threshold  $\sigma_{th}^i$  can either be kept constant for all the breakings (quenched disorder) or new failure thresholds of the same distribution can be chosen (annealed disorder) after each instant of failure, which can model a microscopic rearrangement of the material after failure, cf. cases (a) and (b) of Fig. 6.4 in Sec. 6.3.

We can assume that in an actual experimental situation, the number of times that a constituent of the material can break is an independent realization of an integer random vari-

able. A prime example is the fracture of wood, specifically of glued timber. Actually, only a few large defects and the finite number of glued joints determine the extreme statistics that governs the propagation and arrest of cracks, which will be discussed in Sec. 6.3. This fact can be incorporated by modeling  $k_{\max}$  as a random number, which is governed by a Poissonian distribution

$$n_{\kappa}(k_{\max}) = \frac{\kappa^{k_{\max}} e^{-\kappa}}{k_{\max}!}. \quad (6.1)$$

A new parameter then enters the model, which is the mean value of  $k_{\max}$ ,  $\kappa = \langle k_{\max} \rangle$ .

With this prescription, the constitutive curve can be expressed as

$$\sigma = \varepsilon \sum_{k_{\max}=0}^{\infty} \frac{\kappa^{k_{\max}} e^{-\kappa}}{k_{\max}!} \left[ \sum_{k=0}^{k_{\max}} a^k P_k(\varepsilon) \right], \quad (6.2)$$

i.e. the Poissonian distribution is convoluted with the previously obtained formula for the constitutive behaviour in the continuous damage model. In this section we will only deal with quenched disorder for the failure thresholds, which means that the probabilities  $P_k(\varepsilon)$  that at a given deformation  $\varepsilon$  a randomly chosen fibre has failed exactly  $k$  times is

$$P_k(\varepsilon) = \begin{cases} 1 - P(\varepsilon) & , k = 0; \\ P(a^{k-1}\varepsilon) - P(a^k\varepsilon) & , 1 \leq k \leq k_{\max}; \\ P(a^{k_{\max}-1}\varepsilon) & , k = k_{\max}. \end{cases} \quad (6.3)$$

The damage thresholds in this chapter will be drawn exclusively from a Weibull distribution with  $\lambda = 1$ ,  $m = 2$ , unless otherwise mentioned.

We can in principle also apply this model to the case of annealed disorder, where

$$P_k(\varepsilon) = \begin{cases} [1 - P(a^k\varepsilon)] \prod_{j=0}^{k-1} P(a^j\varepsilon) & , 0 \leq k \leq k_{\max} - 1; \\ \prod_{j=0}^{k_{\max}-1} P(a^j\varepsilon) & , k = k_{\max}, \end{cases} \quad (6.4)$$

however, we restrict this discussion to the quenched disorder case, although it should be stressed that the introduction of a Poissonian distribution factor to the case of annealed disorder is feasible and certainly meaningful. In Sec. 6.3, however, a new concept will be introduced which to a certain extent describes a third alternative to the cases of quenched and annealed disorder.

In the analytical solution for the constitutive behaviour, Eq. (6.2), two physically strongly distinct cases can be realized by appropriate choices of the summation limit of the innermost, bracketed term: if the summation extends from zero to  $k_{\max}$ , as indicated, the fibres will retain a residual stiffness after the limiting case of  $k_{\max}$  failures, i.e. hardening of the fibre bundle occurs in the limit of large  $\varepsilon$ , and the asymptotic behaviour of the bundle is described by

$$\begin{aligned} \sigma_{\text{asympt.}} &= \varepsilon \sum_{k_{\max}=0}^{\infty} \frac{\kappa^{k_{\max}} e^{-\kappa}}{k_{\max}!} a^{k_{\max}} \\ &= \varepsilon e^{-\kappa} (1 - a) \\ &= \varepsilon e^{-\kappa} (-a \varepsilon e^{-\kappa}). \end{aligned} \quad (6.5)$$

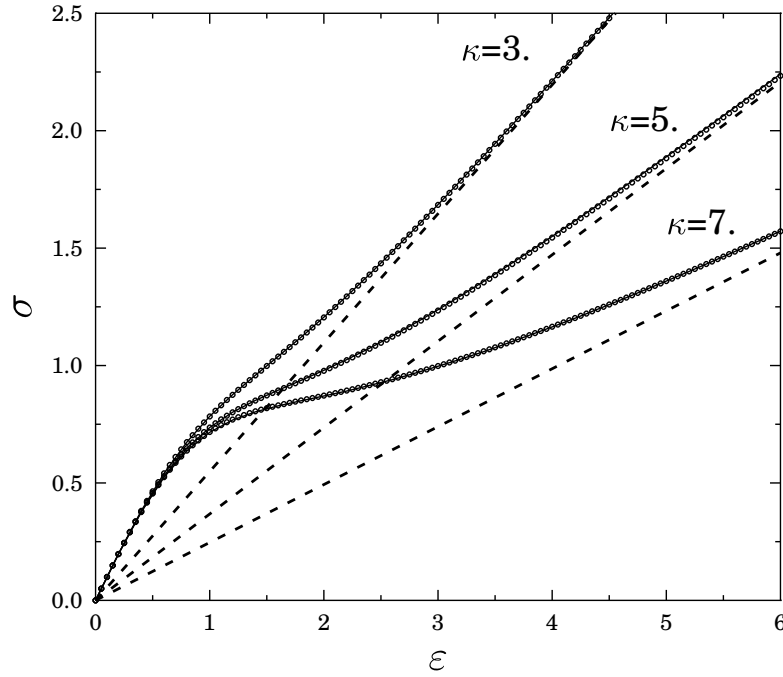


Figure 6.1: Constitutive behaviour for a fibre bundle with quenched disorder and Poisson distributed  $k_{\max}$  for three values of  $\kappa$ , in the presence of the residual stiffness term. Symbols: analytical solution, Eq. (6.2), solid lines: simulation results, dashed lines: asymptotic behaviour, Eq. (6.5).

Fig. 6.1 demonstrates the perfect agreement between the analytical solution, Eq. (6.2), and a strain controlled numerical simulation, where the asymptotic behaviour of Eq. (6.5) is recovered. In order to model the failure of materials, however, the failure law has to be slightly modified: after  $k^* = k_{\max} - 1$  failures, the load on a fibre must be set to zero, and the constitutive behaviour changes to

$$\sigma = \varepsilon \sum_{k_{\max}=0}^{\infty} \frac{\kappa^{k_{\max}} e^{-\kappa}}{k_{\max}!} \left[ \sum_{k=0}^{k^*} a^k P_k(\varepsilon) \right]. \quad (6.6)$$

Again, in this case the constitutive curves displayed in Fig. 6.2 show an excellent agreement between the analytical solution Eq. (6.6) and the simulation data. At first glance, the hardening behaviour that emerges after the main course of loading may appear to contradict the fact that residual stiffness is not explicitly taken into account and the terms  $P_k(\varepsilon)$  with  $k = k_{\max}$  are excluded in the failure law, Eq. (6.6); this regime is dominated by the fibres with  $k_{\max} = 0$ , i.e., fibres that never break, and since the expectation value of these fibres is  $n_{\kappa}(k_{\max} = 0) = e^{-\kappa}$ , the asymptotic behaviour even in the case without an explicit residual stiffness reads

$$\sigma_{\text{asympt}} = \varepsilon e^{-\kappa}. \quad (6.7)$$

Apparently, the dominance of the fibres with  $k_{\max} = 0$  diminishes with increasing  $\kappa$ , and at least for this choice of the disorder distribution, under stress controlled loading



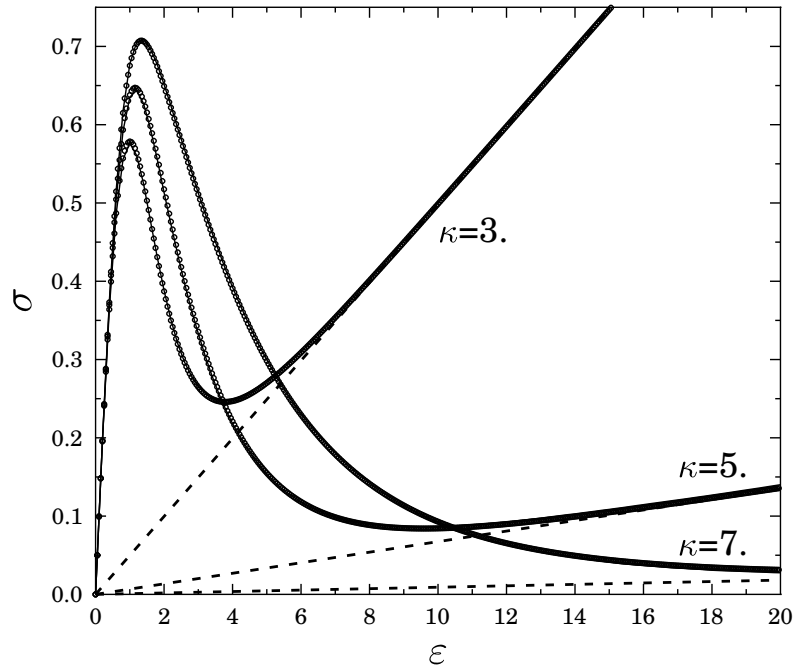


Figure 6.2: Constitutive behaviour for a fibre bundle with quenched disorder and Poisson distributed  $k_{\max}$  for three values of  $\kappa$ , in the absence of the residual stiffness term. Symbols: analytical solution, Eq. (6.2), solid lines: simulation results, dashed lines: asymptotic behaviour, Eq. (6.7), that is governed by fibres that never break with the distribution  $n_{\kappa}(k_{\max} = 0) = e^{-\kappa}$ .

the hardening regime cannot be accessed, i.e., all fibres break before traversing the local minima of the slope. One should note that —with or without a residual stiffness term— the fibres with vanishing  $k_{\max}$  can be excluded from both the simulations and the analytical calculations, in case of which the hardening behaviour in the second case will also disappear. The distribution  $n_{\kappa}(k_{\max})$  will not be purely Poissonian anymore, although we abstain from discussing this case in more detail.

Concerning the avalanche size distribution, this model reproduces the behaviour of the case of fixed  $k_{\max}$ , which has been discussed in [30]. There, it was found that for larger values of  $a$ , corresponding to  $a > 0.3$  for the Weibull distribution, the distribution can be fitted to a power law, the exponent of which also depends on  $k_{\max}$ . For small values of  $k_{\max}$ , the usual mean field behaviour with an exponent  $-5/2$  is obtained, whereas for larger values of  $k_{\max}$  a smaller exponent  $\approx 2.12$  appears. Examining the effect of the Poissonian term with a choice of  $\kappa = \langle k_{\max} \rangle$  corresponding to the ordinary CDFBM, we find in Fig. 6.3 a quantitative agreement between the two models, i.e. the Poissonian term causes no visible change to the avalanche statistics, and even the crossover between the two power law exponents is recovered.

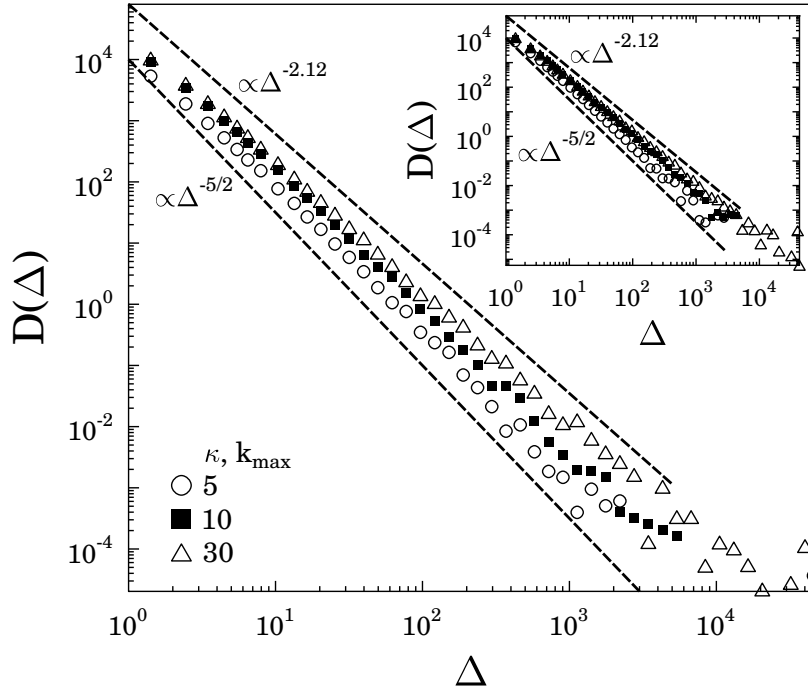


Figure 6.3: Avalanche size distribution for a fibre bundle of size  $L = 201$  with Poisson distributed  $k_{\max}$  for different values of  $\kappa$ . Inset: Avalanche size distribution for a fibre bundle of size  $L = 201$  with fixed  $k_{\max}$ , where the  $k_{\max}$  values shown correspond to the  $\kappa$  values of the main plot.

### 6.3 CDFBM with sorted failure thresholds

In highly disordered materials subjected to an increasing external load, in the early stages of loading cracks nucleate at the weakest locations in a spatially random manner. As the load increases, simultaneously to the nucleation of new microcracks the existing cracks propagate and become unstable. Advancing cracks can be arrested by high strength locations of the material. Before macroscopic failure occurs, advancing cracks can undergo several activation and arrest events. Since stress concentration at the crack tip increases as the crack becomes longer, arresting can only be realized by local materials of increasing strength. These growth and arrest events result in a gradual degradation of the macroscopic sample strength.

In order to provide a more realistic representation of this gradual degradation process sweeping through material elements in the increasing order of their local strength, we modify the CDFBM by considering a fixed number of allowed failures of single fibres  $k_{\max}$  with different threshold values. However, we sort the activation thresholds into increasing order. Fig. 6.4, case (c), provides a graphical illustration of the sorting and the ensuing damage law for a single fibre. It is important to emphasize that from a physical point of view this case is a mixture of the annealed and quenched disorder cases discussed previously [21]. On the one hand, the sorted model bears resemblance to annealed disorder, since the consecutive thresholds are different from each other; on the other hand,

it could also be classified as quenched as the thresholds are fixed in advance. Sorting of a series of random numbers imposes a correlation between these numbers, and we will have to resort to a mathematical theorem from the field of order statistics in order to obtain a complete understanding of the failure mechanism. It should be stressed that in the following discussion we will consider  $k_{\max}$  to assume a fixed value, although the addition of the randomly distributed  $k_{\max}$  can be trivially incorporated.

We want to motivate the aforementioned prescription by invoking the fibre bundle analogue of crack arrest. If a single fibre —seen as a meta-element representing smaller constituents— is to model the progress of a crack, which does not proceed continuously but comes to a halt at certain values of the fibres' strain  $\varepsilon$ , we may apply the damage law of the CDFBM, but impose the additional condition that the load on the fibre at subsequent instants of the arrest should increase. Hence we can draw the failure thresholds from a random distribution, for which we will use again the Weibull distribution, and store them in sorted order. As in the previous discussion, the Weibull distribution employed will have the parameters  $\lambda = 1$  and  $m = 2$ .

As mentioned before, bringing an array of  $n$  random numbers in sorted order necessarily invokes correlations between them, and the distribution of the random variant at the  $i$ th position is not governed by the PDF of the unsorted random numbers anymore. The mathematical field of order statistics deals with the statistical properties of sorted random numbers, and we will quote, with slight alterations, from [104] the following two theorems:

Let the continuous random variables  $X_1, \dots, X_n$  denote a random sample from a population with CDF  $F(x)$  and density  $f(x)$ . Let  $X_{(i)}, i = 1, \dots, n$  be the  $i$ th smallest of these sample observations. We refer to  $X_{(i)} \leq \dots \leq X_{(n)}$  as the order statistics for the random sample  $X_1, \dots, X_n$ . Unlike the  $X$ s themselves, the order statistics are neither mutually independent nor identically distributed.

Theorem: Let  $X_1, \dots, X_n$  be the order statistics for a random sample of continuous random variables from a distribution with CDF  $F(x)$  and density  $f(x)$ . The joint density for the order statistics is then:

$$g(x_{(1)}, \dots, x_{(n)}) = \begin{cases} n! \prod_{i=1}^n f(x_{(i)}) & , -\infty < x_{(1)} < \dots < x_{(n)} < \infty \\ 0 & , \text{elsewhere} . \end{cases} \quad (6.8)$$

Theorem: The marginal statistics for the  $j$ th order statistics  $X_{(j)}, 1 \leq j \leq n$ , under the conditions of the first theorem is

$$g_{(j)}(t) = \frac{n!}{(j-1)!(n-j)!} [F(t)]^{j-1} [1-F(t)]^{n-j} f(t), -\infty < t < \infty . \quad (6.9)$$

The latter marginal statistics is therefore the adequate replacement of the PDF, i.e. the distribution function for the random number at the  $j$ -th position, if  $n$  random numbers

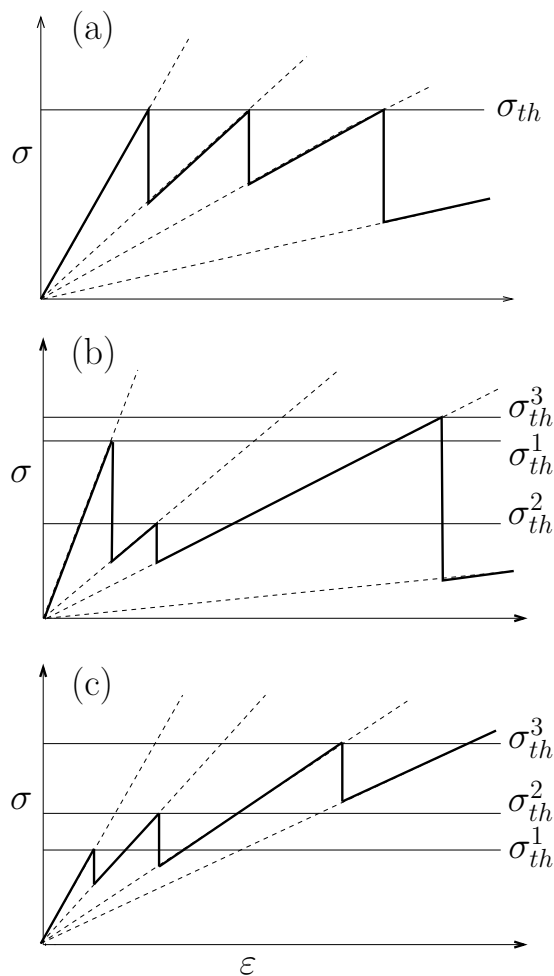


Figure 6.4: Damage law for a single fibre for the cases of quenched (a), annealed (b) disorder, cf. [21], and for the model with sorted thresholds (c). In all cases, after breaking of a fibre upon reaching a failure threshold  $\sigma_{th}^i$ , loading is resumed with a stiffness that is reduced by a factor  $a$ .

have been drawn. In order to illustrate this result, in Fig. 6.5 the marginal statistics for the  $j$ th random number,  $1 \leq j \leq n = 4$ , together with the underlying Weibull distribution with  $\lambda = 1, m = 2$  is shown. It is apparent from Fig. 6.5 that with increasing  $j$ , the marginal statistics share the peaked characteristics of the underlying PDF, and that the position of the maxima reflects the sorting. Also, the marginal statistics become wider with increasing  $j$ , although this effect is not too pronounced.

Having found an analytical expression for the marginal statistics, the constitutive behaviour of this model can be expressed in closed form. In analogy to the annealed case of

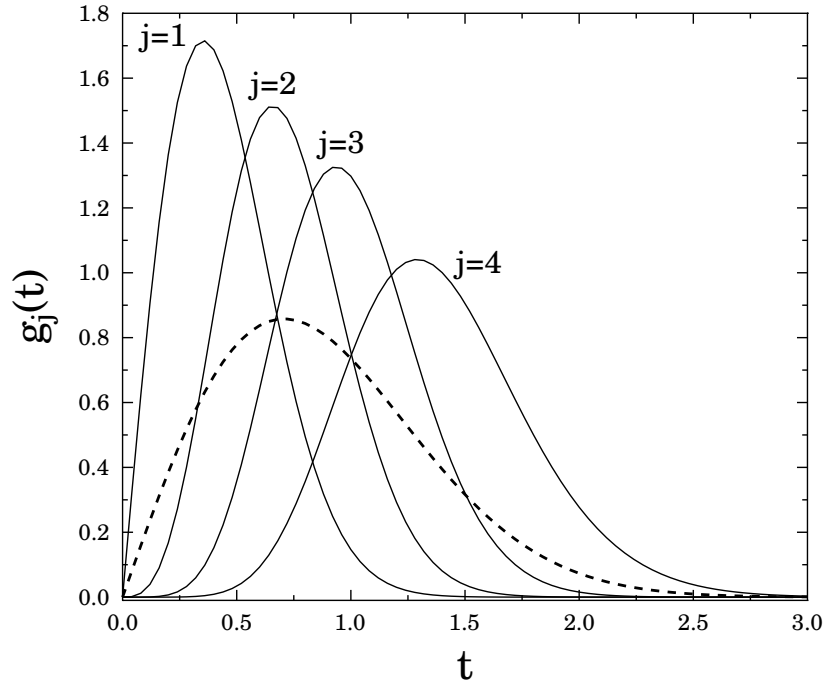


Figure 6.5: Marginal statistics for a Weibull distribution with  $\lambda = 1, m = 2$ , for the respective values  $j = 1, \dots, n = 4$  (solid lines), together with the underlying PDF (dashed line).

the CDFBM, we denote by  $P_k(\varepsilon)$  the probability that a fibre has failed exactly  $k$  times:

$$P_k(\varepsilon) = \begin{cases} [1 - G_{(k+1)}(a^k \varepsilon)] \prod_{j=0}^{k-1} G_{(j+1)}(a^j \varepsilon) & , 0 \leq k \leq k_{\max} - 1 \\ \prod_{j=0}^{k_{\max}-1} G_{(j+1)}(a^j \varepsilon) & , k = k_{\max} , \end{cases} \quad (6.10)$$

where

$$G_{(j)}(x) = \int_0^x g_j(t) dt \quad (6.11)$$

is the integral associated with the marginal statistics  $g_{(j)}(t)$ , corresponding to the CDF of unordered random numbers. The second case in Eq. (6.10) with  $k = k_{\max}$  corresponds to the residual stiffness of the bundle, again in close analogy to the ordinary CDFBM. With this result the constitutive behaviour reads, if the hardening term is skipped in order to account for material failure:

$$\sigma(\varepsilon) = \sum_{k=0}^{k_{\max}-1} a^k \varepsilon [1 - G_{(k+1)}(a^k \varepsilon)] \prod_{j=0}^{k-1} G_{(j+1)}(a^j \varepsilon). \quad (6.12)$$

We have therefore derived an analytical solution for the constitutive behaviour. It should be noted, though, that in the formula for the  $k$ -th failure probability  $P_k(\varepsilon)$ , Eq. (6.10),

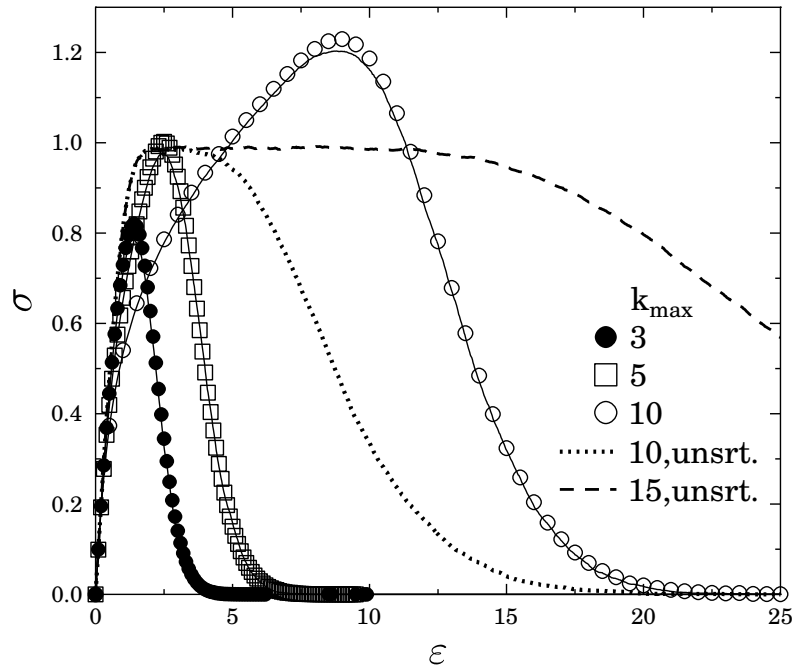


Figure 6.6: Constitutive curves for the model with sorted random thresholds, without residual stiffness. Solid lines; simulation results, symbols: analytical solution Eq. (6.12), dashed lines: simulations for the conventional CDFBM without sorting, shown for comparison. The failure thresholds are drawn from a Weibull distribution with  $\lambda = 1$ ,  $m = 2$ .

the integral Eq. (6.11) appears, which cannot in general be solved analytically due to the structure of the integrand, Eq. (6.9). In order to obtain the constitutive behaviour the integral Eq. (6.11) has to be evaluated numerically. In Fig. 6.6, the stress-strain curves obtained in this way are plotted for three values of  $k_{\max}$ . The agreement between the simulation results and the analytical solution, Eq. (6.12), is very good, although the numerical integration routine introduces some numerical error in the evaluation of the analytical solution, on which we will comment later.

It can be seen in Fig. 6.6 that contrary to the case of unsorted thresholds —whether quenched or annealed disorder is of no importance— that the constitutive curve does not develop a plateau, it always increases monotonically and has a quadratic maximum where macroscopic failure occurs. As a consequence of extreme order statistics, with growing  $k_{\max}$  the critical stress  $\sigma_c$  and strain  $\varepsilon_c$  increase, indicating a higher macroscopic load bearing capacity. It can be seen from the general expression of the constitutive curve, Eq. (6.12), that the macroscopic failure of the system is mainly controlled by the largest thresholds whose distribution can be obtained from Eq. (6.9), setting  $j = k_{\max}$ . Analyzing the constitutive behaviour of the system considering only the largest thresholds,  $j = k_{\max}$ , yields

$$\sigma_c \approx a\lambda [\ln(k_{\max} + 1)]^{1/m} \quad (6.13)$$

and

$$\varepsilon_c \approx a^{-k_{\max}}, \quad (6.14)$$

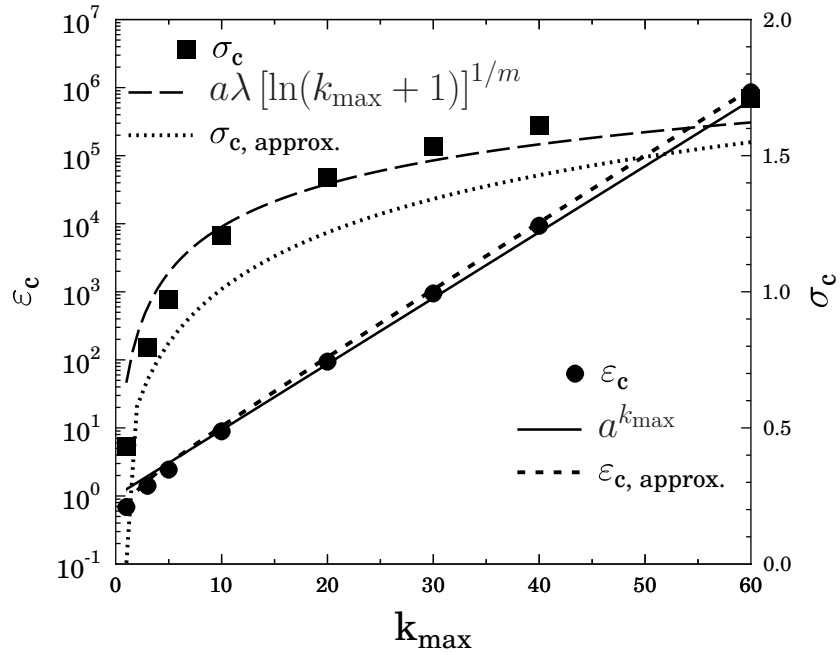


Figure 6.7: The critical stress  $\sigma_c$  and strain  $\varepsilon_c$  for a bundle with sorted random thresholds from a Weibull distribution with  $\lambda = 1, m = 2$  and without residual stiffness as a function of the maximum number  $k_{\max}$  of failures. The symbols represent simulation results, whereas the lines display evaluations of Eqs. (6.13,6.14) and numerically obtained maxima of Eq. (6.15) with the setting  $k = k_{\max}$ , respectively.

for the failure stress and strain, respectively, assuming Weibull distributed failure thresholds with parameters  $\lambda, m$ . Eq. (6.13) implies that the sorted CDFBM does not have a plastic limit as in the conventional CDFBM, i.e. no plateau of the  $\sigma(\varepsilon)$  emerges. Instead, the strength of the bundle is an asymptotically increasing function of  $k_{\max}$ , namely,  $\sigma_c$  increases logarithmically whereas  $\varepsilon_c$  increases exponentially with  $k_{\max}$ . This is illustrated in Fig. 6.7, where the values  $\sigma_c$  and  $\varepsilon_c$  obtained by computer simulations are compared to the analytical results.

For very high values of  $k_{\max}$ , a distinguished regime of ripples appears in the constitutive curves, see Fig. 6.8. This plot shows the constitutive behaviour in a stress controlled simulation with  $k_{\max} = 60$ , together with the avalanche sizes  $\Delta$  recorded at each loading step  $\varepsilon$ . Apparently, the constitutive curve displays a large amount of ripples with horizontal plateaus, which coincide with large scale bursts of breaking events. The position of the peaks suggests a regularity of some kind. In order to quantify this regularity of the peak events, the inset carries information about the ratios  $\varepsilon_{i+1}/\varepsilon_i$  of subsequent failure events  $\Delta$  with  $\Delta_i > 2000$ . Obviously, this ratio assumes a constant value of  $\approx 1/a$  after a brief onset period, where  $a = 0.8$  is the load reduction parameter used in all the simulations presented in this chapter, and a comparison with the case of  $a = 0.7$  is presented in order to confirm the influence of the load reduction parameter. It should also be noted that the envelope of the constitutive curve remains monotonically increasing. In order to analyze this rippling phenomenon an investigation on the evolution of the breakdown process is

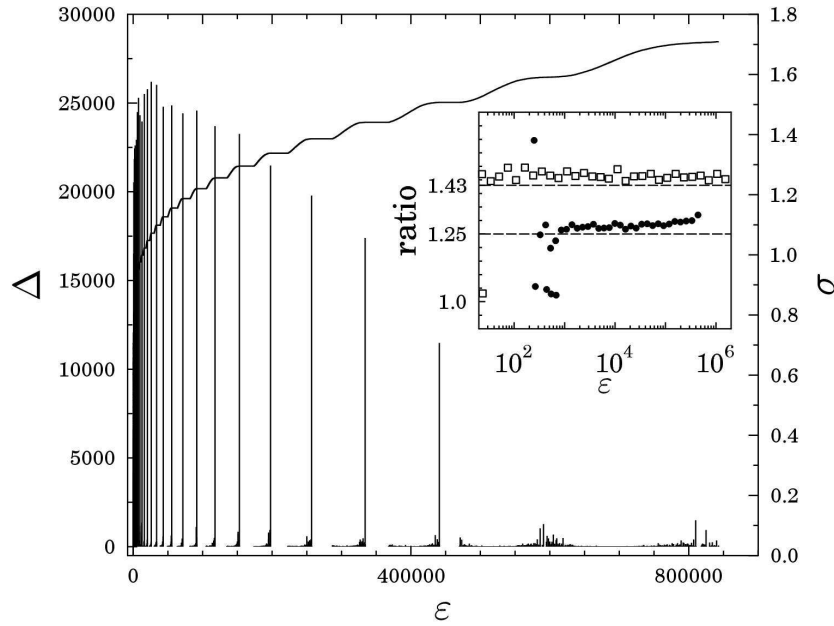


Figure 6.8: Constitutive curve (solid line) and avalanche sizes without residual stiffness as a function of strain  $\varepsilon$  for  $k_{\max} = 60$ ,  $m = 2$ . Inset: ratio  $\varepsilon_{i+1}/\varepsilon_i$  for subsequent bursts with  $\Delta_i > 200$ , for the values  $a = 0.7$  (unfilled circles) and  $a = 0.8$  (filled squares), where the lines indicate the respective values of  $1/a$ .

necessary.

In fact, an analytical argument can be made about the origin of these ripples, and their position relative to the state of loading  $\varepsilon$ . In the constitutive formula, Eq. (6.12), there appears a product of integral marginal statistics  $G_{(j+1)}(a^j\varepsilon)$ , where  $0 \leq j \leq k-1$ , and  $0 \leq k \leq k_{\max}-1$ . From the structure of Eq. (6.9), and if a Weibull distribution with  $m = 2, \lambda = 1$  is assumed as usual, it can be understood that the respective derivatives  $g_{(j+1)}(x)$  take on their maximum value even for very large  $j, n$ , and  $j \lesssim n$  at a numerical value of the argument  $x = \mathcal{O}(1)$ . Therefore, the  $g_{(j+1)}$  for large values of  $j$  possess well defined peaks at very large values of  $\varepsilon$ , where  $a^j\varepsilon \approx 1$ . The positions of these peaks become strongly separated for subsequent indices  $j, j+1$  if  $j = \mathcal{O}(n)$  and  $n$  is large. Consequently, in Eq. (6.12) the product of the integral quantities  $G_{(j+1)}(a^j\varepsilon)$  can be replaced by the largest factor  $G_{(k)}(a^{k-1}\varepsilon)$  for relatively large  $k$ , and together with the leading term  $\varepsilon[1 - G_{(k+1)}(a^k\varepsilon)]$  a peak structure is formed. It was confirmed numerically for  $k_{\max} = 60$  and  $k \gtrsim 30$  that the position  $\varepsilon$  of these maxima, which are defined through the function

$$m_k(\varepsilon) = a^k\varepsilon[1 - G_{(k+1)}(a^k\varepsilon)]G_{(k)}(a^{k-1}\varepsilon) \quad (6.15)$$

correlate well with the observed peaks in the avalanche size distribution and with the setting  $k = k_{\max}$  also yield good estimates for the critical stress and strain, see Fig. 6.7.

A rippled regime also appears if residual stiffness is present, as shown in Fig. 6.9 for stress controlled simulations for various values of  $k_{\max}$ , where ripples are clearly visible for  $k_{\max} \gtrsim 30$ , as in the case without residual stiffness. Again, the appearance of rippling



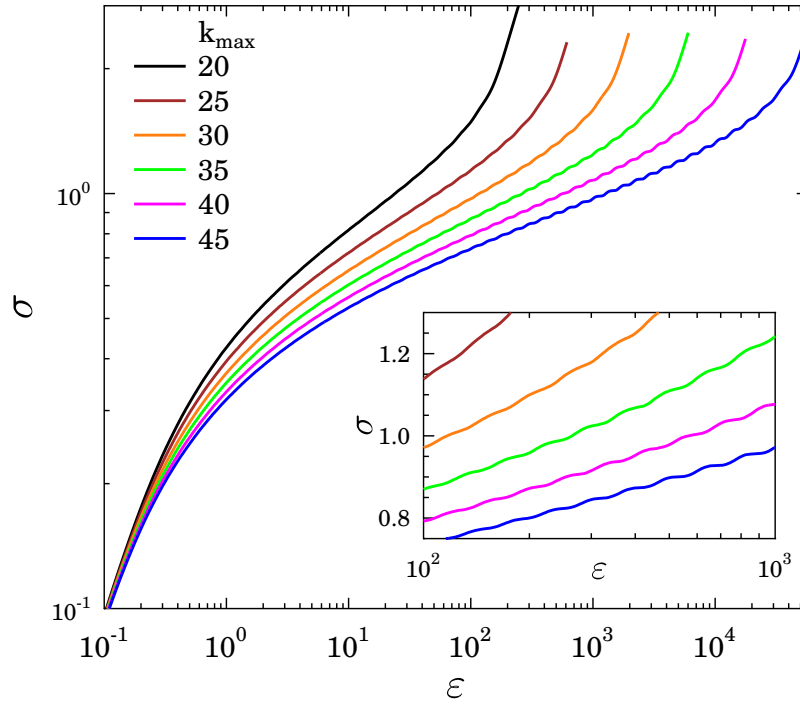


Figure 6.9: Constitutive curve for the model with sorted failure thresholds and residual stiffness with  $\lambda = 1$ ,  $m = 2$  for various values of  $k_{\max}$  in a double-logarithmic plot, under stress controlled loading. The inset shows a section of the constitutive curves on a logarithmic-linear scale, where the onset of rippling with increasing  $k_{\max}$  is better visible.

depends on the choice of  $k_{\max}$ , and sets in at  $k_{\max} \approx 30$ . With increasing  $k_{\max}$  also pronounced strain hardening occurs, whereas in the conventional CDFBM a plastic plateau is present. After passing the strain hardening regime, the bundles attain an asymptotical regime of constant slope  $\alpha^{k_{\max}}$  for all values of  $k_{\max}$ , where also macroscopic failure occurs for all cases investigated. It should be noted that therefore for low values of  $k_{\max}$ , i.e. without rippling, the slope of the constitutive curve is always finite positive, whereas for higher values of  $k_{\max}$ , there are sections of the constitutive curve with zero slope due to the ripples.

The presence of the ripples, and therefore of a locally vanishing slope, has a distinguished effect on the distribution of avalanche sizes, as demonstrated by Fig. 6.10 for the case with residual stiffness, and in Fig. 6.11 for the case without; this is also suggested by the presence of large size avalanches in Fig. 6.8 (no residual stiffness). It can be seen that in the absence of residual stiffness, Fig. 6.10, two remarkable features are present. First, for all values of  $k_{\max}$ , there is a regime with a power law of exponent  $-3/2$  for small avalanche sizes. Secondly, For small values of  $k_{\max}$ , an exponential cutoff appears for the larger avalanches; the presence of the initial power law regime with a following cutoff is confirmed by rescaling both axes by the average size of the largest avalanche,  $\langle \Delta_{\max} \rangle$ . The distributions  $D(\Delta)$  can be collapsed onto a single master curve, which was then fit

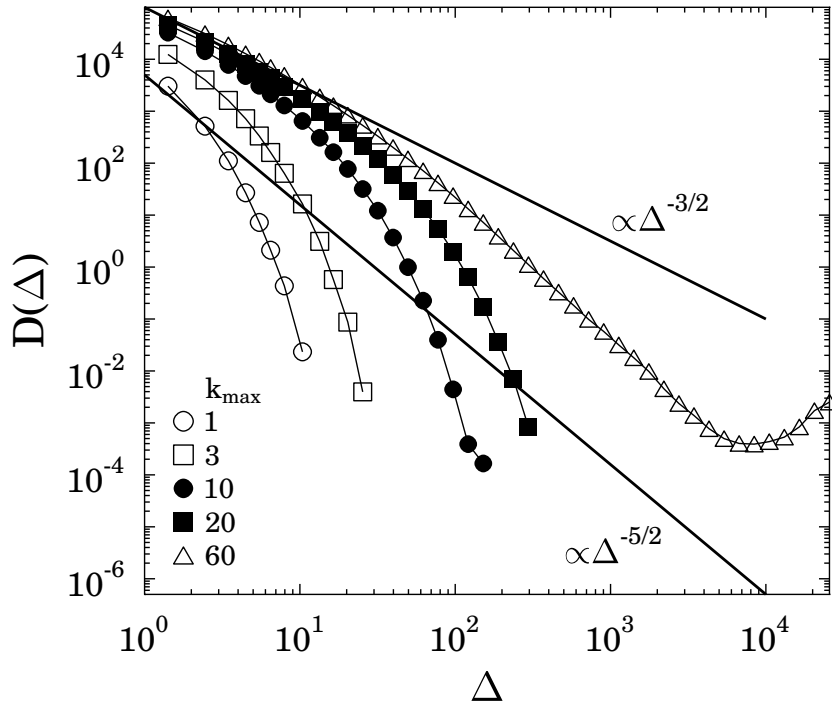


Figure 6.10: Avalanche size distributions for the CDFBM with sorted failure thresholds for various values of  $k_{\max}$ ,  $1 \leq k_{\max} \leq 60$  and residual stiffness. Results from stress controlled simulations of  $L = 201$  fibre bundles, averaged over 100 realizations.

by the exponential form

$$D(\Delta) \propto \left( \frac{\Delta}{\langle \Delta_{\max} \rangle} \right)^{-3/2} \exp \left( -\frac{\Delta}{c \langle \Delta_{\max} \rangle} \right), \quad (6.16)$$

as can be seen in Fig. 6.12, where the curves with low values  $k_{\max} \leq 20$  have been used. The above arguments are supported by the fact that the power law of exponent  $3/2$  with an exponential cutoff provides a perfect fit to the master curve obtained numerically. It should be noted that in the fitting, the value of the exponent was fixed to  $3/2$ , and the fit was obtained solely by varying the parameter  $c$  in Eq. (6.16).

For high values of  $k_{\max}$ , i.e. in the presence of ripples, a crossover is observed from an initial regime with a power law of exponent  $-3/2$ , to another regime with the mean field power law of exponent  $-5/2$ , and finally to a peaked regime for very large avalanches of about the system size.

A similarly complex behaviour is observed in the cases without residual stiffness, see Fig. 6.10. There, for low values of  $k_{\max}$ , the usual mean field behaviour of a power law with an exponent  $-5/2$  is observed. For intermediate values of  $k_{\max}$ , a crossover occurs between an initial  $-3/2$  power law part to a mean field part for larger avalanches, and the position of the crossover shifts to larger avalanche sizes with increasing  $k_{\max}$ . For higher values of  $k_{\max}$ , a limiting curve with a crossover at  $\Delta \approx 10^2$  can be identified, and again a peak of avalanches of the order of the system size is found for  $k_{\max} = 60$ .

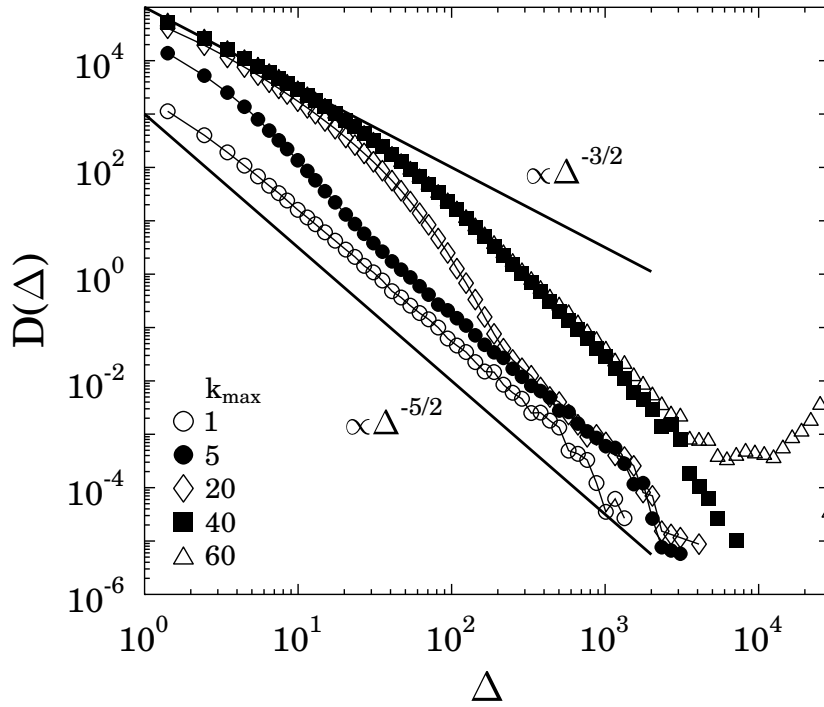


Figure 6.11: Avalanche size distributions for the CDFBM with sorted failure thresholds and no residual stiffness for various values of  $k_{\max}$ ,  $1 \leq k_{\max} \leq 60$ . Results from stress controlled simulations of  $L = 201$  fibre bundles, averaged over 200 realizations.

The features found in the avalanche size distributions can all be explained on the basis of the fine structure of the ripples, which is displayed in Fig. 6.13 for both stress and strain controlled loading, with  $k_{\max} = 15$  and the choice  $m = 10$  for the Weibull parameter. From this illustration it becomes apparent that the horizontal plateaus in the stress controlled simulations actually correspond to regions of decreasing stress  $\sigma$  under strain controlled loading, which cannot be accessed in the stress controlled mode. Also, the validity of the simulation results is supported by a semi-analytical evaluation of Eq. (6.12). It has been mentioned previously that the integral Eq. (6.11) cannot in general be evaluated easily. However, for  $k_{\max} = 15$ , the computer algebraics program MATHEMATICA<sup>®</sup> can perform these integrations analytically and evaluate the results, at least for  $\varepsilon \lesssim 6$ . The excellent agreement with the simulation results, see Fig. 6.13, is convincing proof of the simulation routine.

In general, a fibre bundle model can only produce large avalanches if the constitutive curve has at least one maximum, where the susceptibility to a small increment of the external force diverges. Avalanches with a power law distributions are generated in the vicinity of the maximum of  $\sigma(\varepsilon)$ , where the shape of the maximum determines the value of the exponent  $\tau$ . Quadratic maxima typically result in  $\tau = 5/2$ , the value obtained in the absence of both ripples and a residual stiffness term. If loading is stopped at a strain  $\varepsilon_s$  before reaching the maximum, i.e. before global failure occurs, an exponential cutoff in the avalanche size distribution appears, which is visible in Figs. 6.10 and 6.12, where due to the residual stiffness term the bundle fails macroscopically after passing

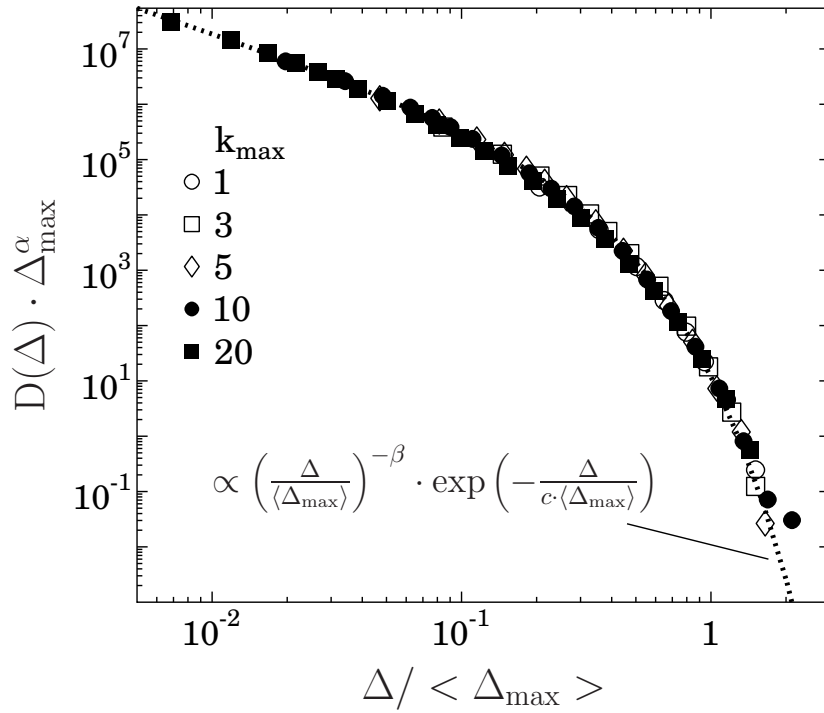


Figure 6.12: Rescaled avalanche size distributions for the CDFBM with sorted failure thresholds and residual stiffness, for small values of  $k_{\max}$  outside the rippling regime. A best fit with the numerical values  $\alpha = 1.22$  and  $\beta = 1.5$  for the exponents has been used to obtain the collapse of the curves and the dashed fit curve.

exclusively through regions of finite positive slope, without quadratic maxima, as for the cases  $k_{\max} \leq 30$  no rippling occurs.

In the rippling regime, however,  $\sigma(\varepsilon)$  passes a series of consecutive maxima with an increasing amplitude. Under stress controlled loading the system jumps from a local maximum of  $\sigma(\varepsilon)$  to the ascending side of the next maximum which is somewhat higher than the previous one, see Fig. 6.13. The jump implies that a large amount of fibre breakings occur in a single avalanche removing all fibres which have breaking thresholds lower than the load of the ending point of the jump on the next peak of  $\sigma(\varepsilon)$ . Consequently, when loading is continued along the ascending side of the peak determined by Eq. 6.15, the response of the system is determined by a disorder distribution which is critical in the sense of Ref. [56], i.e. weak fibres are removed so that the lower cutoff of the disorder distribution falls close to the local critical deformation, the location of the next peak. As it has been shown in Chapter 5, when the disorder distribution approaches criticality, the avalanche size distribution exhibits a power law from an exponent  $\tau = 3/2$  for the small avalanches, to another exponent of  $\tau = 5/2$  for the large ones, irrespective of the effective range of interaction. This effect can be recognized in the  $k_{\max} = 60$  curve in Fig. 6.10.

The same argumentation holds for the case without residual stiffness: here, a global quadratic maximum is always present, so for low values of  $k_{\max}$  the mean field expo-

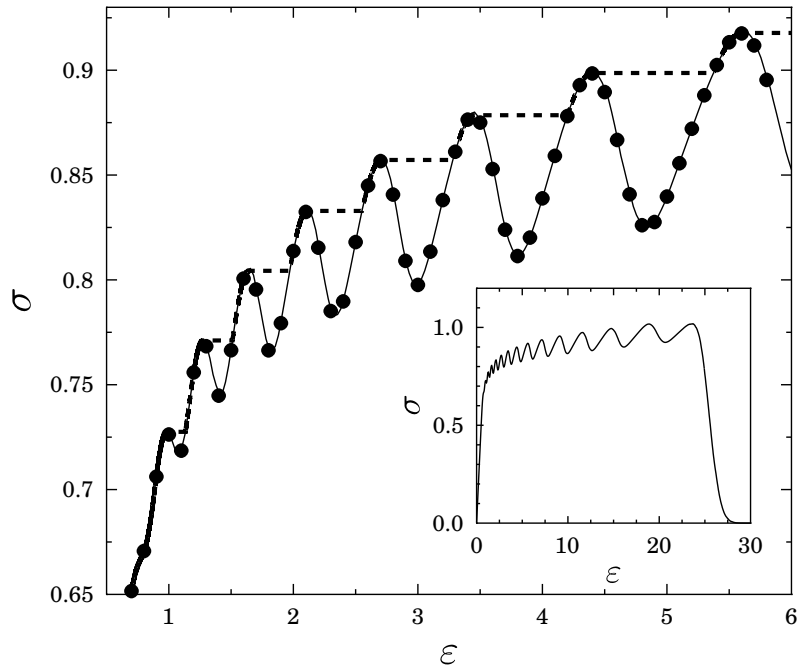


Figure 6.13: Section of the constitutive curve for the model with  $k_{\max} = 15$ ,  $m = 10$  and no residual stiffness. Solid line: strain controlled simulation, dashed line: stress controlled simulation, dots: exact evaluation of the analytical solution, Eq. (6.12).

ment  $-5/2$  is found. However, in the presence of rippling structures, there appear a series of local quadratic maxima, and the stepping effect described above yields a series of local critical threshold distributions, which results in the crossover of exponents visible in the avalanche size distribution, cf. Fig. 6.11.

It has to be stressed that the effects found here in the CDFBM with sorting have no equivalent counterparts in the conventional CDFBM without sorting. There, the macroscopic behaviour yields a plastic plateau and no steps appear in the constitutive curve; consequently, the size distribution of avalanches shows no signatures of criticality. The existence of rippling, synchronized avalanche bursts and a critical crossover of the avalanche size distribution exponents is a genuine peculiarity of the extreme order statistics accompanying sorting.

The analytical argumentation presented above also makes it clear that rippling cannot occur for all disorder distributions and all values of  $k_{\max}$ ; rather, its appearance is restricted to combinations of large  $k_{\max}$  and low disorder corresponding to high values of the Weibull parameter  $m$ , such that the maxima defined through Eq. (6.15) are clearly separated. Fig. 6.14 presents a numerical survey of the apparent occurrence of ripples. One can see that a well defined and smooth separatrix can be found which isolates the regime with ripples from the regime without in the  $\{k_{\max}, m\}$  parameter space.

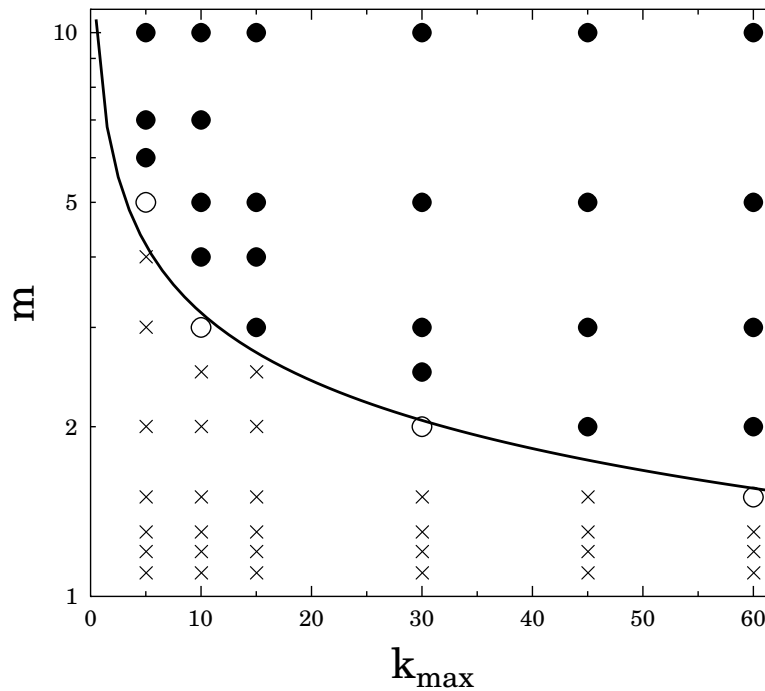


Figure 6.14: Phase diagram denoting the appearance of ripples in the constitutive curves of the model with sorting and no residual stiffness, and the presence of pronounced spikes in the avalanche size distribution. Filled circles: rippled regime; crosses: normal regime; unfilled circles: inconclusive state. The solid line denotes the approximate location of the separatrix between the two regimes.

## 6.4 Conclusions

Motivated by experimental observation on the fracture process of composite systems having a hierarchy of length scales, we extended the continuous damage fibre bundle model by taking into account that a hierarchy of length and energy scales for damage initiation and crack growth and propagation exist. Cracks can also be arrested at particularly strong locations inside a material, and the maximum number of macroscopically visible damage events, which are based on large defects in the material, is not a constant, but varies between samples of the same production batch. Therefore, two new features have been added to the ordinary CDFBM, and their effect on the microscopic and the macroscopic damage evolution has been investigated.

In the first model, the maximum number of failures has been modeled as a Poissonian random variable. It can be concluded that the influence of the additional term on the CDFBM can be well understood in all its effects; the main additional feature is the appearance of a hardening regime in the constitutive curve in all the cases investigated, which can be explained by analytical considerations. The macroscopic behaviour is therefore fully tractable analytically, and we have presented a numerical study for different values of the parameter  $\kappa$ . It should be noted that this strain hardening can also be discarded of by mod-

ifying the distribution prescription for  $k_{\max}$ . The effect of the Poissonian term should have a clearly distinguishable effect on the constitutive behaviour, especially for small values of its mean. In the microscopic behaviour, the extension of the CDFBM by means of a Poissonian term for  $k_{\max}$  leaves the distribution of avalanche sizes invariant, displaying a crossover from a power law with an exponent  $-5/2$  to a power law with another exponent  $-2.12$  for increasing values of  $\kappa$ , in analogy to the conventional CDFBM.

Consequently, the model incorporates the existence of disorder not only with respect to a distribution of failure thresholds for each defect, but also with respect to the finite number of macroscopic defects that may effectively govern the macroscopic breaking of certain materials.

The second model introducing sorted failure thresholds gives rise to complex dynamics and synchronized damage events. A parameter regime has been identified where the damage evolution of all fibres synchronizes and considerable changes to the microscopic quantities can be observed, depending on the amount of disorder and the maximum number of allowed failures.

A combination of both models has been shown to be feasible, and can be useful to obtain a better understanding of the failure process in real disordered materials. The models may be especially helpful if several damage processes coexist in these materials, which differ in their specific damage mechanism and activation energy.





# Chapter 7

## Discussion and Outlook

### 7.1 Summary of the Results

We have proposed several models to address the issue of finding a more realistic description of failure and fracture in disordered —specifically fibrous— materials, as it was mentioned in the introduction: the aim was to provide a description for the shear failure of interfaces in disordered and composite materials; find a simple representation of plasticity, investigate the question of criticality, and to explain some aspects of cracking behaviour in strongly disordered materials, all this with the possible application of fibrous composites under both shear and tension loading in mind. Several models, all of them variants of the fibre bundle kind have been proposed, and they have been investigated numerically and —wherever possible— analytically for a wide range of parameters.

To apply FBMs to the case of transversal loading, a novel type of model for the shear failure of the glued interface between two solid blocks has been introduced in Chapter 3. In the model the interface is discretized in terms of elastic beams which experience stretching and bending deformation under shear. Breaking of a beam can be caused by both deformations resulting in two failure modes; the modes can be independent or coupled by a von Mises type criterion. The mechanical strength of beam elements is characterized by the two threshold values of stretching and bending which the beam can withstand. The beams are assumed to have identical elastic properties, the heterogeneous microstructure is represented by the disorder distribution of the breaking thresholds.

The beam model introduced in Chapter 3 provides a more realistic description of the interface of macroscopic solid bodies than the simple fibre bundle model and is applicable to more complex loading situations. A detailed study of the macroscopic response and the progressive damaging of the interface under quasistatic loading has been presented. The analytic solution for the constitutive behaviour of the model and the damage accumulated in the system has been obtained in the case of global load sharing. An efficient simulation technique has been worked out to study the microscopic damage process in large systems. It has been demonstrated that the disorder distribution and the relative importance of the two failure modes have a substantial effect on both the microscopic damage process and

the macroscopic constitutive behaviour of the interface, and the existence of two failure modes was found to lower the critical stress and strain as compared to the corresponding fibre bundle model. Varying its parameters, the model provides a broad spectrum of material behaviours. The distribution of burst sizes displays power law behaviour with an exponent equal to the one of simple fibre bundles. Under stress controlled loading conditions, the macroscopic failure of the interface occurs analogously to phase transitions, where the beam model proved to be in the same universality class as the equal load sharing fibre bundle model [61; 29; 69]. In the case of localized interaction of beams a more brittle behaviour of the interface has been found, which implies a more abrupt transition at the critical load.

A mapping of the beam model onto the classical fibre bundle model has been worked out; it was found that despite of the different loading situation, the beam model can be treated by the same methods as the fibre bundles for loading parallel to the fibre axis. This has allowed us to restrict all further studies to FBM models.

In Chapter 4, a one-parameter plastic fibre bundle model has been introduced, where failed fibres retain a fraction  $0 \leq \alpha \leq 1$  of their failure load. The value of the parameter  $\alpha$  interpolates between the perfectly rigid failure  $\alpha = 0$  and perfect plasticity  $\alpha = 1$  of fibres.

The plastic fibre bundle model can be relevant for the shear failure of interfaces where failed surface elements can remain in contact still transmitting load. In fibre composites, where fibres are embedded in a matrix material, the fibre-matrix interface—which has a profound influence on the material failure—displays the properties of the glued interfaces discussed in Chapter 3. The finite load bearing capacity of failed elements of the model can account for the frictional contact of debonded fibre-matrix interfaces and also for plastic behaviour of the components.

The effect of the fibres' load bearing capacity after failure has been studied both analytically and numerically. Under GLS, when the fibres attain a state of perfect plasticity with  $\alpha \rightarrow 1$ , the yield stress proved to be equal to the average fibre strength, and the critical strain diverges with a functional form that depends on the failure threshold distribution. Microscopically, with increasing  $\alpha$  the avalanche size distribution shows a crossover from the mean field power law form with an exponent  $-5/2$  to a faster exponential decay. The existence of this crossover was confirmed by analytical calculations, which also show another crossover to an asymptotic power law with the mean field exponent, in the regime of very large avalanche sizes that cannot be reached in simulations.

The behaviour of the plastic fibre bundle under LLS is determined by a competition between failure induced by the presence of disorder, and failure due to stress enhancement around clusters of broken fibres. An increasing value of  $\alpha$  lowers the stress concentration around broken fibres, and an interesting phase transition between the two regimes occurs at a specific value  $\alpha_c$ , which depends on the strength of disorder. Macroscopically, the fibre bundle shows a brittle response below the critical point  $\alpha_c$ , which means that a weak non-linearity is present in the constitutive curve before global failure, whereas above  $\alpha_c$  the constitutive behaviour becomes practically identical to the GLS counterpart.

Computer simulations revealed that the microscopic damage evolution in the LLS bundle shows a continuous transition analogous to percolation as a function of  $\alpha$ . The avalanche size distribution of fibre breakings becomes a power law at  $\alpha_c$  with the universal exponent  $3/2$ , which is equal to the exponent of bundles with critical strength distributions studied in Chapter 5. Also, a spanning cluster of broken fibres appears at the transition point. Simulations showed that these spanning clusters are compact and have a fractal boundary, with a dimension that increases with the amount of disorder.

In Chapter 5, we carried out computer simulations of the failure process of a bundle of fibres with a finite cutoff of the fibres' strength, continuously varying the range of interaction between the limiting cases of global and local load sharing. This was done employing a variable range of interaction model proposed in [29], and our results confirm the analogy between the localized interaction case, and the case of purely global load sharing, which has been investigated in [56]. It was shown that with increasing cutoff strength  $\varepsilon_L$  the macroscopic response of the fibre bundle becomes perfectly brittle as  $\varepsilon_L$  approaches a critical value  $\varepsilon_L^c(\gamma)$ , depending on the range of interaction  $\gamma$ . As the case of localized load sharing is not analytically tractable, extensive numerical simulations have been carried out to substantiate the existence of a macroscopic brittleness regime, and a microscopic crossover behaviour. The numerical results demonstrate the robustness of the crossover of the avalanche size distribution  $D(\Delta)$  to a universal power law of exponent  $3/2$ , irrespective of the range of interaction between the material elements. A thorough investigation of the crossover regime has resulted in a characterization of this regime by means of several quantities, such as the mean avalanche size and the crossover avalanche size. The distinguished properties of these quantities clearly mark the existence of the crossover, and a pronounced change in the degree of macroscopic brittleness, which has also been found in earlier experiments [103] and in the magnitude distribution of earthquakes [102].

In Chapter 6, two new features have been added to the ordinary CDFBM, and their effect on the microscopic and the macroscopic damage evolution has been investigated.

In the first CDFBM variant, the maximum number of failures of a fibre,  $k_{\max}$ , has been modeled as a Poissonian distributed random variable of mean  $\kappa$ . This allows to account for the inter-sample fluctuations of relevant macroscopic defects, which is a disorder effect that pertains not only to the strength of a single defect, but also to the total number of defects. The value of the parameter  $\kappa$  was shown to influence the macroscopic constitutive behaviour by introducing an asymptotic linear regime even in the absence of a residual stiffness term, an effect that becomes less pronounced with increasing  $\kappa$ . However, no apparent changes were found to be present in the microscopic characteristics, where—as in the standard CDFBM—a crossover in the avalanche size distributions from a power law with an exponent  $-5/2$  to a power law with another exponent  $-2.12$  for increasing values of  $\kappa$  occurs.

A second variant takes  $k_{\max}$  to be fixed, whereas the thresholds for subsequent failure events of a fibre are determined by random numbers sorted in increasing order. This sorting can account for crack arrest, since cracks propagate sweeping through the regions of weak and intermediate strength, but can become arrested at regions of high strength. It

was found that with increasing  $k_{\max}$ , a long strain hardening regime appears prior to global failure, and the critical stress and strength,  $\sigma_c$  and  $\varepsilon_c$  diverge, although at a different pace. For certain choices of  $k_{\max}$  and the amount of disorder, which can be controlled through the Weibull parameter  $m$ , ripples appear in the strain hardening regime of the constitutive curve. The ripples mark the presence of synchronized microscopic damage events of a critical nature. Hence, a crossover is present in the avalanche size distribution to a power law with an exponent  $3/2$ , which can be explained on the basis of the results discussed in Chapter 5 for the presence of a cutoff in the failure threshold distribution. It should be noted that no similar effect is present in the CDFBM without sorting, regardless of whether quenched or annealed disorder is taken into account.

A combination of both models has been shown to be feasible, and can be useful to obtain a better understanding of the failure process in real disordered materials. The models may be especially helpful if several damage processes coexist in these materials, which differ in their specific damage mechanisms and activation energies.

Two important conclusions have to be drawn at this time: first, the case of shear loading of composites has been mapped onto the conventional fibre bundle model; this mapping allows to treat the case of shear failure in the framework, with the methods, and including all variants that have been developed for the conventional FBM. Secondly, the question of criticality has emerged as a recurring issue, appearing surprisingly in the context of different models: not only in the case that the threshold distribution is prepared with a cutoff, as in Chapter 5, but it appears also in the plastic FBM with local load sharing, cf. Chapter 4, and in the modified CDFBM in the presence of ripples in Chapter 6.

## 7.2 Open Questions

In this thesis, several models or model variants for fracture have been proposed, and their properties have been explored through analytical calculations and numerical simulations. Having completed the theoretical approach, it will be interesting to see further experimental efforts directed at this field. A first step has been taken by our colleagues from the common research project SFB 381 at the University of Stuttgart to test the predictions of the beam model by investigating the shear failure of a unidirectional glass fibre composite. First results from measurements of the constitutive curve and acoustic emissions from several samples have yielded promising results about the brittle nature of global failure, which will allow us to calibrate the parameters of the beam model. The acoustic emission data however still lacks statistical significance, and it is planned to conduct further experiments on this issue.

Similarly, a microscopic observation of fracture patterns in disordered materials with some degree of plasticity could be very interesting to compare to the plastic fibre bundle model introduced in Chapter 4, specifically to the clusters of broken fibres found therein. We have described some unique features of these clusters in detail, which should make them experimentally distinguishable from microcrack patterns predicted by other methods.

Another ongoing research effort —again within the SFB 381 project, to which we are deeply indebted— focuses on the fracture of glued timber structures, which serve as cost effective, wide-spanning structural elements, *e. g.* in roofs. Preliminary results and observations from this experimental project have motivated us to propose the extension of the CDFBM discussed in Chapter 6, and a calibration of our model parameters and the evaluation of the experimental data gathered so far can hopefully yield new insight into the interesting questions posed by crack propagation and arrest, and the overall influence of large defect structures.

Fortunately the effect of a lower cutoff in failure threshold distributions has been found already in experiments on the brittle vs. plastic fracture of metals, and also in the time series of earthquakes. Naturally, further research efforts should be dedicated to this important issue.

In undue generality, a remark about the availability of experimental data from a physicist's point of view may be in place here: dealing with disordered and especially fibrous composite materials, the engineering community has amassed an incredible wealth of theoretical and experimental knowledge on the issue of fracture and failure. Yet the sharing of knowledge between the engineering and physics communities could probably be improved. We find many experiments described in the engineering literature to be too complex to handle them by statistical physics methods. It may be helpful in the future to design simpler experiments, focusing on a single aspect of a well prepared experimental state, preferably dealing with model materials which may not even have a significant application in engineering, industry or construction.

Having mentioned this, there is also quite some effort to be undertaken for the unification of the existing statistical models of fracture, and their embedding into the formalism of statistical physics, although remarkable progress has been made in the recent years. On a lower level, one may think of two extensions of FBM models which can be implemented with moderate effort. First, the introduction of spatial correlations for the failure thresholds in the beam model can more closely reflect the presence of localized fibre-matrix interfaces in fibre composites. This can yield rewarding insight into fracture patterns and microcracks, when localized load sharing is employed in the model. Even under global load sharing, interesting questions arise due to the mixing of failure threshold distributions, which has been investigated not only in the beam model of Chapter 3, but also in another recent study [76]. Secondly, placing fibre bundle elements on the nodes of networks while retaining their disordered properties and dynamical rules could be a fascinating field to study, and a similar effort has recently been undertaken employing the random fuse model [58]. This could lead to a better understanding for the failure modes of electrical grids, or computer networks.

In addition, a close resemblance of fibre bundle models to models of biological structures [105; 106] has recently been discovered. First steps undertaken in the direction of FBMs with a healing condition [40; 39] make fibre bundles promising candidates for the understanding of the cellular microskeleton, and the possible benefits of further insight in this field can hardly be exaggerated.

Finally, we may direct the reader's attention to a technical application. We have mentioned the catastrophic collapse of a sports facility in Bad Reichenhall in the year 2006 in the introduction, which was followed by a series of other hall collapses in the same winter, fortunately without inflicting any further injuries. Following these incidents were demands for regular checks of public buildings by independent experts. Needless to say, this would impose a heavy financial burden on the owners, and necessarily provide only a snapshot picture of the buildings' state. On the other hand, small, battery powered acoustic sensors have recently been presented and are currently undergoing field tests [20], which can be equipped with long term recording and warning devices. It is through the study of fibre bundles and similar statistical models that criteria can be established, which permit to distinguish ambient and ordinary yield noises from microfractures and impending collapse. A possibly life saving alarm signal could then be triggered if the latter are found. Together with the potential of constant building supervision and the ensuing economic advantages, the early warning capabilities could make these devices —akin to smoke detectors— a cheap and ubiquitous piece of equipment in all areas of life.

### 7.3 A perspective

What is the future of the fibre bundle model? In the field of fracture models, there is hardly a lack of well proven and tested approaches, and FBMs face the competition of atomistic simulations, beam models on lattices, classical fracture mechanics and finite element simulations, to name but a few. It has been the intention of this thesis to highlight the appropriateness and elegance of fibre bundle models, and their particular suitability in terms of modeling disorder and load transfer. From a broader application point of view, the future of all these different models certainly lies in a combination by means of a hierarchical multi-scale approach, using their specific advantages on one scale while overcoming restrictions and shortcomings on other scales. An integration is also feasible in terms of multiple mechanisms and loading conditions; an example can be the mechanism based toolbox [107] that has been developed as a joint effort by several research groups of the SFB 381, where also the beam model of Chapter 3 has been implemented to account for interfacial based failure. It can be ascertained that a considerable number of research projects all over the world are presently devoted to the issue of multi-scale modeling, and computer simulations that make the expertise of hundreds of researchers easily accessible through user friendly interfaces are becoming a widespread tool in industry and the academic world.

We would like to conclude this study with an analogy, which is admittedly a bit far fetched, but nevertheless instructive. Present state of the art simulations allow for tracing crack propagation in a bulk of  $10^9$  atoms on a single-atom level, which has addressed a series of fundamental questions about the microscopic origin of fracture. Given the rapid progress of computational performance, the number given above will certainly strongly increase in the near future. But just as the potential computation of the  $10^{23}$  molecular trajectories present in only one mole of an ideal gas will not render the mean field formulation of thermodynamics useless, there will most likely always be a demand for easily

---

comprehensible statistical models of fracture —such as the fibre bundle model— which capture the almost infinite amount of states by means of a few state variables. The pursuit of statistical models has yielded an abundance of novel information on the fracture process of disordered materials and its connection to statistical physics in recent years. To name an example, despite the decade long study of fibre bundle models, the discovery of a crossover in the power law exponents describing the statistics of fracture events dates back to the last year [56], and we have found further manifestations of this crossover throughout this thesis. It is for this reason we may assume that the field of fibre bundle models can still bear some surprising insights, and that the study of these models is still a worthwhile effort in exploring fundamental principles of fracture.





# Bibliography

- [1] H. J. Herrmann and S. Roux, editors. *Statistical models for the fracture of disordered media*. Random materials and processes. Elsevier, Amsterdam, 1990.
- [2] G. Busse, B.-H. Kröplin, and F. K. Wittel, editors. *Damage and its Evolution in Fiber-Composite Materials: Simulation and Non-Destructive Evaluation*. Universität Stuttgart, 2006.
- [3] G. Dill-Langer, R. C. Hidalgo, F. Kun, Y. Moreno, S. Aicher, and H. J. Herrmann. Size dependency of tension strength in natural fiber composites. *Physica A*, 325:547–560, 2003.
- [4] F. T. Peires. Tensile tests for cotton yarns. v.-'the weakest link', theorems on the strength of long composite specimens. *J. Textile Inst.*, 17:T355–368, 1926.
- [5] H. E. Daniels. The Statistical Theory of the Strength of Bundles of Threads. I. *Proc. R. Soc London A*, 183:405–435, 1945.
- [6] M. Kloster, A. Hansen, and P. C. Hemmer. Burst avalanches in solvable models of fibrous materials. *Phys. Rev. E*, 56:2615–2625, 1997.
- [7] M. J. Alava, P. K. V. V. Nukala, and S. Zapperi. Statistical models of fracture. *Adv. Phys.*, 2006.
- [8] S. Pradhan, A. Hansen, and P. C. Hemmer. Crossover behavior in failure avalanches. *Phys. Rev. E*, 74:016122, 2006.
- [9] L. da Vinci. *I libri di Meccanica*. Hoepli, Milano, 1940.
- [10] G. Galilei. *Discorsi e dimostrazioni matematiche intorno a due nuove scienze*. Boringhieri, Torino, 1958.
- [11] J. Fineberg and M. Marder. Instability in dynamic fracture. *Phys. Rep.*, 313:2, 1999.
- [12] R. W. Cahn, P. Haasen, and E. J. Kramer. *Structure and Properties of Composites*. VCH-Verlag Weinheim, Germany, 1993.
- [13] D. Hull and T. W. Clyne. *An Introduction to Composite Materials*. Cambridge solid state science series. Cambridge University Press, 2nd edition, 1996.

- [14] K. K. U. Stellbrink. *Micromechanics of Composites: composite properties of fibre and matrix constituents*. Carl Hanser Verlag, Munich, 1996.
- [15] I. Solodov and D. Döring. *Damage and its Evolution in Fiber-Composite Materials: Simulation and Non-Destructive Evaluation*, chapter Ultrasonics for NDE of Fiber-Composite Materials. Universität Stuttgart, 2006.
- [16] F. Kun, F. Raischel, R. C. Hidalgo, and H. J. Herrmann. *Modeling Critical and Catastrophic Phenomena in Geoscience*, volume 705 of *Lecture Notes in Physics*, chapter Extensions of Fibre Bundle Models, pp 57–92. Springer Berlin, 2006.
- [17] J. W. Kopp. *Zur Spannungs- und Festigkeitsanalyse von unidirektionalen Faserverbundkunststoffen*. PhD thesis, RWTH Aachen, 1999.
- [18] S. Brelant and I. Petker. *Mechanics of Composite Materials*, chapter Fabrication and Environmental Interaction of Filament-Wound Composites, pp 799–812. Pergamon Press, Oxford, 1970.
- [19] n. n. Gutachten zu den Ursachen des Einsturzes der Eissporthalle in Bad Reichenhall vorgelegt. *Bautechnik*, 83(9):667, 2006.
- [20] C. U. Grosse, A. Wanner, J. H. Kurz, and L. M. Linzer. *Damage and its Evolution in Fiber-Composite Materials: Simulation and Non-Destructive Evaluation*, chapter 1.1.2 Acoustic Emission. Universität Stuttgart, 2006.
- [21] F. Kun, S. Zapperi, and H. J. Herrmann. Damage in fiber bundle models. *Eur. Phys. J. B*, 17:269, 2000.
- [22] S. L. Phoenix and I. J. Beyerlein. Statistical Strength Theory for Fibrous Composite Materials. In A. Kelly and C. Zweben, editors, *Comprehensive Composite Materials*, volume 1, chapter 1.19, pp 1–81. Pergamon-Elsevier Science, New York, 2000.
- [23] B. D. Coleman. Time dependence of mechanical breakdown phenomena. *J. Appl. Phys.*, 27:862, 1956.
- [24] B. K. Chakrabarti and L. G. Benguigui. *Statistical Physics of Fracture and Breakdown in Disordered Systems*. Oxford University Press, 1997.
- [25] F. Kun and H. J. Herrmann. Damage development under gradual loading of composites. *Journal of Materials Science*, 35:4685, 2000.
- [26] S. L. Phoenix, M. Ibnabdeljalil, and C.-Y. Hui. Size effects in the distribution for strength of brittle matrix fibrous composites. *Int. J. Solids Structures*, 34:545, 1997.
- [27] S. L. Phoenix and R. Raj. Scalings in fracture probabilities for a brittle matrix fiber composite. *Acta metall. mater.*, 40:2813, 1992.
- [28] W. A. Curtin. The "tough" to brittle transition in brittle matrix composites. *J. Mech. Phys. Solids*, 41:217, 1993.

- [29] R. C. Hidalgo, Y. Moreno, F. Kun, and H. J. Herrmann. Fracture model with variable range of interaction. *Phys. Rev. E*, 65:046148, 2002.
- [30] R. C. Hidalgo, F. Kun, and H. J. Herrmann. Bursts in a fiber bundle model with continuous damage. *Phys. Rev. E*, 64(6):066122, 2001.
- [31] R. C. Hidalgo, C. U. Grosse, F. Kun, H. W. Reinhardt, and H. J. Herrmann. Evolution of percolating force chains in compressed granular media. *Phys. Rev. Lett.*, 89:205501, 2002.
- [32] R. C. Hidalgo, F. Kun, and H. J. Herrmann. Creep rupture of viscoelastic fiber bundles. *Phys. Rev. E*, 65:032502, 2002.
- [33] F. Kun, Y. Moreno, R. C. Hidalgo, and H. J. Herrmann. Creep rupture has two universality classes. *Europhys. Lett.*, 63(3):347–353, 2003.
- [34] F. Kun, R. C. Hidalgo, H. J. Herrmann, and K. F. Pal. Scaling laws of creep rupture of fiber bundles. *Phys. Rev. E*, 67(6):061802, 2003.
- [35] H. Nechad, A. Helmstetter, R. E. Guerjouma, and D. Sornette. Creep ruptures in heterogeneous materials. *Phys. Rev. Lett.*, 94:045501, 2005.
- [36] H. Nechad, A. Helmstetter, R. E. Guerjouma, and D. Sornette. Andrade and critical time to failure laws in fiber-matrix composites: Experiments and model. *J. Mech. Phys. Solids*, 53:1099, 2005.
- [37] R. Chudoba, M. Vořechovský, and M. Konrad. Stochastic modeling of multifilament yarns. I. random properties within the cross-section and size effect. *Int. J. Solids Struct.*, 43:413–434, 2005.
- [38] R. Chudoba, M. Vořechovský, and M. Konrad. Stochastic modeling of multifilament yarns. II. random properties over the length and size effect. *Int. J. Solids Struct.*, 43:unknown, 2005.
- [39] F. Kun, M. H. A. S. Costa, R. N. C. Filho, J. S. Andrade Jr, J. B. Soares, S. Zapperi, and H. J. Herrmann. Damage and healing in fatigue fracture. *cond-mat/0607606*, 2006.
- [40] H. A. Carmona, F. Kun, J. S. Andrade Jr, and H. J. Herrmann. Numerical simulation of fatigue under diametrical compression. *cond-mat/0610080*, 2006.
- [41] P. A. Vermeer et al., editors. *Continuous and Discontinuous Modeling of Cohesive-Frictional Materials*. Lecture Notes in Physics. Springer, New York and others, 2000.
- [42] G. G. Batrouni, A. Hansen, and J. Schmittbuhl. Heterogeneous interfacial failure between two elastic blocks. *Phys. Rev. E*, 65:036126, 2002.
- [43] A. Delaplace, S. Roux, and G. Pijaudier-Callot. ‘Damage cascade’ in a softening interface. *Int. J. Solids Struct.*, 36:1403–1426, 1999.

- 
- [44] S. Roux, A. Delaplace, and G. Pijaudier-Cabot. Damage at heterogeneous interfaces. *Physica A*, 270:35–41, 1999.
- [45] S. Zapperi, H. J. Herrmann, and S. Roux. Planar cracks in the fuse model. *Eur. Phys. J. B*, 17:131–136, 2000.
- [46] J. Knudsen and A. R. Massih. Breakdown of disordered media by surface loads. *Phys. Rev. E*, 72:036129, 2005.
- [47] R. da Silveira. An introduction to breakdown phenomena in disordered systems. *Am. J. Phys.*, 67:1177, 1999.
- [48] S. Zapperi, P. Ray, H. E. Stanley, and A. Vespignani. Avalanches in breakdown and fracture processes. *Phys. Rev. E*, 59:5049, 1999.
- [49] Y. Moreno, J. B. Gomez, and A. F. Pacheco. Instability of scale-free networks under node-breaking avalanches. *Eur. Phys. Lett.*, 58:630, 2002.
- [50] D.-H. Kim, B. J. Kim, and H. Jeong. Universality class of the fiber bundle model on complex networks. *Phys. Rev. Lett.*, 94:025501, 2005.
- [51] D. L. Turcotte and M. T. Glasscoe. A damage model for the continuum rheology of the upper continental crust. *Tectonophysics*, 383:71–80, 2004.
- [52] D. Sornette. Mean-field solution of a block-spring model of earthquakes. *J. Phys. I. France*, 2:2089, 1992.
- [53] S. Roux. Thermally activated breakdown in the fiber-bundle model. *Phys. Rev. E*, 62:6164, 2000.
- [54] R. Scorretti, S. Ciliberto, and A. Guarino. Disorder enhances the effect of thermal noise in the fiber bundle model. *Europhys. Lett.*, 55:626–632, 2001.
- [55] A. Virgili, A. Petri, and S. R. Salinas. A thermodynamical fiber bundle model for the fracture of disordered materials. *cond-mat/0611721*, 2006.
- [56] S. Pradhan, A. Hansen, and P. C. Hemmer. Crossover behavior in burst avalanches: Signature of imminent failure. *Phys. Rev. Lett.*, 95:125501, 2005.
- [57] S. Pradhan and A. Hansen. Failure properties of loaded fiber bundles having a lower cutoff in fiber threshold distribution. *Phys. Rev. E*, 72:026111, 2005.
- [58] J. O. H. Bakke, A. Hansen, and J. Kertesz. Failure and avalanches in complex networks. *cond-mat/0605461*, 2006.
- [59] P. K. Nukala and S. Simunovic. A continuous damage random thresholds model for simulating the fracture behavior of nacre. *Biomaterials*, 26:6087, 2005.
- [60] P. K. Nukala and S. Simunovic. Statistical physics models for nacre fracture simulation. *Phys. Rev. E*, 72:041919, 2005.

- [61] J. V. Andersen, D. Sornette, and K. Leung. Tricritical Behaviour in Rupture Induced by Disorder. *Phys. Rev. Lett.*, 78:2140–2143, 1997.
- [62] S. Zapperi, P. Ray, H. E. Stanley, and A. Vespignani. First-Order Transition in the Breakdown of Disordered Media. *Phys. Rev. Lett.*, 78:1408, 1997.
- [63] P. Bhattacharyya, S. Pradhan, and B. K. Chakrabarti. Phase transition in fiber bundle models with recursive dynamics. *Phys. Rev. E*, 67(14):046122, 2003.
- [64] E. Vives and A. Planes. Avalanches in a fluctuationless first-order phase transition in a random-bond Ising model. *Phys. Rev. B*, 50:3839, 1994.
- [65] Y. Moreno, J. B. Gomez, and A. F. Pacheco. Fracture and second-order phase transitions. *Phys. Rev. Lett.*, 85(14):2865–2868, 2000.
- [66] Y. Moreno, J. B. Gómez, and A. F. Pacheco. Self-organized criticality in a fibre-bundle-type model. *Physica A*, 274:400, 1999.
- [67] A. Hansen and S. Roux. Statistical toolbox for damage and fracture. In D. Krajcinovic and J. van Mier, editors, *Damage and Fracture of Disordered Materials*, number 410 in CISM Courses and Lectures, chapter 2, pp 17–101. Springer Verlag, 2000.
- [68] P. C. Hemmer and A. Hansen. The Distribution of Simultaneous Fiber Failures in Fiber Bundles. *J. Appl. Mech.*, 59:909–914, 1992.
- [69] S. Pradhan and B. K. Chakrabarti. Failure properties of fiber bundle models. *Int. J. Mod. Phys. B*, 17:5565–5581, 2003.
- [70] S. Pradhan and B. K. Chakrabarti. Failure due to fatigue in fiber bundles and solids. *Phys. Rev. E*, 67(14):046124, 2003.
- [71] S. Pradhan and B. K. Chakrabarti. Precursors of catastrophe in the Bak-Tang-Wiesenfeld, Manna, and random-fiber-bundle models of failure. *Phys. Rev. E*, 65:016113, 2002.
- [72] S. Zapperi, P. Ray, H. E. Stanley, and A. Vespignani. Analysis of damage clusters in fracture processes. *Physica A*, 270:57, 1999.
- [73] S. R. Pride and R. Toussaint. Thermodynamics of fiber bundles. *Physica A*, 312:159–171, 2002.
- [74] R. Toussaint and S. R. Pride. Interacting damage models mapped onto Ising and percolation models. *Phys. Rev. E*, 71:046127, 2005.
- [75] A. Hansen and P. C. Hemmer. Burst Avalanches in Bundles of Fibers: Local Versus Global Load-Sharing. *Phys. Lett. A*, 184:394–396, 1994.
- [76] U. Divakaran and A. Dutta. Critical behaviour of random fibers with mixed weibull distribution. *cond-mat/0608123*, 2006.

- [77] D. Sornette. Elasticity and failure of a set of elements loaded in parallel. *J. Phys. A*, 22:L243–L250, 1989.
- [78] J. B. Gómez, D. Iñiguez, and A. F. Pacheco. Solvable Fracture Model with Local Load Transfer. *Phys. Rev. Lett.*, 71:380, 1993.
- [79] D. G. Harlow and S. L. Phoenix. The Chain-of-Bundles Probability Model For the Strength of Fibrous Materials I: Analysis and Conjectures. *J. Comp. Mater.*, 12:195, 1978.
- [80] W. A. Curtin. Size Scaling of Strength in Heterogeneous Materials. *Phys. Rev. Lett.*, 80:1445–1448, 1998.
- [81] D. G. Harlow and S. L. Phoenix. The Chain-of-Bundles Probability Model for the Strength of Fibrous Materials II: A Numerical Study of Convergence. *J. Comp. Mater.*, 12:314, 1978.
- [82] W. I. Newman and A. M. Gabrielov. Failure of hierarchical distributions of fibre bundles. i. *Int. J. Fracture*, 50:1–14, 1991.
- [83] G. G. Batrouni and A. Hansen. Fracture in three-dimensional fuse networks. *Phys. Rev. Lett.*, 80:325, 1998.
- [84] P. V. V. Nukala, S. Simunovic, and S. Zapperi. Percolation and localization in the random fuse model. *J. Stat. Mech: Theor. Exp.*, p P08001, 2004.
- [85] H. J. Herrmann, A. Hansen, and S. Roux. Fracture of disordered, elastic lattices in two dimensions. *Phys. Rev. B*, 39:637–647, 1989.
- [86] F. Raischel, F. Kun, and H. J. Herrmann. Simple beam model for the shear failure of interfaces. *Phys. Rev. E*, 72:046126, 2005.
- [87] L. D. Landau and E. M. Lifschitz. *Theory of elasticity*. Butterworth-Heinemann, Oxford, 3rd edition, 1986.
- [88] W. Beitz and K.-H. Grote, editors. *Dubbel Taschenbuch für den Maschinenbau*. Springer-Verlag, New York, 20th edition, 2001.
- [89] D. Sornette. Failure thresholds in hierarchical and euclidean-space by real space renormalization-group. *J. Phys. (France)*, 50:745, 1989.
- [90] G. A. D’Addetta, F. Kun, E. Ramm, and H. J. Herrmann. From solids to granulates — Discrete element simulations of fracture and fragmentation processes in geomaterials. In P. Vermeer et al., editors, *Continuous and Discontinuous Modelling of Cohesive-Frictional Materials*, Lecture Notes in Physics. Springer Berlin, 2001.
- [91] F. Raischel, F. Kun, and H. J. Herrmann. Failure process of a bundle of plastic fibers. *Phys. Rev. E*, 73:066101, 2006.
- [92] D. Stauffer and A. Aharony. *Introduction to Percolation Theory*. Taylor & Francis, 1992.

- 
- [93] M. E. J. Newman and G. T. Barkema. *Monte Carlo Methods in Statistical Physics*. Clarendon Press, Oxford, 1999.
- [94] A. Hansen, S. Roux, and H. J. Herrmann. Rupture of central-force lattices. *J. Phys. France*, 50:733, 1989.
- [95] P. Ray and G. Date. Spatial scaling in fracture propagation in dilute systems. *Physica A*, 229:26, 1996.
- [96] S. Roux, A. Hansen, H. Herrmann, and W. Guyon. Rupture of heterogeneous media in the limit of infinite disorder. *J. Stat. Phys.*, 52:237, 1988.
- [97] A. Weinrib. Long-range correlated percolation. *Phys. Rev. B*, 29:387, 1984.
- [98] S. R. Anderson and F. Family. Percolation in an interactive cluster-growth model. *Phys. Rev. A*, 38:4198, 1988.
- [99] H. Saleur and B. Duplantier. Exact determination of the percolation hull exponent in two dimensions. *Phys. Rev. Lett.*, 58:2325, 1987.
- [100] F. Raischel, F. Kun, and H. J. Herrmann. Local load sharing fiber bundles with a lower cutoff of strength disorder. *Phys. Rev. E*, 74:035104(R), 2006.
- [101] S. Pradhan, P. Bhattacharyya, and B. K. Chakrabarti. Dynamic critical behavior of failure and plastic deformation in the random fiber bundle model. *Phys. Rev. E*, 66:016116, 2002.
- [102] H. Kawamura. Spatiotemporal correlations of earthquakes. *cond-mat/0603335*, 2006.
- [103] F. Kun, G. B. Lenkey, N. Takács, and D. L. Beke. Structure of magnetic noise in dynamic fracture. *Phys. Rev. Lett.*, 93:227204, 2004.
- [104] R. H. Randles and D. A. Wolfe. *Introduction to the theory of nonparametric statistics*. Wiley & Sons, New York, 1979.
- [105] T. Erdmann and U. S. Schwarz. Stability of adhesion clusters under constant force. *Phys. Rev. Lett.*, 92:108102, 2004.
- [106] T. Erdmann and U. S. Schwarz. Stochastic dynamics of adhesion clusters under shared constant force and with rebinding. *J. Chem. Phys.*, 121:8997, 2004.
- [107] F. K. Wittel and M. D'Ottavio. *Damage and its Evolution in Fiber-Composite Materials: Simulation and Non-Destructive Evaluation*, chapter 5.1 An Open Toolbox for Damage Simulation. Universität Stuttgart, 2006.





# Acknowledgments

I am greatly indebted to Prof. Hans J. Herrmann for accepting me as a student in his institute and supervising my thesis. He has always been available for invaluable discussions, and his knowledge of physics as well as his focus on progress are the foundation of this effort.

Working with Ferenc Kun has been an unforgettable experience, and I am deeply grateful for his untiring support, and the immense hospitality with which he and his wife, Dora Sohler, have received me in Debrecen. I have benefitted greatly from his guidance throughout my PhD, both personally and with respect to the research presented here.

This PhD has been supported by the DFG in the framework of SFB 381, and the members of the SFB, especially Falk Wittel, have provided many valuable suggestions and ideas.

It has been a constant pleasure to enjoy the company of my friends and colleagues at ICP, namely Bibhu Biswal, Ciprian David, Orencio Duran, Jason Gallas, Ramón García-Rojo, Marta Gonzalez, Jens Harting, Martin Hecht, Rudolf Hilfer, Frank Huber, Christian Kunert, Pedro Lind, Sean McNamara, Andrés Alfonso Peña Olarte, Marlies Parsons, Eric Ribeiro Parteli, Henriette Patzelt, Hansjörg Seybold and Adriano de Oliveira Sousa. Necessarily, this list of persons who have created a uniquely stimulating and amicable atmosphere at the institute is incomplete.

My parents, Christine and Helmut Raischel, have continuously supported and motivated me, for which I am very grateful. And, finally, I cannot imagine the past three years without Joana Freire at my side.





# Lebenslauf

<b>Name:</b>		Frank Raischel
<b>geboren:</b>		am 29.08.1977 in Würzburg
<b>Eltern:</b>		Helmut und Christine Raischel, geb. Filser
<b>Familienstand:</b>		ledig
<b>Schulausbildung:</b>	1983 - 1987	Grundschule Vinzentinum Würzburg
	1987 - 1996	Deutschhaus-Gymnasium Würzburg
	06/1996	Abitur
<b>Studium:</b>	1996 - 1997	Studium der Humanmedizin an der Universität Würzburg bis zum 2. Fachsemester
	1997 - 2003	Studium der Physik an der Universität Würzburg
	2000 - 2001	Studium der Physik an der University of Texas at Austin
	08/2001	M. A., University of Texas Thema der Masterarbeit „A Laser Electron Accelerator System for Radiation Therapy“ Betreuer: Dr. T. Tajima
	10/2003	Diplom, Universität Würzburg Thema der Diplomarbeit: „Computersimulation von epitaktischen Wachstumsprozessen: Einfluss von Desorption auf instabiles Wachstum“ Betreuer: Dr. M. Biehl Lehrstuhl für Theoretische Physik III
<b>Promotion:</b>	2004 - 2006	Doktorarbeit am Institut für Computerphysik der Universität Stuttgart (Prof. Dr. H. J. Herrmann)